Università
Ca'Foscari
Venezia

Centro Euro-Mediterraneo
sui Cambiamenti Climatici

Corso di Dottorato di ricerca in
Scienza e Gestione dei Cambiamenti Climatici
ciclo XXIX

Tesi di Ricerca

Using seasonal climate forecasts to predict rice yield over Nepal's Terai

Settore scientifico Disciplinare Di Afferenza: GEO/12

COORDINATORE DEL DOTTORATO

Prof. Carlo Barbante

SUPERVISORE

Dr. Panos Athanasiadis

CO-SUPERVISORE

Dr. Silvio Gualdi

DOTTORANDO

Prakash Kumar Jha

Matricola 956109

Acknowledgements

I would like to express my sincere gratitude to many people who have made this research possible. First, I need to thank my PhD supervisor Dr. Panos Athanasiadis for his continuous support over the past three years. He was the one who used to guide me whenever I was stuck, from the beginning to end. I am grateful for this continuous inspiration, promptness, and helping me to coordinate with experts in the area other than his expertise. I owe thanks to my co-supervisor Dr. Silvio Gualdi, who helped me strategically.

I am indebted to Professor Gerrit Hoogenboom from University of Florida Gainesville for his time and support in helping me to dig deeper into dynamic crop modelling and using a combination of hypothetical weathers for predictive skill improvement. I cordially thank him for his meticulous guidance in every detail of simulations. I must thank Dr. Vakhtang Shelia for his support in DSSAT calibration and writing a program to convert tens of thousands of weather files in DSSAT format. It would have taken several months had I prepared those files manually.

I would also like to thank Dr. Valentina Mereu and Dr. Antonio Trabucco from CMCC Sassari for orienting me with DSSAT in the beginning.

I thank Dr. Ram Baran Yadab from National Rice Research Program Hardinath along with other scientists from Nepal Agricultural Research Council for helping me to access experimental data and orienting me the basics of rice varietal trial experimentation in Nepal.

My parents used to energize me during the entire process whenever I used to lose confidence.

But most of all I want to thank my wife Usha Mishra and daughter Rosemary Jha for their infinite patience, understanding, encouragement and enduring love despite being far away from me.

Prakash Jha
December 2016

Table of Contents

List of Tables

List of Figures

Executive Summary

The gradual improvements in dynamical seasonal forecasts provide an opportunity to link coming season's weather with the dynamic crop models for agricultural applications including in-season crop yield prediction and management optimization.

Climate variability is a major source of crop yield variability, explaining roughly a third of the observed yield variability globally (Ray et al., 2015). Thus advance information on coming season weather can help in estimating crop yield. Crop yield prediction is an important part of the famine early warning system (Thornton et al., 1997). Subjective methods of crop yield estimation without properly accounting for the weather related variability result in less accurate yield prediction. Lack of proper estimation of food supply limit country's ability to manage food insecurity, and in some cases, lead to famine.

The high interannual variability in weather variables, including rainfall, makes the return on investment from agriculture uncertain and therefore is a major disincentive for farmers to tap full potential of farming. In an extreme case, hundred thousands of farmers in India have committed suicide due to crop failures related to no irrigation and poor water storage (Besten et al., 2016). Therefore, the risk-averse famers adopt low-risk (conservative) strategies with a lower expected profit than those which are more profitable on average. This reflected on the lowest rate of fertilizer applications and lowest rice yields in Nepal compared to the other South-Asian countries (WorldBank, 2015). Thus advance information on coming season weather can help farmers to maximize their benefits during the favourable seasons and minimize loss of inputs during unfavourable seasons. This is possible by evaluating yields under a variety of input options for the coming season weather using a dynamic crop model before the actual planting starts.

The importance of weather related variability on crop yield is high particularly for rainfed farming systems and for crops needing high amount of water. One such example is Nepal's Terai, where most of the rice cultivable lands are still rainfed and depend entirely on the monsoon rain (MOAC, 2008; IRRI, 2010). We selected rice crop because it needs high amount of water to grow (Bouman and Aureus, 2009). Moreover, the seasonal prediction systems (SPSs) have some skill to predict monsoon in the Indian region (Pokhrel Samir et al., 2013).

Various studies have been conducted in this direction using different types of seasonal forecasts. Some of them have used the El Nino Southern Oscillations (ENSO) to predict yields and optimize management (Ramirez-Rodrigues et al., 2014; Mavromatis et al., 2002). ENSO-based seasonal forecasts for yield

prediction, however, have several limitations. First, ENSO explains only part of the Indian Summer Monsoon (ISM) interannual variability (Goswami et al., 2006; Saji et al., 1999). Second, the strength of ENSO signal for the study area has been debated (Ichiyanagi et al., 2007). Moreover, there is a mismatch in the life cycles of ENSO and the ISM.

Other studies have used seasonal forecasts from the seasonal prediction systems (SPSs) (Pal et al., 2013; Mishra et al., 2008; Hansen et al., 2004). The SPSs are general circulation models (GCMs), which run with realistic initial conditions to predict the climatic anomalies for the coming season. The skill of the SPSs in predicting anomalies is associated with slowly varying boundary conditions such as the sea surface temperature (SST), sea ice, snow cover and soil moisture.

However, the mismatch in the temporal and spatial resolutions of SPSs and crop models is a challenge. Since the SPSs do not have skill to predict daily weather for a particular grid point, usually the seasonal forecasts from the SPSs are issued in the form of monthly or seasonal means anomalies for a larger area. On the other hand, the crop models run on a station level using daily data. Therefore, for crop modelling and other applications, Weather Generators (WGs) are commonly used to generate daily data from the seasonal or monthly means anomalies.

The WGs have difficulty in accurately estimating precipitation especially for the tropical and sub-tropical regions (Schmidt et al., 1996). Moreover, WGs generate daily data based on the statistical properties of the historical climate, which might not remain constant under the context of climate change. Using daily weather outputs from dynamic climate models have potential to reduce biases.

In our knowledge, this is the first study to use seasonal forecasts' daily data from an SPS into a dynamic crop model for predicting rice yield and optimizing management for the Nepali regions.

Nonetheless, before using seasonal forecasts from SPSs, we need to be sure that the SPSs have prediction skill for our regions of interest. Therefore, this study has the following objectives:

- To evaluate the ability of the Climate Forecast System Version 2 (CFS v2) (Saha et al., 2010) and Centro Euro-Mediterraneo sui Cambiamenti Climatici Version 1.5 (CMCC v1.5) (Borrelli et al., 2012) SPSs to predict the South Asian Monsoon with a focus on Nepal's Terai region and on parameters relevant to crop modelling;
- To explore potential of seasonal forecasts to predict yield for Nepal's Terai region; and
- To use seasonal forecasts to optimize crop management.

These are described separately in the following three chapters.

Chapter-I deals with evaluating SPSs. However, comparing all available SPSs was beyond the scope of this study. We took two state-of-the-art SPSs the CFS v2 and the CMCC v1.5. Potential of the CFS v2 and CMCC v1.5 SPSs to predict the ISM in a season advance is analysed in this chapter. We evaluated SPSs by comparing the hindcasts against observed and reanalysis data. We found that the CFS v2 has better skill in predicting temperature maximum/minimum and solar radiation demonstrated by the low biases and high correlation coefficients for both the Terai-East (TE) and All-India (AI) regions compared with the ERA-Interim reanalysis (Dee et al., 2011). CFS v2 was warmer, drier and it overestimated solar radiation than the ERA-Interim for both the AI and TE domains. However, the CFS v2 had a large systematic cold bias (upto -7^0C) when compared to the weather station data. Although, hindcasts from the one-month lead experienced lower biases than the hindcasts from longer lead times, considering the sensitivity of the crop models to temperature this reduction is not sufficient. Therefore, bias correction is needed. Also, as expected, the correlation coefficients between the hindcasts and reanalysis data were found higher for the short lead times hindcasts.

In contrast, both the models were less skill full in predicting precipitation. Although, the CFS v2 performed better than CMCC v1.5 in simulating precipitation over the Terai-East region, both SPSs were drier than the observed data from APHRODITE (Yatagai et al., 2012) and GPCP (Adler et al., 2003). Neither CFS v2 nor CMCC v1.5 was able to successfully simulate the monsoon climatology peak (both timing and magnitude). Similarly, both SPSs were able to capture the large-scale circulation features such as the ENSO-ISM teleconnection, strength of the Monsoon Indices, Flindlater Jet and monsoon onset and withdrawal. However, both SPSs failed to reproduce the Indian Ocean Dipole Index-ISM teleconnection and movement of the Inter Tropical Convergence Zone (ITCZ) above 20^0 N latitude in July as seen in observation.

In chapter II, we calibrated the Crop Estimation through Resource and Environment Synthesis (CERES)-Rice model of the DSSAT v4.6 (Hoogenboom et al., 2015) with the experimental data from the regional agricultural research station from Nepal. The hindcasts simulations of the CERES-Rice model fed with station and reanalysis meteorological data were less able to capture the inter-annual variations in district yield data. This could be because the district average yield comprised yields averaged from tens of thousands of farmers. These farmers practice dissimilar management in individual years on different farms. In contrast, the simulations were conducted for only one cultivar, soil and management practice.

After that we used yields simulated using observed weather as a reference for comparison. We used those reference yields, so as to capture the random errors related to the seasonal forecasts, while ignoring the crop model's errors (Hansen et al., 2004). Even using a combination of one-month lead seasonal forecasts from June to December, we did not find satisfactory skill in predicting reference yields. The one-month

lead seasonal forecasts consisted of July data from forecasts initialized in June, August data from forecasts initialized in July and so forth to December. Also, we used the one-and-two-month lead forecasts in which July and August data came from forecasts initialized in June, August and September data came from forecasts initialized in July and so forth to December.

Finally, we compared performances of predictions involving climatology alone with the predictions involving climatology combined with seasonal forecasts. The seasonal forecasts consisted of one-month and one-and-two-month lead. For each year, weather data included observed weather data until the forecast date, combined with seasonal forecasts and climatology or climatology alone for the remainder of the growing season. With the progress in growing season weather data were updated with the observed data. The model was run separately for each hybrid weather time series. For every month of prediction, we calculated average yield for each ensemble member by averaging 28 years of simulated yields.

In general, yield forecasts were better when combining observations for the past with climatological data for the remaining of the crop period compared to using observations and forecast data. This is evident from the lower mean percentage error (MPE), root mean square deviation (RMSD) and respective higher correlation coefficients. The prediction skill was even lower when using one- and two-month lead seasonal forecasts compared to using only one-month lead seasonal forecasts. The poor prediction skill when using seasonal forecasts is associated with the low skill of the seasonal forecasts, particularly in predicting precipitation. Given that the SPSs were able to capture the large scale circulation features, there is a potential to improve prediction using CFSv2 seasonal or monthly mean anomalies with spatial and temporal downscaling.

As expected, yield forecasts improved by incorporating successive monthly weather updates due to the increase in duration of observed weather. Predicting yield within 5% of error and with 0.99 correlation coefficient two and a half months before harvest using climatology alone is a promising result. However, it is important to note that this is not a true skill verified against observed yield.

Given that the model did not have satisfactory skill to predict yield using daily forecasts from CFS v2, it cannot be used for optimizing management before planting starts. Since we found that the ENSO signal was stronger in western Terai, we selected a station (Bhairahawa) in that domain as the study area for using ENSO categories of weather for management optimization. Admittedly, even the ENSO signal in that area is not particularly strong, and this imposes limitations to the applicability of our conclusions.

Using ENSO-phases for management optimization is described in the third chapter. To that end, the CERES-RICE model was run using the weather station data from 1983 to 2010. The years were categorized on the basis of the El Nino-Southern Oscillation (ENSO) phases: El Nino, La Nina and

Neutral years using the Nino 3.4 seasonal (JJAS) sea surface temperature (SST) anomaly. Additionally, we classified years according to the amount of precipitation as above average, below average and average based on standardized precipitation anomaly. The model was run under a given weather category for different planting dates and levels of Nitrogen (N) fertilizer. The average yields under various weather categories and management options were compared to select the best management option for a given weather category.

The rice yields simulated by the models were high in El Nino years, low in La Nina years and medium in the ENSO neutral years. Also, the yield increased in proportion to the amount of N fertilizer applied in all years. The rice yields were higher for the early planting date on June 14 than the existing practices in mid-July. These conclusions must be verified by the research stations.

The lower yields in La Nina years were associated with high (low) N leaching (uptake) due to the high drainage and runoff. Moreover, the lower yield during the La Nina years were associated with high minimum temperature anomaly during the second half of the growing season (Peng et al., 2004).

Considering the existing practices of mid-July planting and low level of N fertilizer application, rice yields could be increased in El Nino years, by adopting earlier planting dates. The net gross margin of US $34/ha can be achieved for the increase in N fertilizer application to 90 kg/ha and by planting on 14 June in El Nino years compared with the similar changes in other years. Since not every El Nino years are dry years, the study's conclusions have a statistical value but may lead to failures and losses. Therefore, before putting these findings into practice, one should assess the probabilities and cost of these "failures".

References

ADLER, R. F., HUFFMAN, G. J., CHANG, A., FERRARO, R., XIE, P.-P., JANOWIAK, J., RUDOLF, B., SCHNEIDER, U., CURTIS, S., BOLVIN, D., GRUBER, A., SUSSKIND, J., ARKIN, P. & NELKIN, E. 2003. The Version-2 Global Precipitation Climatology Project (GPCP) Monthly Precipitation Analysis (1979–Present). *Journal of Hydrometeorology,* 4, 1147-1167.

BESTEN, N., PANDE, S. & SAVENIJE, H. H. G. 2016. A socio-hydrological comparative assessment explaining regional variances in suicide rate amongst farmers in Maharashtra, India. *Proc. IAHS,* 373, 115-118.

BORRELLI, A., MATERIA, S., BELLUCCI, A., ALESSANDRI, A. & GUALDI, S. 2012. Seasonal Prediction System at CMCC. *Research Papers Issue RP0147*.

BOUMAN, B. & AUREUS, A. 2009. Every drop counts. *Rice Today.*: International Rice Research Institute. Los Banos, Laguna, Phillipines.

DEE, D. P., UPPALA, S. M., SIMMONS, A. J., BERRISFORD, P., POLI, P., KOBAYASHI, S., ANDRAE, U., BALMASEDA, M. A., BALSAMO, G., BAUER, P., BECHTOLD, P., BELJAARS, A. C. M., VAN DE BERG, L., BIDLOT, J., BORMANN, N., DELSOL, C., DRAGANI, R., FUENTES, M., GEER, A. J., HAIMBERGER, L., HEALY, S. B., HERSBACH, H., HÓLM, E. V., ISAKSEN, L., KÅLLBERG, P., KÖHLER, M., MATRICARDI, M., MCNALLY, A. P., MONGE-SANZ, B. M., MORCRETTE, J. J., PARK, B. K., PEUBEY, C., DE ROSNAY, P., TAVOLATO, C., THÉPAUT, J. N. & VITART, F. 2011. The ERA-Interim reanalysis: configuration and performance of the data assimilation system. *Quarterly Journal of the Royal Meteorological Society,* 137, 553-597.

GOSWAMI, B. N., MADHUSOODANAN, M. S., NEEMA, C. P. & SINGUPTA, D. 2006. A physical mechanism for North Atlantic SST influence on the Indian Summer Monsoon. *Geophysical Research Letters,* 33.

HANSEN, J. W., POTGIETER, A. & TIPPETT, M. K. 2004. Using a general circulation model to forecast regional wheat yields in northeast Australia. *Agricultural and Forest Meteorology,* 127, 77-92.

HOOGENBOOM, G., J.W. JONES, P.W. WILKENS, C.H. PORTER, K.J. BOOTE, L.A. HUNT, U. SINGH, J.I. LIZASO, J.W. WHITE, O. URYASEV, R. OGOSHI, J. KOO, V. SHELIA & TSUJI., G. Y. 2015. Decision Support System for Agrotechnology Transfer (DSSAT) Version 4.6 (http://dssat.net). Prosser, Washington: DSSAT Foundation.

ICHIYANAGI, K., YAMANAKA, M. D., MURAJI, Y. & VAIDYA, B. K. 2007. Precipitation in Nepal between 1987 and 1996. *International Journal of Climatology,* 27, 1753-1762.

IRRI 2010. Household survey data for Nepal collected under IFAD upland rice and STRASA (Stress tolerant rice for poor farmers in Africa and South Asia) projects. Social Sciences Division, International Rice Research Institute, Los Banos, Phillipines.

MAVROMATIS, T., JAGTAP, S. S. & JONES, J. W. 2002. El NiÃƒÂ±o-Southern Oscillation effects on peanut yield and nitrogen leaching. *Climate Research,* 22, 129-140.

MISHRA, A., HANSEN, J. W., DINGKUHN, M., BARON, C., TRAORÉ, S. B., NDIAYE, O. & WARD, M. N. 2008. Sorghum yield prediction from seasonal rainfall forecasts in Burkina Faso. *Agricultural and Forest Meteorology,* 148, 1798-1814.

MOAC 2008. Statistical informaton on Nepalese Agriculture, 2008/09, Government of Nepal, Ministry of Agricultural Development, Agribusiness Promotion and Statistics Division, Singh Durbar, Kathmandu,Nepal.

PAL, R. K., SEHGAL, A. K., MISRA, A. K., GHOSH, K., MOHANTY, U. C. & RANA, R. S. 2013. Application of Seasonal Temperature and Rainfall Forecast for Wheat Yield Prediction for

Palampur, Himachal Pradesh *International Journal of Agriculture and Food Science Technology,* 4, 453-460.

PENG, S., HUANG, J., SHEEHY, J. E., LAZA, R. C., VISPERAS, R. M., ZHONG, X., CENTENO, G. S., KHUSH, G. S. & CASSMAN, K. G. 2004. Rice yields decline with higher night temperature from global warming. *Proceedings of the National Academy of Sciences of the United States of America,* 101, 9971-9975.

POKHREL SAMIR, DHAKATE, A., CHAUDHARI, H. S. & SAHA, S. K. 2013. Status of NCEP CFS vis-a-vis IPCC AR4 models for the simulation of Indian summer monsoon. *Theor. Appl Climatol,* 11, 65-78.

RAMIREZ-RODRIGUES, M. A., ASSENG, S., FRAISSE, C., STEFANOVA, L. & EISENKOLBI, A. 2014. Tailoring wheat management to ENSO phases for increased wheat production in Paraguay. *Climate Risk Management,* 3, 24-38.

RAY, D. K., GERBER, J. S., MACDONALD, G. K. & WEST, P. C. 2015. Climate variation explains a third of global crop yield variability. *Nature Communications,* 6, 5989.

SAHA, S., MOORTHI, S., PAN, H.-L., WU, X., WANG, J., NADIGA, S., TRIPP, P., KISTLER, R., WOOLLEN, J., BEHRINGER, D., LIU, H., STOKES, D., GRUMBINE, R., GAYNO, G., WANG, J., HOU, Y.-T., CHUANG, H.-Y., JUANG, H.-M. H., SELA, J., IREDELL, M., TREADON, R., KLEIST, D., VAN DELST, P., KEYSER, D., DERBER, J., EK, M., MENG, J., WEI, H., YANG, R., LORD, S., VAN DEN DOOL, H., KUMAR, A., WANG, W., LONG, C., CHELLIAH, M., XUE, Y., HUANG, B., SCHEMM, J.-K., EBISUZAKI, W., LIN, R., XIE, P., CHEN, M., ZHOU, S., HIGGINS, W., ZOU, C.-Z., LIU, Q., CHEN, Y., HAN, Y., CUCURULL, L., REYNOLDS, R. W., RUTLEDGE, G. & GOLDBERG, M. 2010. The NCEP Climate Forecast System Reanalysis. *Bulletin of the American Meteorological Society,* 91, 1015-1057.

SAJI, N. H., GOSWAMI, B. N., VINAYACHANDRAN, P. N. & YAMAGATA, T. 1999. A dipole mode in the tropical Indian Ocean. *Nature,* 401, 360-363.

SCHMIDT, G. M., SMAJSTRLA, A. G. & ZAZUETA, F. S. 1996. Parametric uncertainty in stochastic precipitation models: wet day amounts. *Transactions of the ASAE,* 39, 2093-2103.

THORNTON, P. K., BOWEN, W. T., RAVELO, A. C., WILKENS, P. W., FARMER, G., BROCK, J. & BRINK, J. E. 1997. Estimating millet production for famine early warning: an application of crop simulation modelling using satellite and ground-based data in Burkina Faso. *Agricultural and Forest Meteorology,* 83, 95-112.

WORLDBANK 2015. Fertilizer consumption rate (kg/ha) of arable land. Data catalogue of the World Bank datasets. The World Bank Group

YATAGAI, A., KAMIGUCHI, K., ARAKAWA, O., HAMADA, A., YASUTOMI, N. & KITOH, A. 2012. APHRODITE: Constructing a Long-Term Daily Gridded Precipitation Dataset for Asia Based on a Dense Network of Rain Gauges. *Bulletin of the American Meteorological Society,* 93, 1401-1415.

CHAPTER I: Evaluating the ability of the CMCC v1.5 and CFS v2 Seasonal Prediction Systems (SPSs) to predict the South Asian Monsoon

Abstract

Interannual weather variability is an important source of crop yield variability globally and particularly for the rainfed farming systems. Seasonal forecasts from the dynamic seasonal prediction systems (SPSs) have potential to contribute to better agricultural decision making by predicting crop yield and by evaluating crop management options in a season advance. The reliability of such predictions, however, depends, to a large extent, on the quality of seasonal forecasts. Therefore, it is important to evaluate the skill of the SPSs before using Seasonal forecasts for any applications. This part of the study analyses the Climate Forecast System Version 2 (CFS v2) and the Centro Euro-Mediterraneo sui Cambiamenti Climatici Version 1.5 (CMCC v1.5) SPSs' potential use in predicting the Indian Summer Monsoon (ISM) in a season advance. It compares the SPSs' hindcasts with mean monsoon climatic features. We found that the CFS v2 model has an excellent skill to predict temperature maximum (T_{max}) at 2 meters, temperature minimum (T_{min}) at 2 meters, and total incoming total surface solar radiation (S_{rad}). Both of the models, however, less precisely predicted precipitation (Precip). The CFS v2 model has an edge over the CMCC v1.5 model in simulating precipitation over the Terai East (TE) region, while the CMCC v1.5 performs better in Central India (CI). Both SPSs are unable to simulate the monsoon peak (timing and magnitude both). In the contrary, both SPSs can capture the large-scale negative correlation between the Nino 3.4 index and precipitation over the Indian land region. However, both SPSs fail to replicate the positive correlation between the Indian Ocean Dipole (IOD) index and precipitation over the Indian land region. The study's findings indicate that the SPSs' direct weather outputs are less skilful in predicting monsoon precipitation.

Keywords: CMCC v1.5, ISM, Nepal, Terai

I.1 Introduction

The simulation and prediction of the Indian Summer Monsoon (ISM) strongly affects the livelihoods of billions of people in Asia. The agricultural productivity of the South Asian region in general – and of Nepal, in particular – depends on the ISM, as most arable lands (79%) are still rainfed (MOAC, 2008; IRRI, 2010; IRRI, 2009).

If the comprehensive seasonal forecast (SF) is based on local farmers' real needs and is disseminated

through the proper channels, it can provide an opportunity to manage climate-related risks and to maximize production (Hansen, 2002). Precipitation is one of the most essential factors for determining crop productivity, especially in rainfed farming systems. However, from a physiological perspective, crop growth depends also on solar radiation. To predict yields, crop models (such as DSSAT-CERES) need, at minimum, the following input variables: Precip, S_{rad}, T_{min}, and T_{max} on a daily basis for a particular location.

Climate models have some degree of skill at predicting anomalies that depart from climate at seasonal lead times. In other words, models have some ability to forecast whether a particular region will experience below or above average rainfall, temperature, or any other weather variable, in the coming season. Nevertheless, they are unable to predict, for example, how much rain a certain region will receive on a particular date in the subsequent season.

This skill of predicting anomalies at seasonal lead time is associated with the slowly varying boundary conditions at the earth's surface, such as the sea surface temperature (SST), soil moisture, and snow cover. Since these slowly changing boundary conditions have remarkable impact on atmospheric development for the coming season on the tropics, they provide clue to the dynamic models for seasonal prediction. For example, when the SST in the equatorial Pacific region is higher (lower) than average SST (a condition called El Nino [La-Nina]), the summer monsoon is lower (higher) than normal (Sikka, 1980).

Before utilizing SPS forecasts as inputs for a crop model, one must first determine whether the model has adequate predictive skill. Moreover, multiplication of high forecasts error with the error inherent in DSSAT can make the yield simulations far from reality. The lack of reliability of forecasts demotivate farmers to use seasonal forecasts a permanent component of their climate risk-management approach.

However, as various studies and model inter comparison projects have demonstrated, general circulation models (GCMs) significantly differ in their ability to predict the ISM (Kripalani et al., 2007; Annamalai et al., 2007; Kulkarni et al., 2013; Jiang et al., 2012). Pokhrel Samir et al. (2013) and Chaudhari et al. (2013) have indicated that the National Centres for Environmental Prediction (NCEP) CFS v2 is the best-performing SPS for the Indian region. However, their focus was not on the Nepali region and neither did they evaluate the CFS v2's ability to predict parameters other than precipitation required for crop modelling.

Furthermore, monsoon climatology widely varies from region to region within South Asia. Therefore, forecasters must test a model's ability to simulate and predict the monsoon in a particular region before encouraging the use of that model's seasonal forecasts for that area. Therefore, we utilized the NCEP CFS v2 along with another state-of-the-art SPS CMCC v1.5 with a focus on Nepal and North Central India

regions and all variables required for crop modelling.

The study concentrates on Nepal's Terai, because rice is the region's main crop, cultivated on 66% of its arable land. Furthermore, most of the Terai's rice production areas are rainfed, and thus depend on monsoon rain (MOAC, 2008; IRRI, 2010; IRRI, 2009). Moreover, there is a lack of similar studies focusing on this region.

This research project began by evaluating the SPSs' ability to predict the ISM and other weather variables, including S_{rad}, T_{max}, and T_{min}. To that end, we employed numerous diagnostics, including mean, standard deviation, coefficients of variation, correlation coefficient, spatial correlation, bias and root mean square error (RMSE).

Section Two of this chapter describes the models, data, and methodology, while Section Three presents and discusses the results. Finally, the conclusions are in Section Four.

I.2 Data, models and methodology

I.2.1 Data

Forecasts were taken from the CFS v2 SPS, which have been made available by NCEP (http://nomads.ncdc.noaa.gov/modeldata/cfs_reforecast_6-hourly_9mon_flxf). The CFS v2 consisted of a set of nine-month hindcasts initialized at every five days' interval and four times a day (00, 06, 12, and 18 UTC) from 1982 to 2010. There were thus 24 forecasts per month, which were considered as an ensemble. October and November were exceptions; each had only 20 members. We gave each ensemble member a three-digit name. The first digit referred to the date of the initialization month, and the following two digits signified the forecast hour. For example, for ensemble member "100", "1" denoted the first date of the initialization month, while "00" referred to the forecast hour.

The first date of a month was not necessarily the first calendar day of that month. For example, June 5^{th} was the first date in the June initialization. And, the 4^{th}, 3^{rd}, and 2^{nd} were the initial dates in the August, September, and December initializations, respectively. We constructed 24 different time series of daily hindcasts from 1983-2010 for seven months (June, July, August, September, October, November, and December) for four variables (Precip, T_{max}, T_{min}, and S_{rad}). As we only had five initialization dates in both October and November, the time series from 17 to 24 employ November and December forecasts from the fifth initialization dates in October and November, respectively.

We constructed the time series by taking forecasts with a one-month lead time. For instance, we took June forecasts from May initialization, July forecasts from June initialization and so on. We utilized this

approach to minimize the predictability error, although from an operational perspective, this would not be feasible. In practice, a set of nine-month forecasts are issued from each initialization time. Although our forecasting approach had less practical relevance, it minimized the predictability error, which was important, as we were primarily interested in the seasonal forecasts' ability to predict yield. In general, the predictability errors drop with the reduction in lead times. Thus, we had 24 different time series for each ensemble member. These consisted of daily hindcasts from 1983-2010 for Precip, T_{max}, T_{min}, and S_{rad}. We selected the months from June to December, as these represent the main rice-growing season in Nepal's Terai. We henceforth named this set of 24 time series the Hybrid-one-month lead-time series. Averaging the 24 time series created an ensemble mean.

Theoretically, the ensemble mean time series should minimize the forecast errors resulting from differences in initial conditions. To assess the predictability error stemming from the lead times, we compared the monthly means of the forecasts with different lead times for all variables.

Moreover, CMCC v1.5 six-month hindcasts are available from 1981-2010 for four initialization times (February 1st, May 1st, August 1st, November 1st). To account for uncertainty resulting from initial conditions, the start date of each initial condition consisted of eight initial atmospheric conditions from the last four days at 12-hours interval along with initial condition of the start date. Thus we had nine different initial conditions including the start date from where the CMCC v1.5 evolved producing a probability distribution of the forecasts (Borrelli et al., 2012).

I.2.2 Models

The NCEP CFS v2 (Saha et al., 2010) is a fully coupled SPS, and it is comprised of the NCEP GFS (Moorthi et al., 2001) atmospheric model and the Modular Ocean Model version 4 (MOM4) p0d (Griffies et al., 2004) ocean GCM. The GFS has T126 (100 km) resolution and 64 hybrid vertical levels. Model physics include rapid radiative transfer model (RRTM) short-wave radiation (Iacono et al., 2000; Clough et al., 2005), Arakawa-Schubert convection with momentum mixing, orographic gravity drag from (Kim and Arakawa (1995) and sub-grid scale mountain blocking, based on Lott and Miller (1997). The MOM4 is a finite differencing model with 0.25^0 - 0.5^0 grid and 40 vertical levels. The CFS v2 and MOM4 models are coupled with no flux adjustment. Also the CFS v2 has a separate sea ice model (Wu et al., 1997; Winton, 2000) and Noah land surface model (Ek et al., 2003).

The CMCC v1.5 coupled General Circulation model (GCM) consists of four components: the ECHAM5 (Roeckner et al., 2006; Roeckner et al., 2003; Roeckner et al., 1996) representing atmosphere; SILVA (Alessandri et al., 2007) for the land-surface; OPA8.2 (Madec et al., 1998) for the ocean component; and LIM (Timmermann et al., 2005) for the sea ice component. These different components are coupled with

the OASIS3 coupler (Valke et al., 2000). The ECHAM5 is a global spectral model with T63 truncation and has 192 points along the longitude and 96 points along the latitude with a horizontal resolution of about 200 km. Moreover, it includes 19 vertical levels in sigma coordinates. It is coupled to the SILVA, a dynamic vegetation model with the same resolution. The OPA8.2 is an ocean GCM with ORAC2 grid. This is a quasi-isotropic tri-polar grid with two poles in the northern hemisphere: one above Siberia and the other above Canada. It has a horizontal resolution of 1.5^0 along the latitude and 2^0 along the longitude, with an increase of 0.5^0 near the equator. It has 31 levels in the vertical, with a resolution of 10-meter in the top 100 meters. It was coupled with the LIM sea ice model, which has the same resolution. Flux exchange was conducted with the coupler, without any adjustment in frequency.

This study uses CMCC v1.5 SPS, in which all components (atmosphere, ocean and land surface) were initialized with a realistic state close to the observed data. The ECHAM5 was initialized using the ERA-Interim reanalysis (Berrisford et al., 2009). And, the OPA8.2 is initialized using CMCC v1.5-INGV Global Ocean Data Assimilation (CIGODAS) (Di Pietro and Masina, 2009; Bellucci et al., 2007), which is based on the assimilation of temperature and salinity profiles and is forced by the ECMWF operational analysis using an optimum interpolation scheme. The sea ice initial condition was from simulation of CMCC v1.5-SPS.

The model was run from 1960 to 2010 in the 'present climate' state, in which the radiative forcing changes according to the actual greenhouse gases (GHG) concentration in the atmosphere every year. The sea ice concentration of the last 20 years was used.

I.2.3 Methodology

We assessed the models' ability to simulate the ISM by comparing their simulations with mean monsoon features (DelSole and Shukla, 2010). The mean monsoon features this study investigated included the mean seasonal cycle, the Flindlater Jet, monsoon indices, proper representation of the maximum rainfall band's movement, monsoon onset and withdrawal dates, and air-sea interactions. We also included the Indian monsoon teleconnections, including the El Nino Southern Oscillation (ENSO) and IOD.

The hindcasts precipitation was evaluated against the APHRODITE precipitation data (Yatagai et al., 2012) and GPCP precipitation data (Adler et al., 2003). Similarly, the Nino 3.4 and IOD indices were calculated from the SST simulated by the models and compared against these indices using the SST from NOAA Optimum Interpolation v2 reanalysis (Reynolds and Smith, 1994). Moreover, the variables total incoming surface S_{rad}, T_{max} at 2 m and T_{min} at 2 meter were validated against ERA-Interim reanalysis (Dee et al., 2011).

We calculated bias and grid-by-grid anomaly correlation. We also compared the area average daily

climatology data for the All India (AI) and Terai East (TE) domains, as well as for one grid point in Nepal. The AI domain was bounded by 5-35^{0}N and 65-95^{0}E, while the TE domain fell between 26-26.9^{0}N and 84.6-88.2^{0}E. The grid point in Nepal was located in Hardinath, at 26.8^{0}N/85.9^{0}E. While the AI region is one of the most commonly researched domains in monsoon-related studies, this study focused on the TE domain. We used bilinear interpolation to get data for the exact point from the gridded data. We computed the daily climatology for the variables by averaging the daily weather from 1983-2010 and applying a 15-day moving average. The CFS v2 hindcasts were only available for June-December, but the APHRODITE and ERA-Interim data spanned the entire year. Furthermore, weather station data from the Department of Hydrology and Meteorology (DHM) and data from the NASA POWER project (http://power.larc.nasa.gov/cgi-bin/agro.cgi?email=agroclim@larc.nasa.gov) were used to cross-check. The reason for using weather station data is because some studies such as the van Wart et al. (2013) have pointed out that results from the studies relying on the reanalysis or satellite based gridded weather data for simulating yield are highly uncertain.

I.3 Results and Discussion (Representation of the monsoon circulation)

I.3.1 Bias

I.3.1.1 Precipitation

In Nepal, the observed climatology from 1976 to 2005 indicated a trend in which precipitation decreased moving from east to west (Marahatta et al., 2009). Similarly, the hill and mountain regions experienced increasing trends of precipitation, while the opposite was observed in the Terai region (MOPE, 2004). The orographic effect further altered precipitation, with the windward side receiving high amounts, while the leeward side saw significantly less (Marahatta et al., 2009).

Neither GPCP nor CMCC v1.5 model was able to capture the observed high precipitation pattern in the hilly areas of the eastern and central regions of Nepal (Fig. I.1(a) and (b)). However, the APHRODITE and CFS v2 had clearly captured the east-west and hill-plain gradient in precipitation (Fig. I.1(c) and (d)). Compared to the hilly regions the southern plain regions received less precipitation.

Both CFS v2 and CMCC v1.5 underestimated rain in TE by 2-5 mm/day, although both were very wet (>10mm/day) in the Himalaya region (Table I.1). The excessive bias in the Himalayan region was related to the orography, which could not be resolved in the low-resolution models.

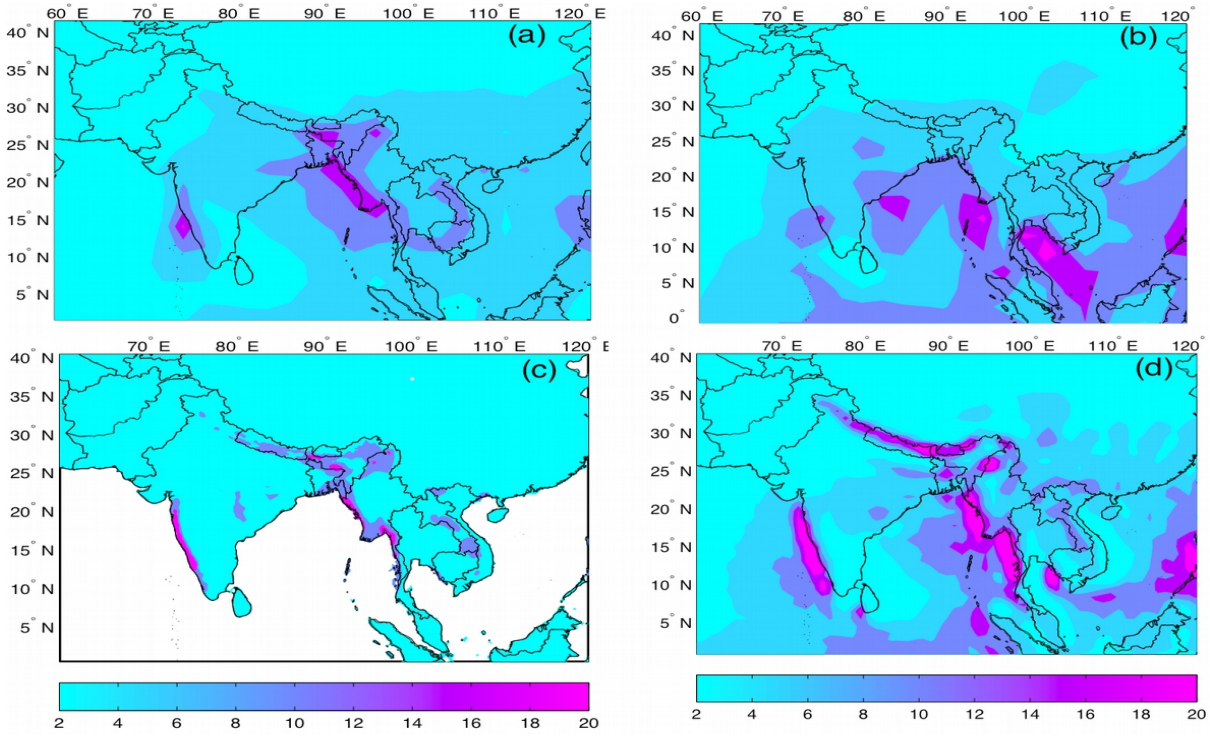

Fig. I.1 Seasonal (JJAS) climatology for the Indian region for the period of 1982-2005 for a) GPCP b) CMCC c) APHRODITE d) CFS v2.

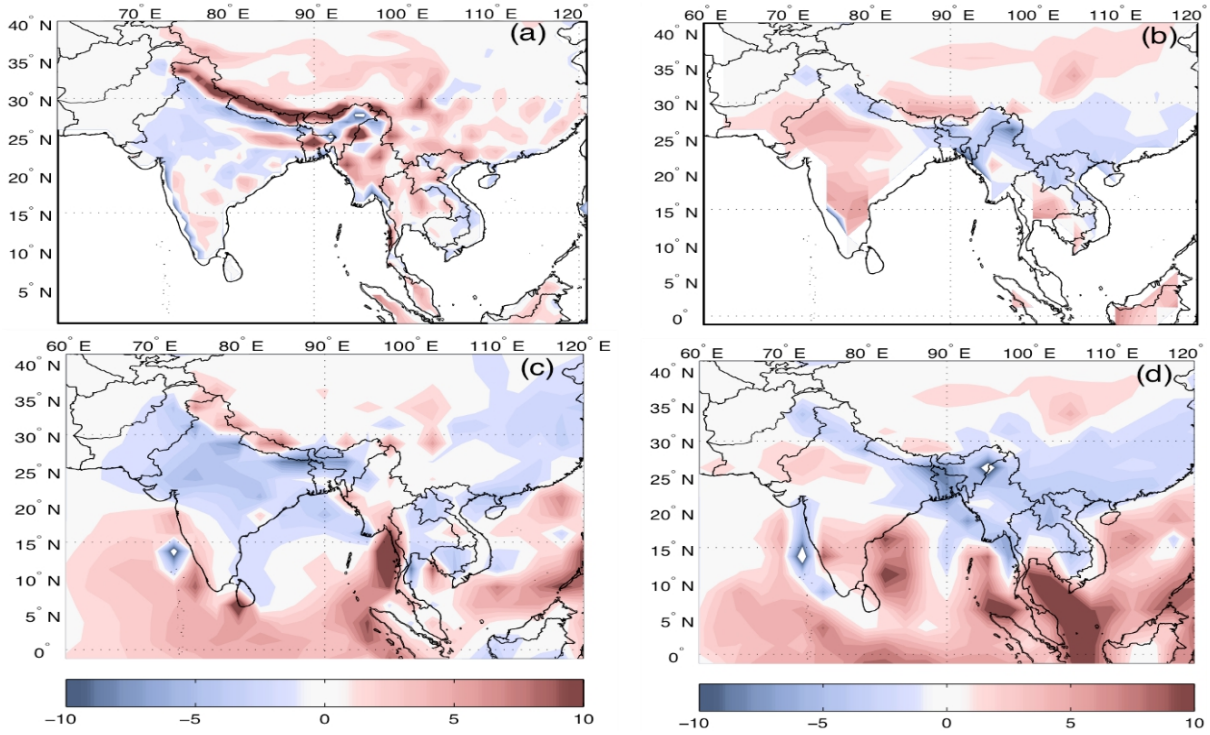

Fig. I.2 Bias in seasonal (JJAS) average precipitation (mm/day) from 1982-2005 for a) CFS v2 b) CMCC v1.5 with respect to APHRODITE and c) CFS v2 d) CMCC with respect to GPCP.

Except some patches of wet bias in the Northeast regions, CFS v2 has dry bias in most other land regions of India. However, the average seasonal (JJAS) precipitation for the AI land only region in both models was close to observation (Table I.1).

In contrast to the other models, including the CFS v2, which demonstrated a dry bias over central India (Rajeevan and Nanjundiah, 2009; Krishnamurthy and Shukla, 2001), the CMCC v1.5 model more successfully captured the precipitation climatology over central India, although it had a somewhat wet bias (Fig. I.1(b), I.2 (b) and I.2 (d)). However, unlike CFS v2, the CMCC v1.5 was not able to capture the higher precipitation along the North East India, the Himalayan region, the Western Ghat region. The CMCC v1.5 thus had a dry bias over these regions (Fig. I.1(b), I.2 (b) and I.2 (d)).

Both models underestimated daily precipitation climatology and variability averaged for the AI (land-only) and TE domains (Fig. I.3a). However, both more successfully captured higher precipitation trends in TE region than in the AI domain. As Figure I.3a indicates, the CFS v2 predicted an earlier start to the rain than what was observed in both the AI and TE domains (Fig. I.3a). Also, the CFS v2 was unable to capture the peak intensity, or the timing of the peak. In the CFS v2 model, rainfall peaked at the end of June, while observations illustrated that rainfall actually peaked at the end of July. Moreover, the CFS v2 had a dry bias for both the AI and TE domains.

In a study that compared 22 IPCC-AR4 models' ability to simulate the monsoon, (Kripalani et al., 2007) found that, for the seven best-performing IPCC-AR4 models, the AI-averaged monsoon (JJAS) season precipitation varied from 5.73 to 8.11 mm/day and the coefficient of variation (CV) was between 5-10 % (Kripalani et al., 2007). For the AI land-ocean domain, both models' mean and CV fell within the range of those seven models (Table I.1).

The RMSE was lower (higher) for AI (TE) for both these models when compared to the GPCP. However, the RMSE values for the CFS v2 and CMCC v1.5 were comparable with APHRODITE (Table I.2). But, the observations were not perfect as shown by the high RMSE between the two observational datasets in the TE domains (Table I.2).

The correlation coefficients for the CFS v2 model's simulated interannual seasonal average (JJAS) precipitation and observed values (GPCP/APHRODITE) demonstrate that the CFS v2 was moderately skilled for the AI domain (Table I.3). The CMCC v1.5 model, however, was not appropriate for the TE domain, as demonstrated by the very low and insignificant correlation coefficients (Table I.3).

Similar to the precipitation averages for the AI and TE domains, the CFS v2 hindcasts daily climatology for Hardinath grid point predicted an early start to the rain and also estimated that the peak would occur in June, rather than in July, as in the observations (Fig I.4a). It also dropped more rapidly after July than

what was observed. To further cross-check the observation data, we employed weather station data and NASA POWER project data at the same point. The CFS v2 forecasts had wet bias in June and dry bias in other months compared to the weather station data. But, the NASA POWER and APHRODITE data had dry bias until July end, after that until mid-September, NASA POWER data had wet bias and APHRODITE had dry bias. From mid-September onwards, both NASA POWER and APHRODITE were very close to the weather station data (Fig. I.4a). Although most of the CFS v2 ensemble members had negative bias in estimating daily precipitation climatology, the observed data (from weather station and APHRODITE) fell inside the ensemble spread (Fig. I.4a).

We also analysed biases in distribution of precipitation. We found that in 9 out of the 28 years, CFS v2 less accurately captured precipitation's distribution. For example, in 2009 and 2010 from August end to December end (almost 4 months) observation did not show any rain, except a few events in October (Fig. I.5). Similar were the case in 1991 and 1995, albeit to a lesser extent. But all ensemble members were showing regular rain during those periods. Similarly, in 2007 none of the ensemble members were able to represent the extreme rain (535 mm in 3 days) during July end. Also in 1994, observation did not show any regular and large rain until mid-July but all members were showing regular and high rainfall.

Table I.1: Seasonal (JJAS) area average precipitation (mm/day), SD and CV for AI and the TE domains for models and observation for the period from 1981-2005. Values of the TE domain are shown in parenthesis.

	Land only		**Land and ocean**
	Mean	CV (%)	Mean
CMCC v1.5	3.3 (7.6)	5 (4)	7.7
CFS v2	3.0 (7.3)	4 (10)	7.6
GPCP	3.5 (12)	6 (14)	6.7
APHRODITE	5.3 (9.4)	8.5 (20)	5.3

Table I.2: RMSE (mm/day) between models and observations for precipitation in the AI and TE domains. The values for the TE are in parenthesis.

CFS v2/APHRODITE	CMCCv1.5/ APHRODITE	CFS v2/GPCP	CMCC v1.5/GPCP	GPCP/ APHRODITE
2.3 (2.7)	2.1 (2.6)	0.6 (5.0)	0.3 (4.6)	1.8 (3.6)

Table I.3: The correlation coefficients, along with their significance values (p), for the interannual variation of seasonal (JJAS) mean precipitation between the models' (CMCC v1.5 and CFS v2) simulations and observations (GPCP and APHRODITE) for the AI domain and TE domain. The values in parentheses are for the TE domain.

	r	**p**
CFS v2/APHRODITE	0.4 (0.3)	0.02 (0.11)
CMCCv1.5/APHRODITE	0.4 (0.0)	0.1 (0.96)
CFS v2/GPCP	0.5 (0.4)	0.00 (0.07)
CMCC v1.5/GPCP	0.5 (0.2)	0.00 (0.45)
GPCP/APHRODITE	0.9 (0.9)	0.00 (0.00)

In 1992, higher than normal rain fell during later part of the growing season but all ensemble members showed opposite. In 2000 observation did not show any high rain from September onwards but all members were showing high rain. Similarly, in 1988 October and November model showed unrealistically high rains.

I.3.1.2 Temperature maximum

The CFS v2's seasonal (JJAS) mean T_{maxs}, averaged from the monthly mean from 1983 to 2010, were colder than the ERA-Interim for the AI region, although the extent of biases varied over the regions (Fig. I.6a). Biases were smaller in TE and its immediate south near Indo-Nepal border than the Himalayan regions and its north. Saha et al. (2014) echoed our finding and showed that the CFS v2's 2-meter air temperature has cold bias than the ERA-Interim for the AI region. In contrast, the CFS v2's daily T_{max} forecasts had positive biases than the ERA-Interim (Fig. I.3b). The reason for the difference between the CFS v2's T_{max} seasonal mean and daily climatology is because the daily forecasts were taken from the maximum of the 6-hourly forecasts for each day, while the seasonal mean was averaged from monthly mean forecasts. Although CFS v2's daily T_{maxs} had warm biases in both domains, the magnitude of these biases was higher in TE (Fig. I.3b). The bias in the AI region was reduced, since it was averaged over a larger region than the TE. The CVs for the CFS v2's and ERA-Interim's T_{maxs} were 0.3 (1.6) and 1.0 (1.8) for the AI (TE) domains respectively. The CFS v2's T_{maxs} had RMSEs 1.5 (3.1) for the AI (TE) domains compared to the ERA-Interim.

Although, the CFS v2 predicted daily T_{max} climatology was closer to the ERA-Interim and NASA POWER data, all of them had very high negative bias when compared to the weather station data for the Hardianth grid point. The CFS v2's, ERA-Interim's and NASA POWER's T_{max} had significant systematic negative biases of up to -6^0C compared to the weather station (Fig. I.4b). Differences between the reanalysis and observation data could stem from the nonlinear interaction among various errors including observational errors, model errors and methodological errors (Thorne and Vose, 2010; Dee et al., 2011).

Considering the mean monsoon season temperature from ERA-Interim averaged for the Indian region has negative bias (Shah and Mishra, 2014) and the CFS v2 daily T_{max} has positive bias than the ERA Interim, the average bias in CFS v2 daily T_{max} forecasts is less than the ERA Interim.

I.3.1.3 Temperature minimum

The CFS v2 model almost perfectly predicted seasonal (JJAS) mean T_{min} for the TE and South Indian region compared to the ERA-Interim reanalysis (Fig. I.6c). For the north Indian regions, however, the

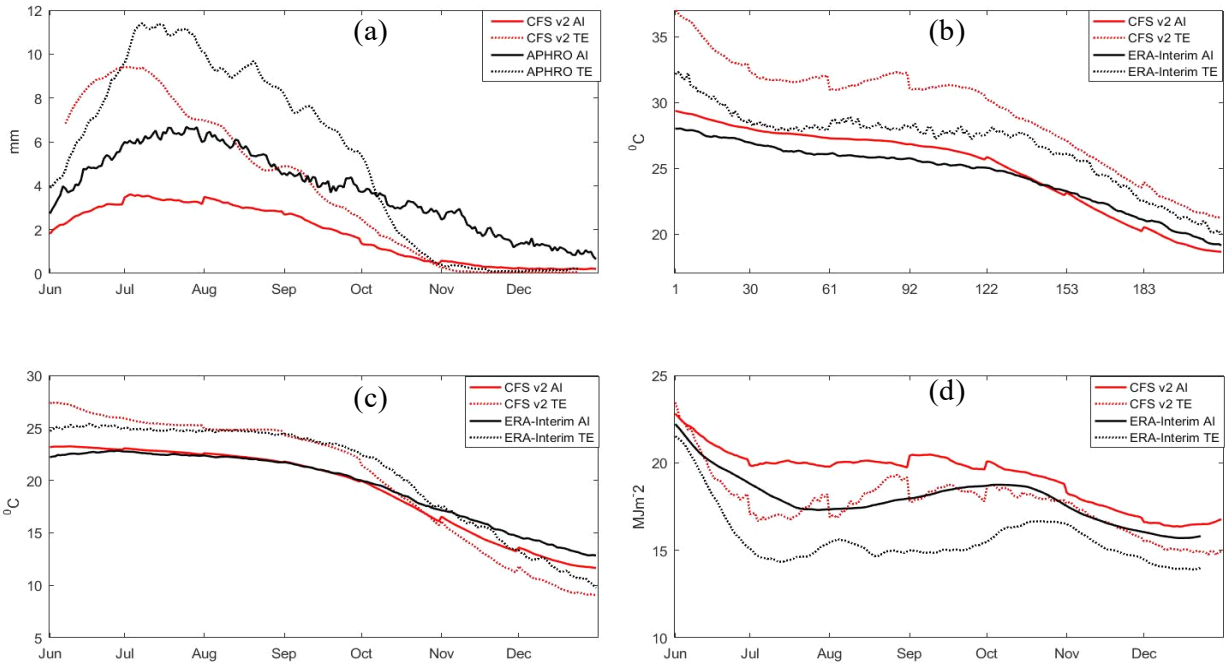

Fig. I.3 Daily climatology from 1983-2010, averaged for the AI and TE domains for: (a) precipitation, (b) temperature maximum, (c) temperature minimum, and (d) solar radiation. The AI domain is shown with solid lines, and TE with dotted lines.

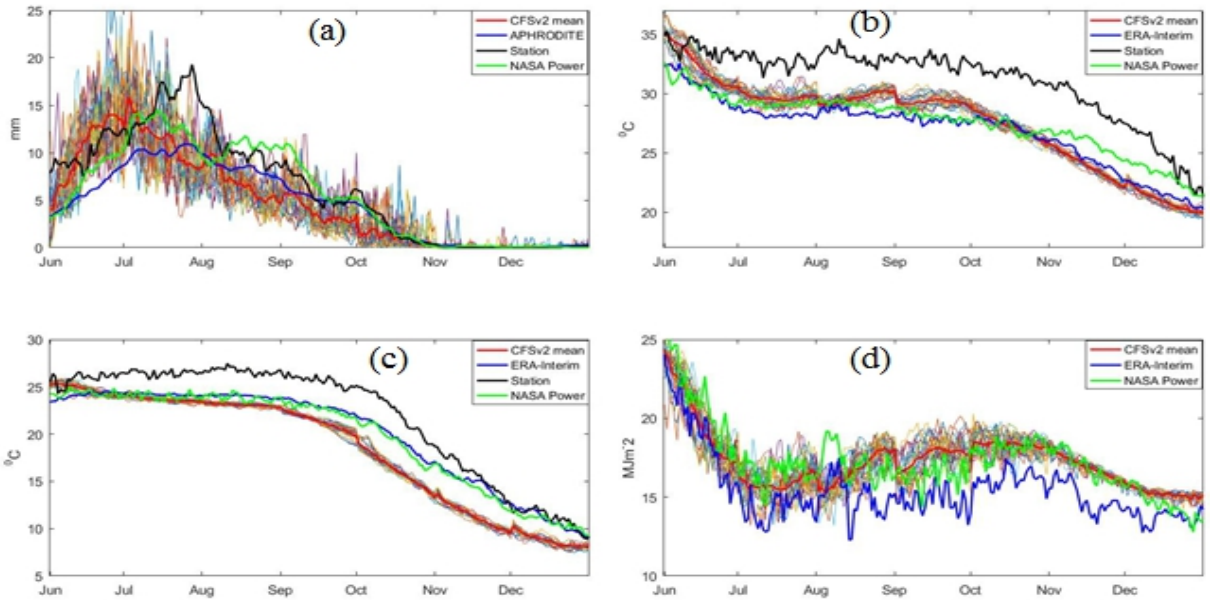

Fig. I.4 Daily climatology from 1983-2010 for Hardinath, Nepal for: (a) precipitation, (b) temperature maximum, (c) temperature minimum, and (d) solar radiation.

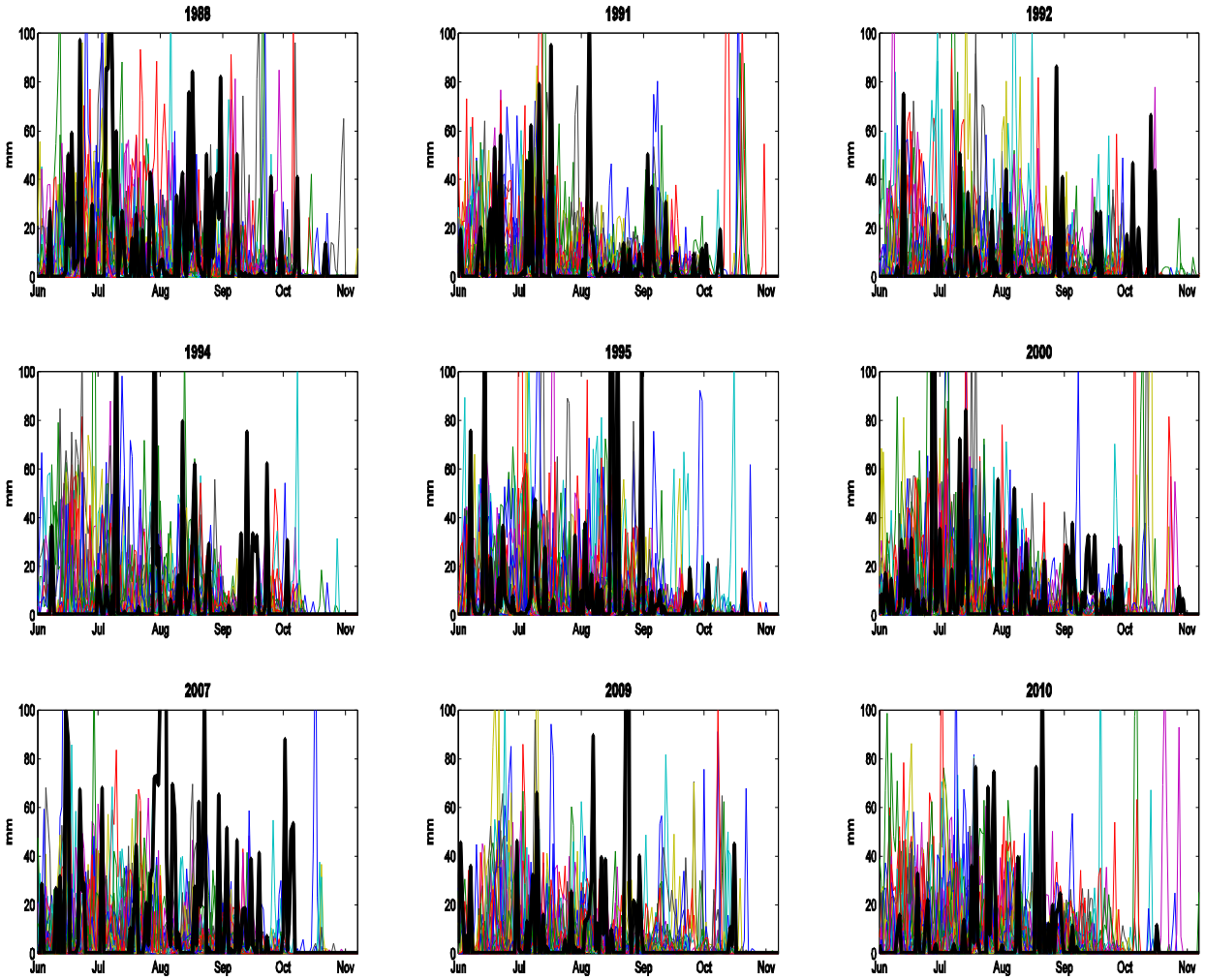

Fig I.5 Daily precipitation observed versus CFS v2 ensemble members for Hardinath grid point from 1983 to 2010. Precipitation intensity (mm) are shown in vertical axis and number of days starting from June are shown in horizontal axis. The thick black line represents the observed precipitation and the thin 24 lines are the CFS v2 ensemble members.

CFS v2 predicted seasonal (JJAS) mean T_{mins} were slightly overestimated. The CFS v2's and ERA-Interim's T_{min} CVs for the AI (TE) domains were 1.2 (1.5) and 1.0 (1.7) respectively. The CFS v2's T_{min} RMSEs for the AI (TE) domains were 0.3 (0.7) respectively.

The CFS v2 T_{min} daily climatology for the AI domain were almost perfect until October, after which the bias increased (Fig. I.3c). Also, the temperature in the TE domain dropped more rapidly than in the AI domain during the cold season. Presence of the ocean and coastal areas in the AI domain resulted in less intense temperature drops than in the inland region. The reduction in T_{min}, however, was more rapid in hindcasts than in the observations.

The CFS v2 ensemble mean daily climatology for T_{min} was quite close to ERA-Interim and NASA POWER data until August after that biases in CFS v2 forecasts increased gradually. Except for the first few days, differences between CFS V2's and ERA-Interim's T_{min} were upto -1^0C until August followed by sharp increase and then steady decline. Compared to the weather station data, the CFS v2's, ERA-Interim's and NASA POWER's T_{min} had bias upto -7^0C, -3^0C and -4^0C respectively. The ensemble spread reached a minimum for T_{min} (Fig. I.4c). These biases are very high considering the sensitivity of dynamic crop models to temperature change. Therefore, proper bias correction is needed before using these forecasts into crop models.

I.3.1.4 Solar radiation

CFS v2 overestimated solar radiation compared with the ERA-Interim reanalysis over a narrow strip along the Indo-Nepal border. This band extended west northward, running parallel to the Himalayas (Fig. I.6c). Furthermore, the model yielded an excessive positive bias of approximately 3 MJ/m^2/day for the TE region. The CFS v2 and ERA-Interim's S_{rad} CVs for the AI (TE) domains were 1.1 (2.5) and 6.7 (7.5) respectively. The CFS v2's S_{rad} RMSEs for the AI (TE) domains were 1.8 (3.0) respectively. Also, in the Northeast regions, the CFS v2 deeply overestimated S_{rad}. Except for a few patches of overestimation in coastal regions, the CFS v2 underestimated S_{rad} in the inlands regions of India.

Unlike temperature, S_{rad} was higher for the AI domain than for the TE domain (Fig. I.3d). Furthermore, the CFS v2 displayed a large, positive bias (approximately 3-4 MJ/m2/day) in both domains during the monsoon season. From November onwards, S_{rad} began to rapidly decline in both domains. Since the AI domain contained more areas at lower latitudes than did the TE domain, S_{rad} was higher in the AI domain.

The ensemble spread for S_{rad} daily climatology was larger during the monsoon season, due to differences in the initial cloud cover conditions (Fig. I.4d). The CFS v2 ensemble mean daily climatology was closer to the NASA Power data than the ERA-Interim. When compared to the ERA-Interim more of a bias was present from July onwards.

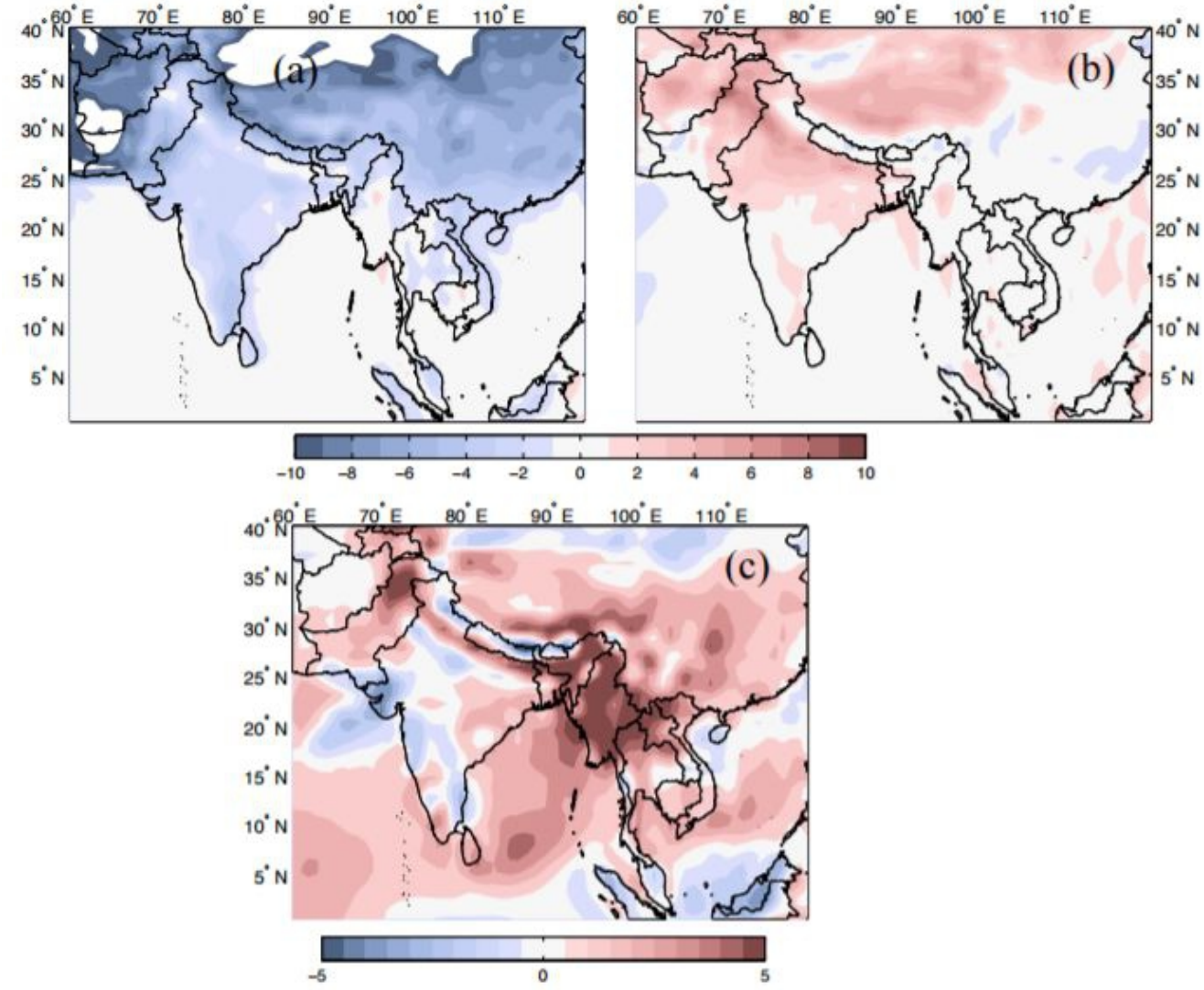

Fig. I.6 Seasonal (JJAS**)** bias for one-month lead-time for (a) maximum temperature (b) minimum temperature and (c) solar radiation. The bias is calculated as the difference between CFS v2 and ERA-Interim for the seasonal (JJAS) average of 1983-2010. Units are in degree Celsius for temperature and in MJ/m2/day for the solar radiation.

I.3.2 Anomaly correlation

We computed the anomaly correlation between the CFS v2 and APHRODITE for precipitation, and between the CFS v2 and the ERA-Interim reanalysis for all other variables. The time series consisted of a 28-year (1983-2010) series of data covering seasonal (JJAS) anomaly of each year.

I.3.2.1 Precipitation

The anomaly correlation value was between 0.4-0.6 in the upper half of the Indian region, while there was either a very weak relationship (or no relationship) from the CI to the Southern tip of India (Fig. I.7a). In the northern regions, the anomaly correlation values slightly increased from east to west. For the TE region, the figure was from 0.2 to 0.4, with westward regions seeing higher values. Despite the fact that North Nepal and South Nepal had opposite biases, both regions had positive anomaly correlation values.

I.3.2.2 Temperature maximum

The CFS v2 models' forecasted T_{maxs} were strongly correlated with the ERA-Interim, except for certain areas in the Himalayas and in South India, where the relationship was weaker (Fig. I.7b). In most other regions (including the TE), the correlation coefficient was higher than 0.7. Shah and Mishra (2014) found ERA-Interim reanalysis as the best performing reanalysis for reproducing observed temporal variability related to mean monsoon season temperature, with the correlation coefficients of 0.8 between the observed and ERA-Interim AI-averaged monsoon season mean temperature.

I.3.2.3 Temperature minimum

Similar to T_{max}, the ERA-Interim's T_{mins} were strongly correlated with T_{mins} from the CFS v2 model except South India and coastal regions (Fig. I.7c). The correlation coefficient was greater than 0.8 in North Indian regions, including the TE.

I.3.2.4 Solar radiation

CFS v2 was very skilled at forecasting S_{rad}, as illustrated by its strong correlation with the ERA-Interim for most of the Indian region, except for the eastern coastal region (Fig. I.7d). This model was also highly predicative for the TE, with a correlation coefficient of approximately 0.7, which increased moving westward.

I.3.3 Effect of lead time on the bias

I.3.3.1 On the bias

We attempted to examine whether these biases were systematic or whether decreasing the lead time could reduce them. To that end, we compared the biases for all four variables for the AI and TE domains. Fig. I.8a illustrates the magnitude of the biases for both domains. As Figure I.8a makes it clear, decreased lead times reduced the biases for both domains for all variables. The exception was T_{min} in the TE domain, where biases slightly increased for the Hybrid initialization than the May initialization. The marginal lead time-driven reduction in the biases was greater for the TE domain than for the AI domain, partly because averaging the biases over large geographic areas reduced them.

I.3.3.2 On the anomaly correlation

The correlation coefficients between CFS v2's hindcasts and APHRODITE's precipitation and ERA-Interim's variables for the AI and TE domain were compared for different lead times – March, April, May, and a hybrid one-month lead. All weather variables were averaged for the AI and TE monsoon season (JJAS) from 1983 to 2010. Figure I.8 (b) clearly indicates that the correlation coefficients for the AI domain did not considerably change compared with the TE domain, regardless of the lead times. For T_{max}, T_{min}, and S_{rad}, the correlation coefficients remained constant at around 0.9. For Precip in the AI domain, however, the correlation coefficient slightly improved, shifting from 0.50 to 0.55. In contrast to the AI domain, the TE domain exhibited a slight improvement in the correlation coefficients for all variables. Specifically, the correlation coefficient increased from 0.19 to 0.30 for Precip, and up to 0.15 for other variables in the TE region.

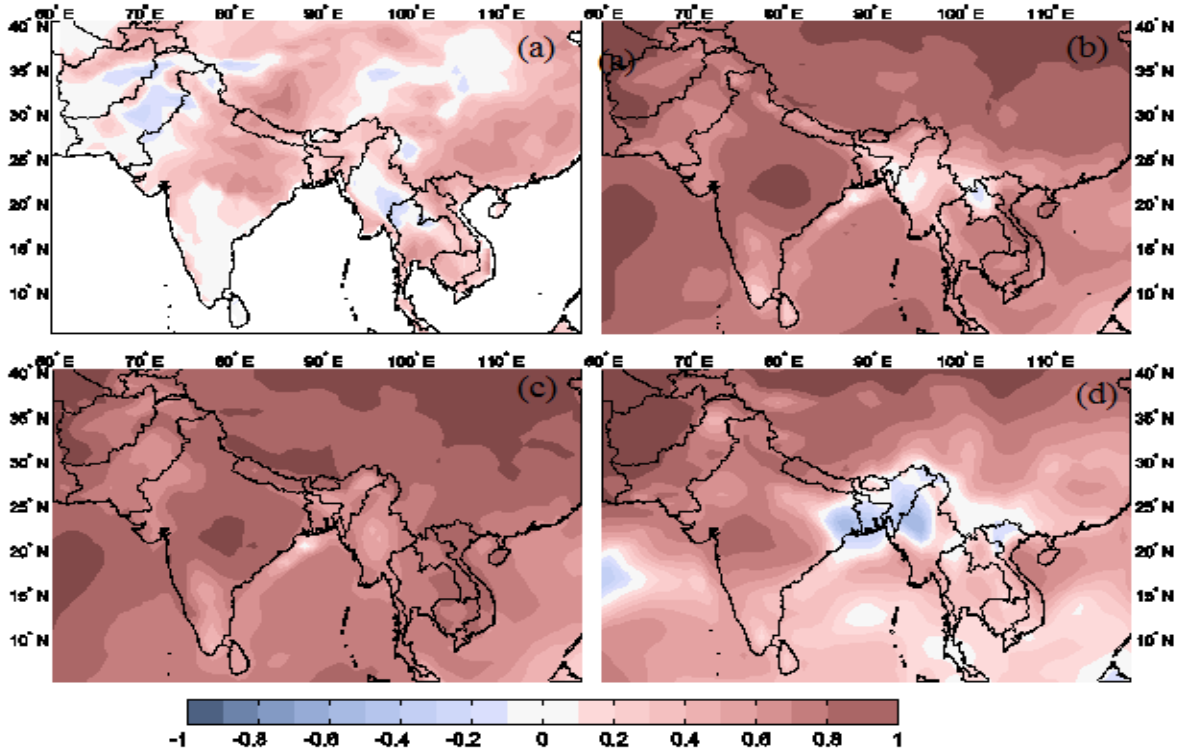

Fig. I.7 Spatial correlation grid-by-grid for a one-month lead-time, from 1983-2010 JJAS for: (a) precipitation, (b) maximum temperature, (c) minimum temperature, and (d) solar radiation. The correlations were computed between the CFS v2 and APHRODITE for precipitation, and between the CFS v2 and the ERA-Interim for all other variables.

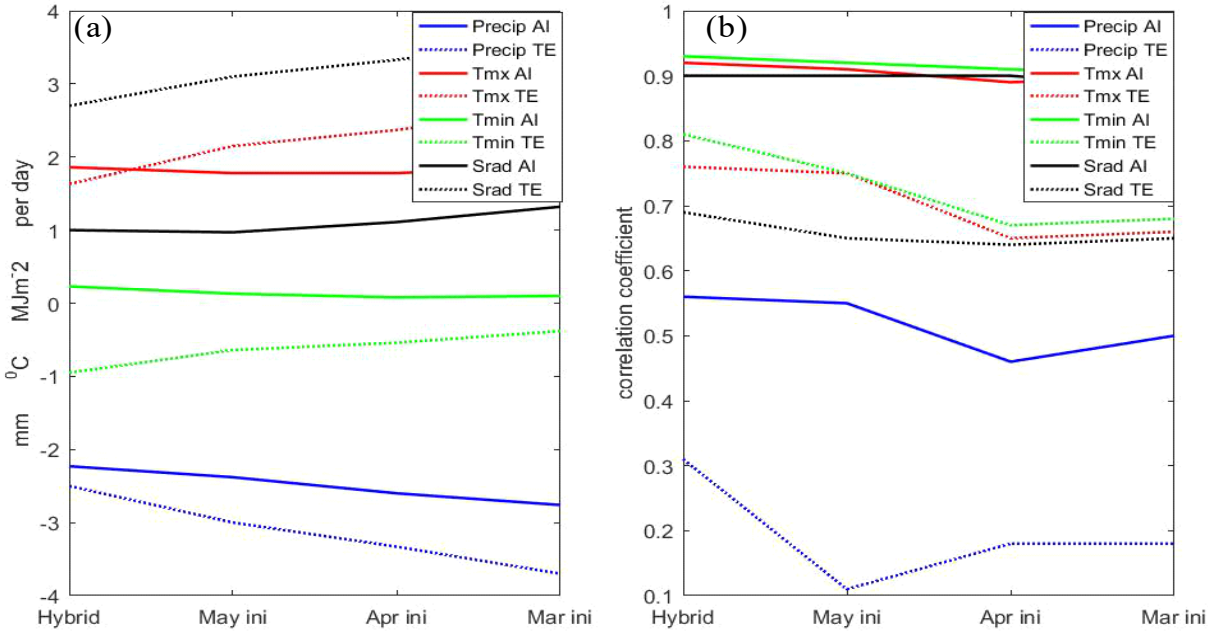

Fig. I.8 Effect of lead times on: (a) bias, and (b) correlation coefficient. Dashed lines are for Terai-East and solid lines are for AI domains.

The following sections evaluate the models (CMCC v1.5 and CFS v2) ability to capture key monsoon's circulation features. Capturing these feature is very important in order to accurately simulate the South Asian monsoon, although it does not guarantee accurate predictions at the grid-point level. Nonetheless, if models are able to capture these large scale circulation feature, prediction can be improved by statistical downscaling.

I.3.4 Movement of the Inter Tropical Convergence Zone (ITCZ)

The monsoon rainfall evolves as the ITCZ makes its seasonal movement from ocean toward the continents, due to seasonal variations in the latitude of maximum insolation. The GPCP observation data demonstrated that the maximum rainfall band (>10 mm/day) shifted to 25^0N in July (Fig. I.9a). However, both models limited that movement to 20^0N (Fig. I.9 b-c). As various other studies have described, this is a common problem found in most models (Rajeevan and Nanjundiah, 2009; Pokhrel Samir et al., 2013). Also unlike the observations, both models exhibited two ITCZs, with a second one positioned between the equator and 10^0S for the entire monsoon season.

I.3.5 Monsoon indices

Different monsoon indices have been used to examine the strength of the ISM including the Webster and Yang (WY) index (Webster and Yang, 1992) and the Goswami index (Goswami et al., 1999). If models are able to capture the strength of these indices accurately, it is highly likely that the skill of the model to predict precipitation at the grid point level can be increased through statistical downscaling.

The WY index is the shear of the zonal winds between 850 hPa and 200 hPa over the domain from 40^0E-110^0E/0^0N-20^0N, and it illustrates the monsoon's thermally driven nature. The index's high (low) value signifies strong (weak) monsoon circulation.

Similarly, the Goswami index measures the meridional wind shear between 850 hPa and 200 hPa over the domain from 70^0E-110^0E/0^0N-30^0N), and it is a good indicator of the Hadley circulation. The meridional wind shear is positive (negative) during the boreal summer (winter) season. The Goswami index is better related to the ISM's inter-annual variability.

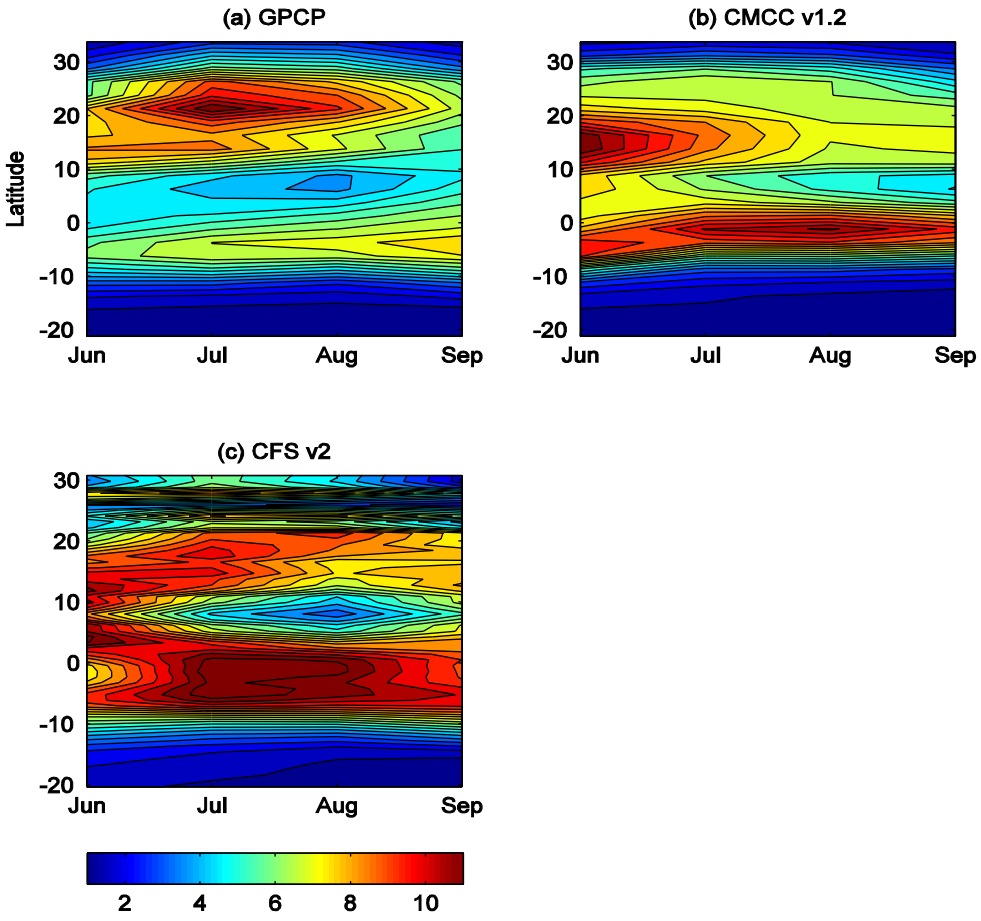

Fig. I.9: Seasonal (JJAS) movement of the maximum rainfall band (mm/day) for: (a) GPCP (observation), (b) the CMCC v1.5, and (c) the CFS v2 averaged for the 70^0E to 90^0E longitudes.

We calculated these indices for observations from the NCEP reanalysis data and for the CFS v2 data from 1982 to 2005. Although the CFS v2 simulated mean values for both the WY and Goswami indices were closer to observation, the correlation coefficient was only satisfactory (r=0.6) and significant at 1% level for the WY index (Fig. I.10, Table I.4-5). The simulated means for the WY and Goswami indices were close to the values found by Chaudhari et al. (2013). The correlation's significance was calculated using the student's t-distribution

Table I.4: Dynamic monsoon indices simulated by the CFS v2, as compared to observations.

Indices	**CFS v2**	**Observation**
WY index	24	24.9
Goswami index	1.9	3.2

Table I.5: Correlation coefficient the models' simulated monsoon indices and observations

Indices	r	p
WY index (CFS v2/NCEP)	0.6	0.001
Goswami index (CFS v2/NCEP)	0.2	0.289

I.3.6 Air-Sea interaction

The ISM is a coupled air-sea interaction phenomenon. The interaction between air and sea can be seen in the correlations between atmospheric variables (e.g. Precip) and oceanic variables (e.g. SST). Although various factors influence precipitation, it only occurs after a certain SST threshold has been crossed, for example, 27.5^0C in the tropical Indian Ocean (Gadgil et al., 2004). The correlation between the SST and rainfall suggests that changes in the SST lead to quick fluctuations in rainfall, thanks to surface evaporation and low-level moisture convergence (Wang et al., 2005).

Both the CMCC v1.5 and CFS v2 SPSs were able to capture the strong positive correlation over the tropical Pacific, although the bands were narrower for the CFS v2 and stronger for the CMCC v1.5 (Fig. I.11b-c). Neither of them could capture the strong negative correlation off the east coast of China, although the CMCC v1.5 replicated the negative correlation off the coast of the Philippines (Fig. I.11b-c). Unlike the observations, the CMCC v1.5 exhibited the positive correlation over the South China Sea (Fig. I.11b).

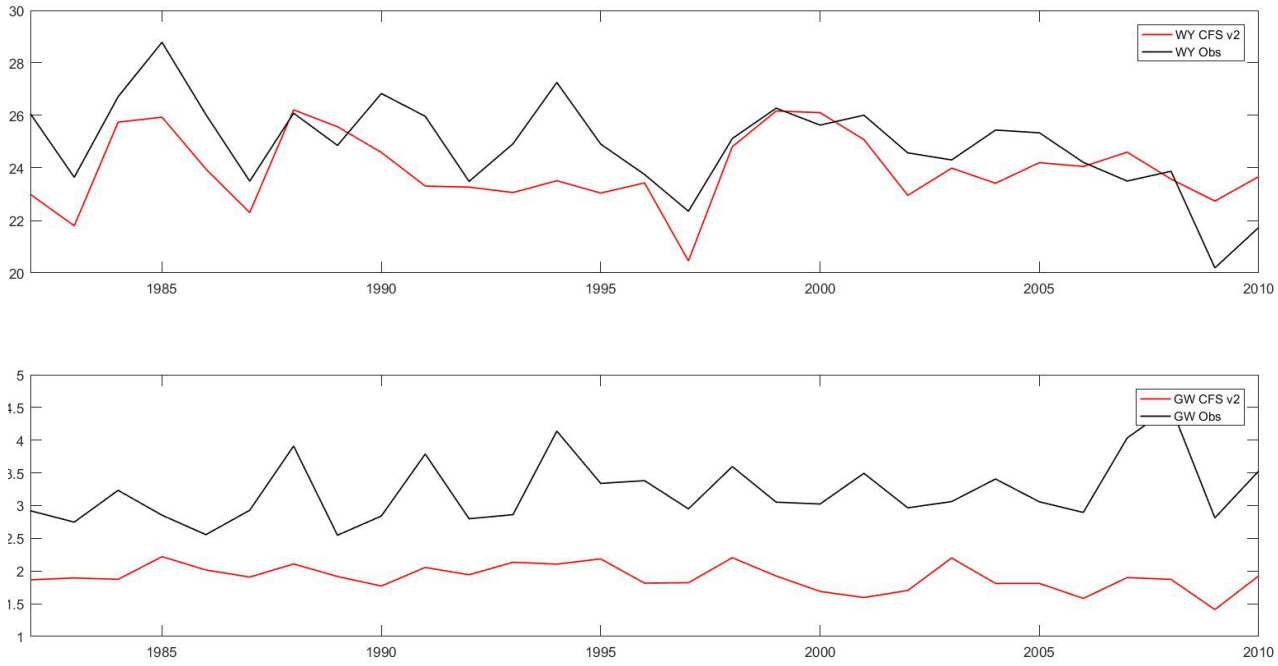

Fig. I.10 Interannual variation of monsoon indices: (a) Webster Yang index, (b) Goswami index in the models (CFS v2/CMCC v1.5) and observations (NCEP reanalysis). The data are from 1982 to 2010.

However, both the CMCC v1.5 and CFS v2 models were able to capture the positive correlation over the Maritime Continent (Fig. I.11b-c). However, patches of negative correlations over the Gulf of Thailand and the Celebes Sea were found for the CMCC v1.5, and the positive correlation was weaker in the CFS v2 (Fig. I.11b-c).

Observations demonstrated a weaker positive correlation over the Indian Ocean, except for few patches of negative correlation off the coast of India's southern tip and in the Northeast BOB (Fig. I.11a). Nonetheless, the CMCC v1.5 demonstrated a positive correlation everywhere over the Indian Ocean, and this correlation was weaker in the CFS v2.

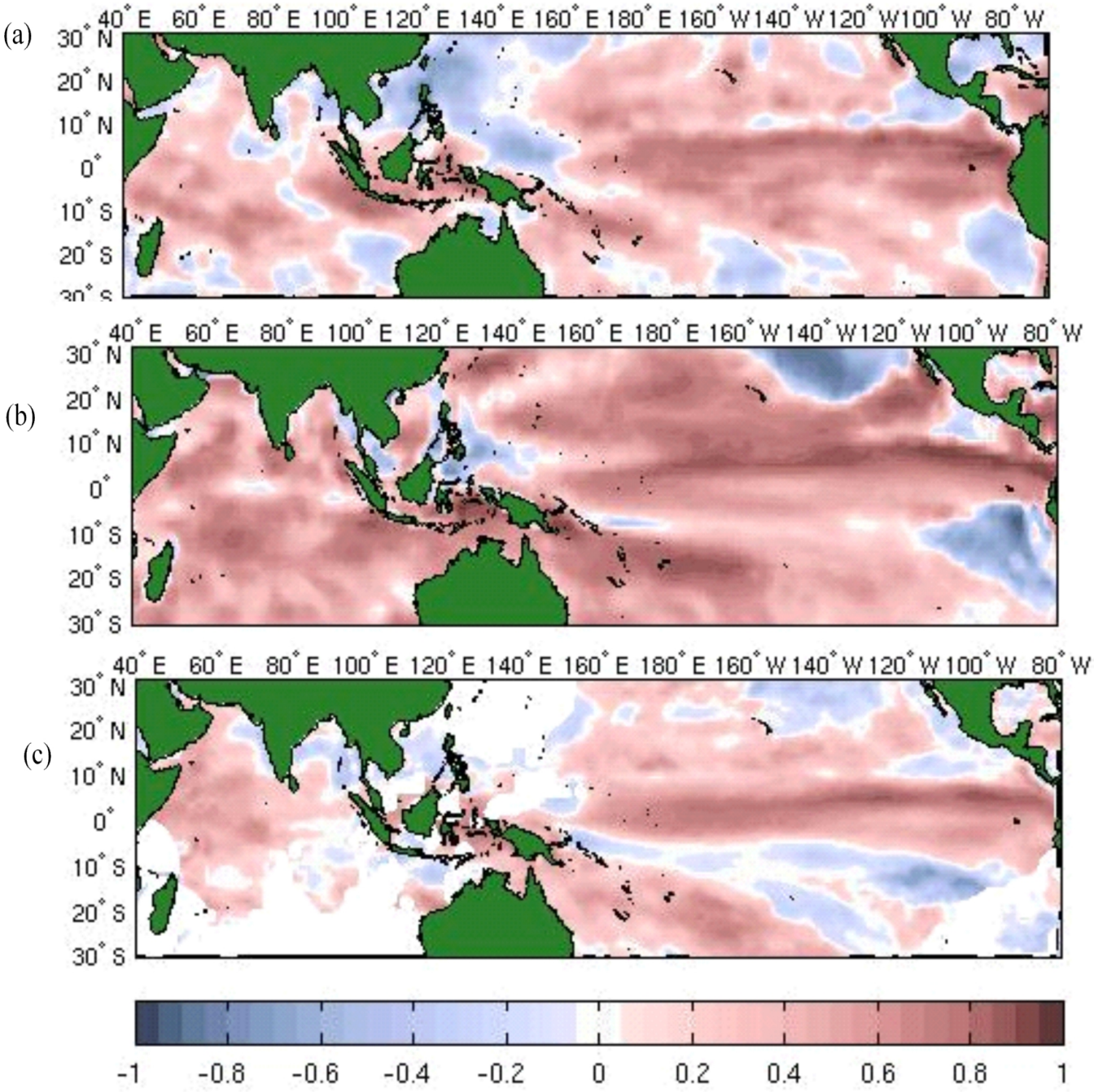

Fig. I.11 Correlation between JJAS averaged SST and rainfall (grid point correlation) for a) GPCP rainfall and Reynold's SST, b) CMCC v1.5 and c) CFS v2 for the period 1981-2005.

I.3.7 Monsoon teleconnections

I.3.7.1 ENSO

Many studies have clearly established the relationship between the interannual variation of the ISM and ENSO (Shukla, 1987; Rasmusson and Carpenter, 1983; Sikka, 1980). The ISM is negatively correlated with the ENSO. Thus the information on coming season's ENSO phase can be used to get indications on the coming season weather. Various studies have used ENSO condition's forecasts for agricultural applications (Jones et al., 2000; Fraisse et al., 2006; Asseng et al., 2012).

The correlation coefficients between the precipitation averages over the AI land-only domain simulated by the models and the Nino 3.4 SST were -0.61 and -0.46 for the CFS v2 and the CMCC v1.5, respectively, as compared to -0.46 for the GPCP (Table I.6). The correlation was significant at the 1% level for the CMCC v1.5 and the CFS v2, but only significant at the 5% level for the GPCP. Correlations' significant levels were calculated using the student's t-distribution for the 28 degree of freedom. For longer periods (1958-2004), the correlation coefficient between the ISM and ENSO was -0.5 and significant at the 1% level.

Table I.6: Correlation coefficient (r) between the AISMR and Nino 3.4 index, along with their significance values (p) for the models and observations

	r	p
CFS v2	-0.61	0.001
CMCC v1.5	-0.46	0.010
GPCP	-0.46	0.020

Regarding the large-scale spatial distribution of correlation coefficients, the CMCC v1.5 was more successful than was the CFS v2 at capturing the negative correlation between the Nino 3.4 SST and precipitation over CI. Moreover, the CFS v2 SPS displayed an excessive negative correlation for regions above 20^0N, and it underestimated the positive correlation in the Northeast and in the BOB (Fig. I.12a-c). However, for Nepal, the CFS v2 was closer to the observed data in predicting the relationship between the ENSO and the summer monsoon. The CFS v2 found a weak to non-existent relationship in the Eastern Terai and a negative relationship for other areas, including a strong, negative relationship in Western Nepal (correlation coefficients varying from -0.4 to -0.8). In contrast, the CMCC v1.5 showed unrealistic strong positive correlation for the Eastern Terai region including some bordering Indian regions.

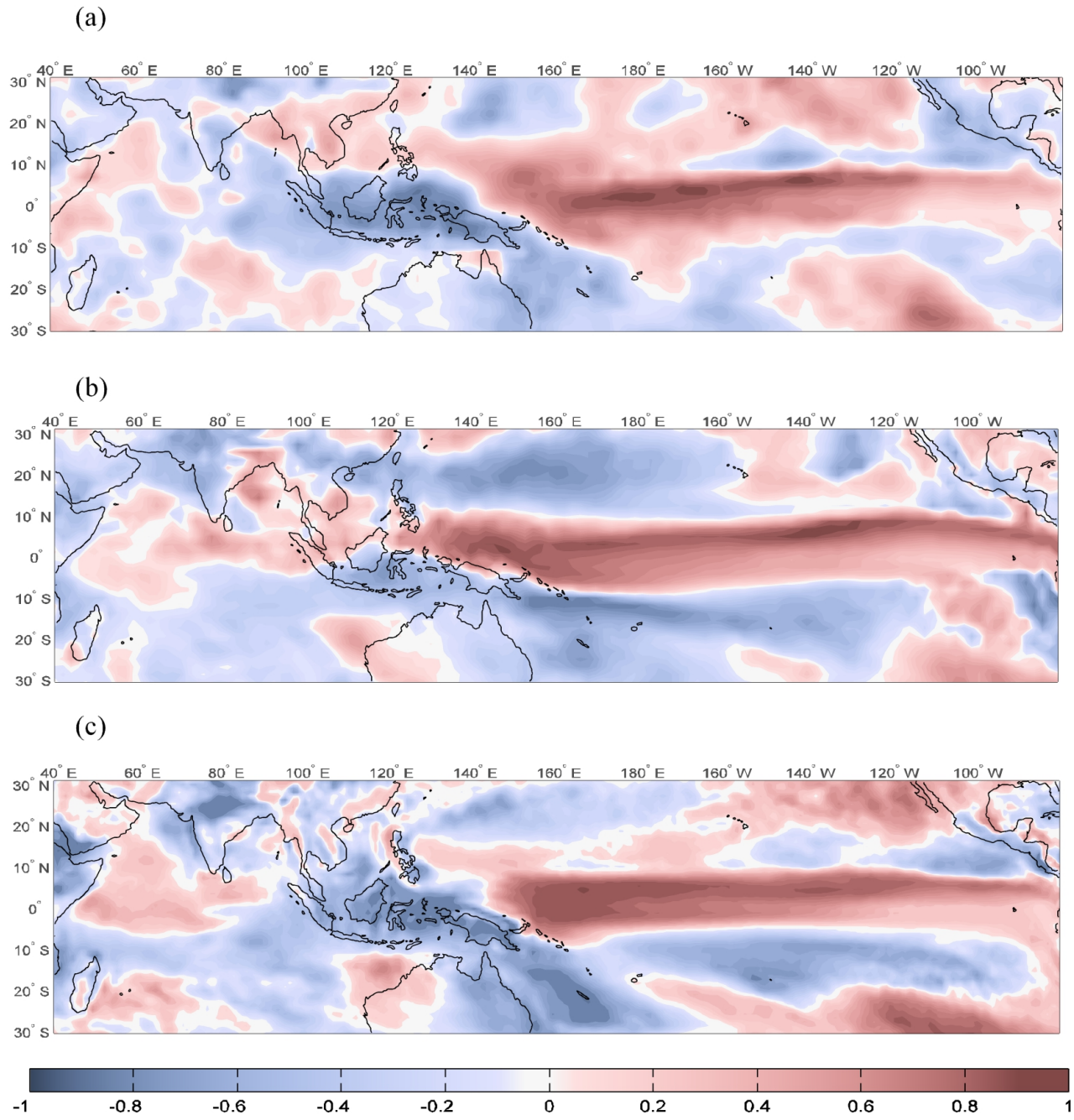

Fig. I.12 Mean seasonal (JJAS) one-point correlation between Nino 3.4 index and precipitation for a) GPCP, b) CMCC v1.5 and c) CFS v2 for the period 1982-2005.

However, ENSO only explains part of the interannual ISM variability, and other sources include: snow cover variations over Eurasia (Blanford, 1884), the North Atlantic Ocean circulation (Goswami et al., 2006), the IOD (Saji et al., 1999; Ashok et al., 2001) and internal dynamics (Krishnamurthy and Shukla, 2000; Cherchi and Navarra, 2003).

I.3.7.2 The IOD

The combined influence of ENSO and the IOD on the ISM's interannual variability has become important in recent decades (Ashok et al., 2001) which have seen a weakening of the ENSO-ISM relationship (Kumar et al., 1999). The IOD is a mode of climate variability, which occurs interannually in the Indian Ocean and is measured by the difference in seasonal (JJAS) SST anomalies between the western (50^0E-70^0E, 10^0S-10^0N) tropical Indian Ocean and the eastern (90^0E-110^0E, 10^0S-Equator) tropical Indian Ocean (Saji et al., 1999). Although the IOD alone does not have a significant correlation with the ISM's interannual variation, the combined effect of the IOD and ENSO on ISM is considerable. Ashok et al. (2001) found that whenever the ENSO-ISMR correlation is weak (strong), the IOD-ISMR correlation is stronger (weaker). Ashok and Saji (2007) and Ashok et al. (2004), used the atmospheric GCM and observation data to demonstrate that a positive IOD remarkably reduces ENSO's negative impact on ISMR, whenever the IOD and ENSO occur together with the same phase.

Both the CMCC v1.5 and CFS v2 models were able to capture the positive correlation between the IOD index and precipitation along the equatorial Pacific, as seen in observations (Fig. I.13a-c). However, the band was narrower in the CMCC v1.5, in which unrealistic patches of positive correlation prevailed over the eastern part of the Maritime Continent. The models also replicated the positive correlation in the western and central equatorial Indian Ocean, although the models unrealistically extended this correlation to the eastern part of that ocean. However, both SPSs failed to simulate the positive correlation in most of India's land regions.

Observations did not indicate a strong and significant correlation between the ISM and the IOD indices, although the relationship was relatively stronger and significant in the CMCC v1.5 (Table I.7). The significant levels were calculated using the student's t-distribution for the 23 degree of freedom.

Table I.7: Correlation between IOD index and ISM index for the months of JJAS from 1982 to 2005.

	r	p
CFS v2-IOD	-0.3	0.200
CMCC v1.5-IOD	0.6	0.001
GPCP-IOD	0.3	0.170
APHRODITE-IOD	0.4	0.080

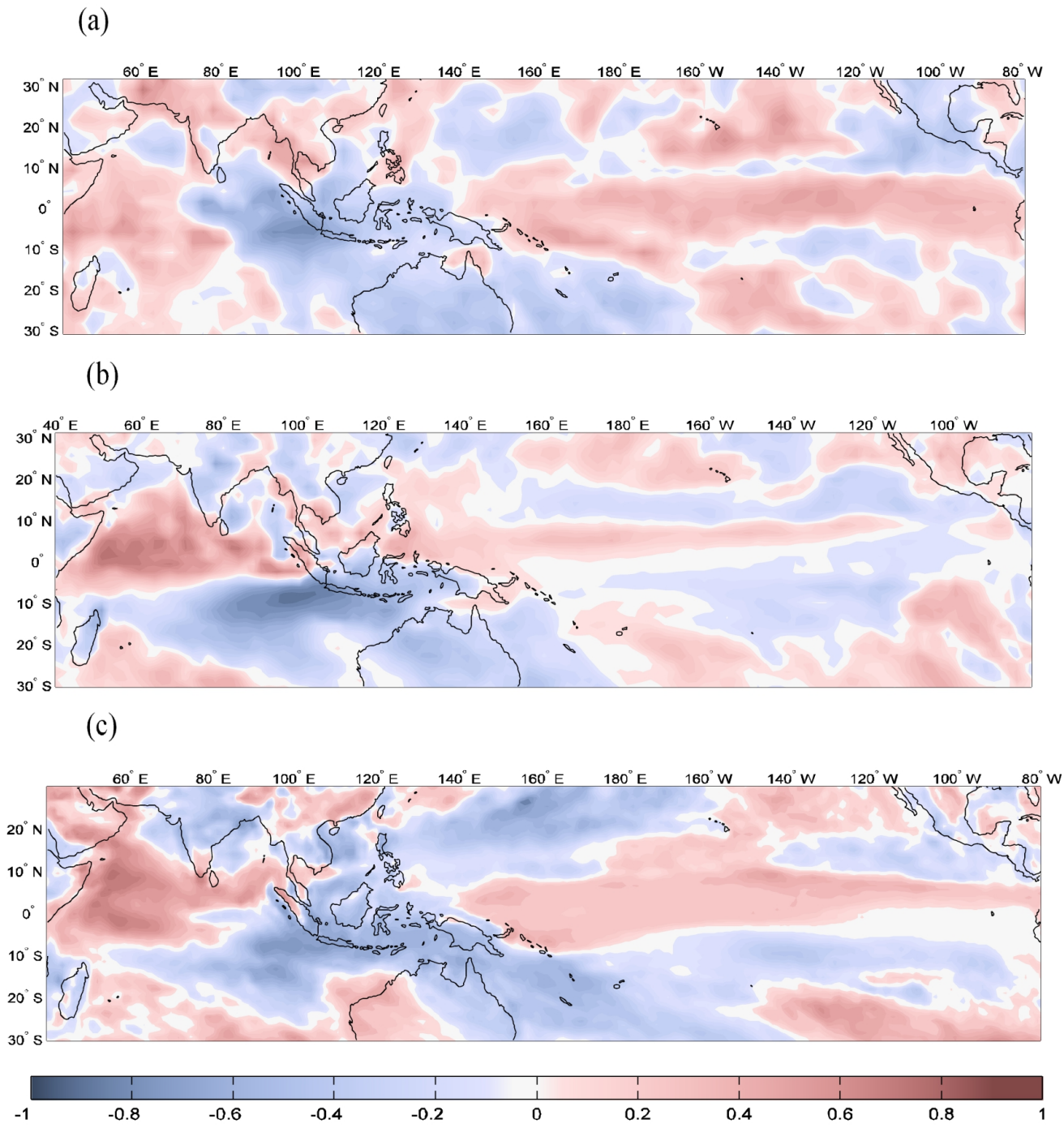

Fig. I.13 One-point correlation maps between the IOD index (difference between SST JJAS anomalies between the western and equatorial Indian Ocean) and seasonal (JJAS) mean precipitation at all other points for: (a) GPCP and Reynold's SST, (b) the CMCC v1.5, and (c) the CFS v2.

I.3.8 Monsoon onset and withdrawal

In this study, the monsoon onset and withdrawal dates refer to the monsoon's start and end dates over Kerala. These dates can be calculated using the Wang et al. (2009) index, which defined the monsoon onset as the date on which the 850 hPa zonal winds averaged over the southern Arabian Sea (40^0E - 80^0E, 5^0N - 15^0N) had sustained speed of 6.2 $m.s^{-1}$ for at least six consecutive days. The withdrawal date is the date on which this threshold is not met. The mean onset date simulated by the CMCC v1.5 was 11 days earlier than observed, and the model's mean withdrawal date was delayed by 15 days (Table I.8). Saha et al. (2014) found the mean onset date simulated by the CFS v2 was 4 days later than observed, and its withdrawal date was delayed by 12 days. They used the Wang et al. (2009) to calculate the onset date, while the withdrawal date was computed using the tropospheric temperature gradient (Xavier et al., 2007).

The CMCC v1.5 provided a longer duration for the monsoon, as compared to the NCEP. Furthermore, the CMCC v1.5 and NCEP's onset/withdrawal dates were not closely related to each other, with a correlation coefficient of approximately 0.1 (Fig. I.14).

Table I.8: Monsoon onset and withdrawal dates for the NCEP, CFS v2, and CMCC v1.5, using the Wang index

	Mean onset (SD)	Mean withdrawal (SD)	Source
NCEP	May 31 (3.9)	September 14 (8.7)	This study
CMCC v1.5	May 20 (7.7)	September 29 (5.4)	This study
CFS v2	June 5 (9.78)	September 26 (9.9)	Saha et al. (2013)

I.3.9 Wind Circulation-Low level

The low-level (850 hPa) monsoon circulation consists of the Flindlater Jet connecting the Mascarene High with the Monsoon trough over India, forming the lower branch of the Hadley cell (Flindlater, 1969). The CMCC v1.5 correctly simulated both the magnitude and direction of the Flindlater Jet, as seen in the NCEP reanalysis, although the model overestimated its intensity between the regions of 0^0N-10^0N and 40^0E-90^0E (Fig. I.15a-c). This overestimation of the cross-equatorial flow was related to the CMCC v1.5 model's wet rainfall bias over CI. Saha et al. (2014) also found the CFS v2 simulated Flindlater jet closer, in both magnitude and direction, to the NCEP-II and ERA-Interim reanalyses than the CFS v1.

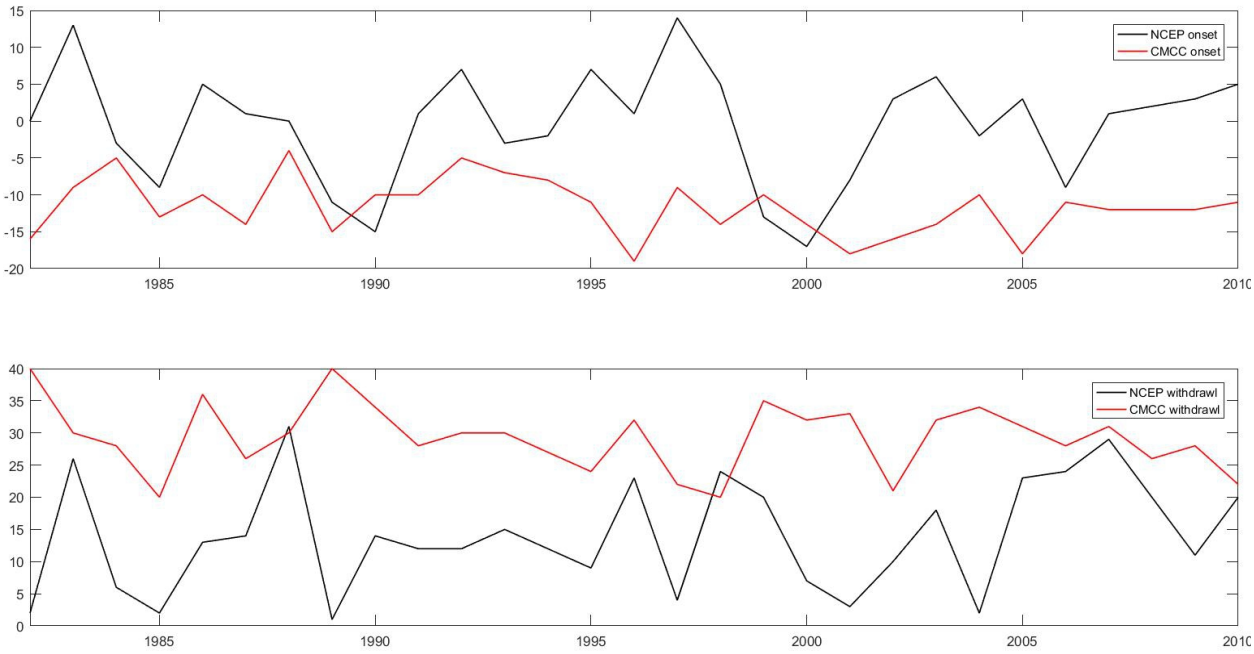

Fig. I.14 Monsoon onset and withdrawal dates for model (CMCC v1.5) and observations (NCEP), calculated using Wang et al. (2009) index, from 1982 to 2010 for: (a) onset and (b) withdrawal. Onset and withdrawal dates were calculated using June 1 as '0' for the onset date and September 1 as '1' for the withdrawal date.

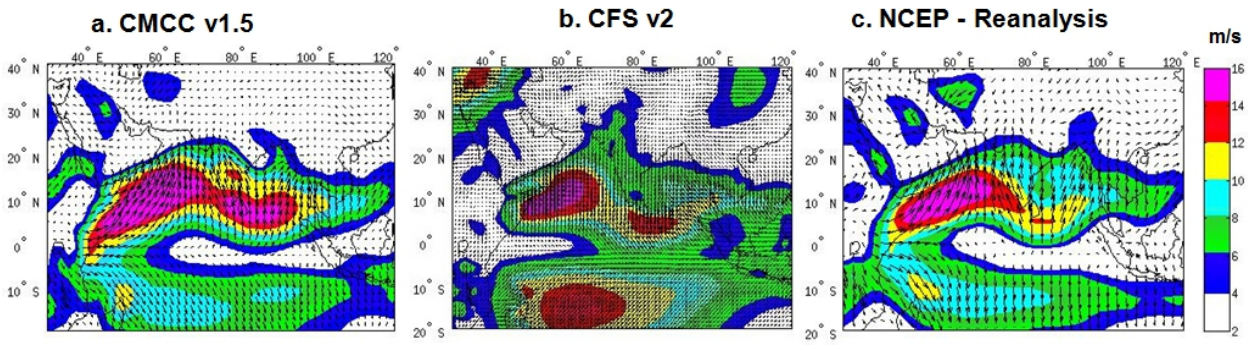

Fig. I.15 Seasonal (JJAS) average climatological mean winds at 850 hPa (in m/s) for: (a) the CMCC v1.5, (b) the CFS v2, and (c) the NCEP reanalysis. The shaded colouring represents the magnitude, and the arrows represent the direction.

I.4 Conclusions

In this part of our study we evaluated the ability of the CFS v2 and CMCC v1.5 models to predict Precip, T_{min}, T_{max}, and S_{rad}, with a focus on Nepal's Terai region. This was done by comparing model hindcasts to observed data. In the case of precipitation, the study found that both models have moderate skill over the AI domain. Both models underestimated precipitation's daily climatology as well as seasonal mean and neither of them were able to simulate the monsoon peak. However, for the TE domain, the CMCC v1.5 did not have satisfactory ability to predict precipitation, as shown by the low correlation skill, the high RMSE and mean and CV not closer to the observation. At a grid point resolution, however, even the CFS v2 had problems in capturing the distribution of precipitation. For agricultural applications distribution of precipitation is more important than the total amount (Baigorria et al., 2007). The good news is that the observed daily climatology of precipitation is included within the ensemble spread of CFS v2. Therefore, there is a possibility of improving prediction skill using all ensemble members.

In terms of teleconnections, both the CMCC v1.5 and the CFS v2 captured the large-scale negative correlation between the Nino 3.4 index and summer monsoon rainfall over the Indian region but the CMCC v1.5 displayed unrealistic positive correlations for the Terai East and its bordering Indian regions. Nonetheless, both models failed to capture the positive correlation between the IOD and ISMR. The CMCC v1.5 SPS simulated an early onset and late withdrawal for the monsoon, and thus overestimated its duration. Both models correctly replicated the low-level cross equatorial Flindlater Jet, while slightly overestimating its magnitude. The CFS v2 model's simulated mean values for both the WY and Goswami indices were closer to observation, but only the correlation coefficient for the WY index was satisfactory. On the basis of the above analysis, it can be concluded that neither the CMCC v1.5 model nor the CFS v2

model are able to predict precipitation precisely for the grid points in the TE region. As the CFS v2 was more successful in capturing the general circulation features, another possibility for improving precipitation prediction skill is through statistical downscaling.

In contrast, the CFS v2 was quite skilled at predicting T_{max}, T_{min}, and S_{rad} considering the ERA-Interim reanalysis as observations. The CFS v2 was warmer and drier than the ERA-Interim, and it overestimated S_{rad} for both the AI and TE domains. However, at a grid point resolution in the TE, the CFS v2's T_{max} and T_{min} daily climatology, from the Hybrid-one-month-lead time forecasts, had a large systematic negative bias of up to -6^0C and -7^0C compared to the observed data from the weather station. Even the ERA-Interim's T_{max} and T_{min} daily climatology experienced a negative bias of up to -6^0C and -3^0C compared to the weather station data. Hindcasts from the nearest initialization months reduced biases, except for T_{min} in the TE region. Unlike the bias, the correlation skill remained unchanged, regardless of the lead-time, for the AI domain. For the TE domain, however, the correlation increased as the lead time of initialization decreased. Considering the sensitivity of the dynamic crop models to temperature change, the systematic bias in CFS v2's T_{max} and T_{min} daily forecasts needs to be corrected before using them in the crop models.

Based on the above analysis, it can be concluded that the SPSs' potential use for agricultural applications is limited by their skill. In order to exactly understand to what extent these biases are translated into crop growth and yield prediction a separate study is needed.

References

ADLER, R. F., HUFFMAN, G. J., CHANG, A., FERRARO, R., XIE, P.-P., JANOWIAK, J., RUDOLF, B., SCHNEIDER, U., CURTIS, S., BOLVIN, D., GRUBER, A., SUSSKIND, J., ARKIN, P. & NELKIN, E. 2003. The Version-2 Global Precipitation Climatology Project (GPCP) Monthly Precipitation Analysis (1979–Present). Journal of Hydrometeorology, 4, 1147-1167.

ALESSANDRI, A., GUALDI, S., POLCHER, J. & NAVARRA, A. 2007. Effects of land surfacevegetation on the boreal summer surface climate of a GCM. Journal of Climate, 20, 255-277.

ANNAMALAI, H., HAMILTON, K. & SPERBER, K. R. 2007. The South Asian Summer Monsoon and Its Relationship with ENSO in the IPCC AR4 Simulations. Journal of Climate, 20, 1071-1092.

ASHOK, K., GUAN, Z. Y., SAJI, N. H. & YAMAGATA, T. 2004. Individual and combined influences of ENSO and the Inidan Ocean Dipole on the Indian summer monsoon. Journal of Climate, 17, 3141-3155.

ASHOK, K., GUAN, Z. Y. & YAMAGATA, T. 2001. Impact of the Indian Ocean Dipole on the relationship between the Indian monsoon rainfall and ENSO. Geophysical Research Letters, 28, 4499-4502.

ASHOK, K. & SAJI, N. H. 2007. On the impacts of ENSO and Indian Ocean dipole events on the sub-regional Indian summer monsoon rainfall. Nat Hazzards, 42, 273-285.

ASSENG, S., MCINTOSH, P. C., WANG, G. & KHIMASHIA, N. 2012. Optimal N fertiliser management based on a seasonal forecast. European Journal of Agronomy, 38, 66-73.

BAIGORRIA, G. A., JONES, J. W., SHIN, D., MISHRA, A. & BRIEN, J. J. 2007. Assessing uncertainties in crop model simulations using daily bias-corrected Regional Circulation Model outputs. Climate Research, 34, 211-222.

BELLUCCI, A., MASINA, S., DI PIETRO, P. & NAVARRA, A. 2007. Using temperature–salinity relations in a global ocean implementation of multivariate data assimilation scheme. Monthly Weather Review, 135, 3785–3807.

BERRISFORD, P., DEE, D., FIELDING, K., FUENTES, M., KALLBERG, P., KOBAYASHI, S. & UPPALA, S. 2009. The ERAInterim archive. Tech. Rep. ERA Rep. Series 1. ECMWF.

BLANFORD, H. 1884. On the connection of Himalayan snowfall and seasons of drought in India Proc R Soc Lond, 37, 3-22.

BORRELLI, A., MATERIA, S., BELLUCCI, A., ALESSANDRI, A. & GUALDI, S. 2012. Seasonal Prediction System at CMCC. Research Papers Issue RP0147.

CHAUDHARI, H., POKHREL, S., MOHANTY, S. & SAHA, S. 2013. Seasonal prediction of Indian summer monsoon in NCEP coupled and uncoupled model. Theoretical and Applied Climatology, 114, 459-477.

CHERCHI, A. & NAVARRA, A. 2003. Reproducibility and predictability of the Asian summer monsoon in the ECHAM4-GCM. Climate Dynamics, 20, 365-379.

CLOUGH, S. A., SHEPHARD, M. W., MLAWER, E. J., DELAMERE, J. S., IACONO, M. J., CADY-PEREIRA, K., BOUKABARA, S. & BROWN, P. D. 2005. Atmospheric radiative transfer modeling: a summary of the AER codes. Journal of Quantitative Spectroscopy and Radiative Transfer, 91, 233-244.

DEE, D. P., UPPALA, S. M., SIMMONS, A. J., BERRISFORD, P., POLI, P., KOBAYASHI, S., ANDRAE, U., BALMASEDA, M. A., BALSAMO, G., BAUER, P., BECHTOLD, P., BELJAARS, A. C. M., VAN DE BERG, L., BIDLOT, J., BORMANN, N., DELSOL, C., DRAGANI, R., FUENTES, M., GEER, A. J., HAIMBERGER, L., HEALY, S. B., HERSBACH, H., HÓLM, E. V., ISAKSEN, L., KÅLLBERG, P., KÖHLER, M., MATRICARDI, M., MCNALLY, A. P., MONGE-SANZ, B. M., MORCRETTE, J. J., PARK, B. K., PEUBEY, C.,

DE ROSNAY, P., TAVOLATO, C., THÉPAUT, J. N. & VITART, F. 2011. The ERA-Interim reanalysis: configuration and performance of the data assimilation system. Quarterly Journal of the Royal Meteorological Society, 137, 553-597.

DELSOLE, T. & SHUKLA, J. 2010. Model Fidelity versus Skill in Seasonal Forecasting. Journal of Climate, 23, 4794-4806.

DI PIETRO, P. & MASINA, S. 2009. The CMCC INGV global ocean data assimilation system (CIGODAS). Tech. Rep. RP0071. Bologna: Centro EuroMediterraneoper i Cambiamenti Climatici.

EK, M. B., MITCHELL, K. E., LIN, Y., ROGERS, E., GRUNMANN, P., KOREN, V., GAYNO, G. & TARPLEY, J. D. 2003. Implementation of Noah land surface model advances in the National Centers for Environmental Prediction operational mesoscale Eta model. Journal of Geophysical Research: Atmospheres, 108, n/a-n/a.

FLINDLATER, J. 1969. A major low-level air current near the Indian Ocean during the northern summer. Quart. J. Roy. Meteor. Soc., 95, 362-380.

FRAISSE, C. W., BREUER, N. E., ZIERDEN, D., BELLOW, J. G., PAZ, J., CABRERA, V. E., GARCIA Y GARCIA, A., INGRAM, K. T., HATCH, U., HOOGENBOOM, G., JONES, J. W. & O'BRIEN, J. J. 2006. AgClimate: A climate forecast information system for agricultural risk management in the southeastern USA. Computers and Electronics in Agriculture, 53, 13-27.

GADGIL, S., VINAYACHANDRAN, P. N., FRANCIS, P. A. & GADGIL, S. 2004. Extremes of the Indian summer monsoon rainfall, ENSO and equatorial Indian Ocean oscillation. Geophysical Research Letters, 31, L12213.

GOSWAMI, B. N., KRISHNAMURTHY, V. & ANNMALAI, H. 1999. A broad-scale circulation index for the interannual variability of the Indian summer monsoon. Quarterly Journal of the Royal Meteorological Society, 125, 611-633.

GOSWAMI, B. N., MADHUSOODANAN, M. S., NEEMA, C. P. & SINGUPTA, D. 2006. A physical mechanism for North Atlantic SST influence on the Indian Summer Monsoon. Geophysical Research Letters, 33.

GRIFFIES, S. M., HARRISON, M. J., PACANOWSKI, R. C. & ROSATI, A. 2004. Technical guide to MOM4. GFDL Ocean Group Technical Report 5. NOAA/Geophysical Fluid Dynamics Laboratory.

HANSEN, J. W. 2002. Realizing the potential benefits of climate prediction to agriculture: Issues, approaches , challenges. Agricultural System, 74, 309-330.

IACONO, M. J., MLAWER, E. J., CLOUGH, S. A. & MORCRETTE, J.-J. 2000. Impact of an improved longwave radiation model, RRTM, on the energy budget and thermodynamic properties of the

NCAR community climate model, CCM3. Journal of Geophysical Research: Atmospheres, 105, 14873-14890.

IRRI 2009. World Rice Statistics 2009 derived from FAO 2004-2006 Database - three years' average. International Rice Research Institute. Los Banos, Laguna, Phillipines.

IRRI 2010. Household survey data for Nepal collected under IFAD upland rice and STRASA (Stress tolerant rice for poor farmers in Africa and South Asia) projects. Social Sciences Division, International Rice Research Institute, Los Banos, Phillipines.

JIANG, X., YANG, S., LI, Y., KUMAR, A., LIU, X., ZUO, Z. & JHA, B. 2012. Seasonal-to-Interannual Prediction of the Asian Summer Monsoon in the NCEP Climate Forecast System Version 2. Journal of Climate, 26, 3708-3727.

JONES, J. W., HANSEN, J. W., ROYCE, F. S. & MESSINA, C. D. 2000. Potential benefits of climate forecasting to agriculture. Agriculture, Ecosystems & Environment, 82, 169-184.

KIM, Y.-J. & ARAKAWA, A. 1995. Improvement of Orographic Gravity Wave Parameterization Using a Mesoscale Gravity Wave Model. Journal of the atmospheric sciences, 52, 1875-1902.

KRIPALANI, R. H., OH, J. H., KULKARNI, A., SABADE, S. S. & CHAUDHARI, H. S. 2007. South Asian summer monsoon precipitation variability: Coupled climate model simulations and projections under IPCC AR4. Theoretical and Applied Climatology, 90, 133-159.

KRISHNAMURTHY, V. & SHUKLA, J. 2000. Intraseasonal and interannual variability of rainfall over India. Journal of Climate, 13, 4366-4377.

KRISHNAMURTHY, V. & SHUKLA, J. 2001. Observed and model simulated interannual variability of the Indian monsoon. Mausam, 52, 133–150.

KULKARNI, A., PATWARDHAN, S., KUMAR, K. K., ASHOK, K. & KRISHNAN, R. 2013. Projected Climate Change in the Hindu Kush–Himalayan Region By Using the High-resolution Regional Climate Model PRECIS. Mountain Research and Development, 33, 142-151.

KUMAR, K. K., RAJAGOPALAN, B. & CANE, M. A. 1999. On the Weakening Relationship Between the Indian Monsoon and ENSO. Science, 284, 2156-2159.

LOTT, F. & MILLER, M. 1997. A new sub grid scale orographic drag parameterization: its performance and testing. Quarterly Journal of the Royal Meteorological Society, 123, 101-127.

MADEC, G., DELECLUSE, P., IMBARD, M. & LEVY, C. 1998. OPA version 8.1 ocean general circulation model reference manual. Tech. Note 11. LODYC/IPSL.

MARAHATTA, S., DONGOL, B. S. & GURUNG, G. B. 2009. Temporal and spatial variablity of climate change over Nepal (1976-2005). Kathmandu: Practical Action Nepal Office.

MOAC 2008. Statistical informaton on Nepalese Agriculture, 2008/09, Government of Nepal, Ministry of Agricultural Development, Agribusiness Promotion and Statistics Division, Singh Durbar, Kathmandu,Nepal.

MOORTHI, S., PAN, H. & CAPLAN, P. 2001. Changes to the 2001 NCEP operational MRF/AVN global analysis/forecast system. NWS Technical Procedures Bulletin. NCEP.

MOPE 2004. Initial National Communication to the Conference of Parties of the United Nations Framework Convention on Climate Change. In: MINISTRY OF POPULATION AND ENVIRONMENT, G. O. N. (ed.). Kathmandu.

POKHREL SAMIR, DHAKATE, A., CHAUDHARI, H. S. & SAHA, S. K. 2013. Status of NCEP CFS vis-a-vis IPCC AR4 models for the simulation of Indian summer monsoon. Theor. Appl Climatol, 11, 65-78.

RAJEEVAN, M. & NANJUNDIAH, R. S. 2009. Coupled model simulations of twentieth century climate of the Indian summer monsoon. Curr Sci, 537–567.

RASMUSSON, E. M. & CARPENTER, T. H. 1983. The relationship between eastern equatorial Pacific sea surface temperatures and rainfall over India and Sri lanka. Mon. Wea. Rev, 111, 517-528.

REYNOLDS, R. W. & SMITH, T. M. 1994. Improved Global Sea Surface Temperature Analyses Using Optimum Interpolation. Journal of Climate, 7, 929-948.

ROECKNER, E., ARPE, K., BENGTSSON, L., CHRISTOPH, M., CLAUSSEN, M., D¨UMENIL, L., ESCH, E., GIORGETTA, M., SCHLESE, U. & SCHULZWEIDA, U. 1996. The atmospheric general circulation model ECHAM4:Model description and simulation of present day climate. Tech. Rep. 218. MaxPlanckInstitut fur Meteorologie.

ROECKNER, E., AUML, G. B., BONAVENTURA, L., BROKOPF, R., ESCH, M., GIORGETTA, M., HAGEMANN, S., KIRCHNER, I., KORNBLUEH, L., MANZINI, E., RHODIN, A., SCHLESE, U., SCHULZWEIDA, U. & TOMPKINS, A. 2003. The atmospheric general circulation model ECHAM5. Part I: Model description. Rep.No. 349. Hamburg, Germany: MaxPlanckInstitut fur Meteorologie.

ROECKNER, E., BROKOPF, R., ESCH, M., GIORGETTA, M., HAGEMANN, S., KORNBLUEH, L., MANZINI, E., SCHLESE, U. & SCHULZWEIDA, U. 2006. Sensitivity of Simulated Climate to Horizontal and Vertical Resolution in the ECHAM5 Atmosphere Model. Journal of Climate, 19, 3771-3791.

SAHA, S., MOORTHI, S., PAN, H.-L., WU, X., WANG, J., NADIGA, S., TRIPP, P., KISTLER, R., WOOLLEN, J., BEHRINGER, D., LIU, H., STOKES, D., GRUMBINE, R., GAYNO, G., WANG, J., HOU, Y.-T., CHUANG, H.-Y., JUANG, H.-M. H., SELA, J., IREDELL, M., TREADON, R., KLEIST, D., VAN DELST, P., KEYSER, D., DERBER, J., EK, M., MENG, J.,

WEI, H., YANG, R., LORD, S., VAN DEN DOOL, H., KUMAR, A., WANG, W., LONG, C., CHELLIAH, M., XUE, Y., HUANG, B., SCHEMM, J.-K., EBISUZAKI, W., LIN, R., XIE, P., CHEN, M., ZHOU, S., HIGGINS, W., ZOU, C.-Z., LIU, Q., CHEN, Y., HAN, Y., CUCURULL, L., REYNOLDS, R. W., RUTLEDGE, G. & GOLDBERG, M. 2010. The NCEP Climate Forecast System Reanalysis. Bulletin of the American Meteorological Society, 91, 1015-1057.

SAHA, S. K., POKHREL, S., CHAUDHARI, H. S., DHAKATE, A., SHEWALE, S., SABEERALI, C. T., SALUNKE, K., HAZRA, A., MAHAPATRA, S. & RAO, A. S. 2014. Improved simulation of Indian summer monsoon in latest NCEP climate forecast system free run. International Journal of Climatology, 34, 1628-1641.

SAJI, N. H., GOSWAMI, B. N., VINAYACHANDRAN, P. N. & YAMAGATA, T. 1999. A dipole mode in the tropical Indian Ocean. Nature, 401, 360-363.

SHAH, R. & MISHRA, V. 2014. Evaluation of the Reanalysis Products for the Monsoon Season Droughts in India. Journal of Hydrometeorology, 15, 1575-1591.

SHUKLA, J. 1987. Interannual variability of monsoons. In: FEIN, J. S. & STEPHENS, P. L. (eds.) Monsoons. Wiley and Sons.

SIKKA, D. R. 1980. Some aspects of the large scale fluctuations of summer monsoon rainfall over India in relation to fluctuations in the planetary and regional scale circulation parameters. Earth and Planetary Sciences, 89, 179-195.

SPERBER, K. R., ANNAMALAI, H., KANG, I. S., KITOH, A., MOISE, A., TURNER, A., WANG, B. & ZHOU, T. 2013. The Asian summer monsoon: an intercomparison of CMIP5 vs. CMIP3 simulations of the late 20th century. Climate Dynamics, 41, 2711-2744.

THORNE, P. W. & VOSE, R. S. 2010. Reanalyses Suitable for Characterizing Long-Term Trends. Bulletin of the American Meteorological Society, 91, 353-361.

TIMMERMANN, R., GOOSSE, H., MADEC, G., FICHEFET, T., ETHEB, C. & DULIERE, V. 2005. On the representation of high latitude processes in the ORCALIM global coupled sea ice ocean model. Technical Report 8, Ocean Modell.

VALKE, S., TERRAY, L. & PIACENTINI, A. 2000. The

OASIS coupled user guide version 2.4. Technical Report TR 0010. CERFACS.

VAN WART, J., GRASSINI, P. & CASSMAN, K. G. 2013. Impact of derived global weather data on simulated crop yields. Global Change Biology, 19, 3822-3834.

WANG, B., DING, Q., FU, X., KANG, I.-S., JIN, K., SHUKLA, J. & DOBLAS-REYES, F. 2005. Fundamental challenge in simulation and prediction of summer monsoon rainfall. Geophysical Research Letters, 32, L15711.

WANG, B., DING, Q. & JOSEPH, P. V. 2009. Objective Definition of the Indian Summer Monsoon Onset*. Journal of Climate, 22, 3303-3316.

WEBSTER, P. J. & YANG, S. 1992. Monsoon and Enso: Selectively Interactive Systems. Q.J.R. Meteorol. Soc, 118, 877-926.

WINTON, M. 2000. A Reformulated Three-Layer Sea Ice Model. Journal of Atmospheric and Oceanic Technology, 17, 525-531.

WU, X., SIMMONDS, I. & BUDD, W. F. 1997. Modeling of Antarctic Sea Ice in a General Circulation Model. Journal of Climate, 10, 593-609.

XAVIER, P. K., MARZIN, C. & GOSWAMI, B. N. 2007. An objective definition of the Indian summer monsoon season and a new perspective on the ENSO–monsoon relationship. Quarterly Journal of the Royal Meteorological Society, 133, 749-764.

YATAGAI, A., KAMIGUCHI, K., ARAKAWA, O., HAMADA, A., YASUTOMI, N. & KITOH, A. 2012. APHRODITE: Constructing a Long-Term Daily Gridded Precipitation Dataset for Asia Based on a Dense Network of Rain Gauges. Bulletin of the American Meteorological Society, 93, 1401-1415.

CHAPTER II: Using seasonal climate forecasts to predict rice yield over Nepal's Terai

Abstract

Skilful seasonal climate predictions paired with a dynamical crop model can assist with agricultural management and help farmers minimize risk. However, until now, the potential applicability of this approach have not been assessed. This study's goal was to link seasonal forecasts with the Decision Support System for Agrotechnology Transfer's (DSSAT) Cropping System Model (CSM) Crop Estimation through Resource and Environment Synthesis (CERES)-Rice crop model for predicting rice yields in Nepal's Terai. The predictive skill of the coupled forecast system model version 2 (CFS v2) hindcasts initialized at different lead times was examined against ERA-Interim reanalysis, weather station data and other observational data sets. Prior to running the hindcasts the CSM-CERES-Rice crop model was calibrated using the varietal trial data from the Hardinath station of the Nepal Agricultural Research Council and evaluated using the district yield data from the Ministry of Agriculture. Rice growth, development and yield, were simulated using weather station data, other observational datasets and daily hindcasts from CFSv2 at different lead times. The hindcasts simulation with the CSM-CERES-Rice model using station meteorological data shows that climatic variability, especially rainfall, can only explain a small part of the interannual variability of rice yield. This variability is further reduced when using the forecasts. The results from our study indicate that the potential application of seasonal climate forecasts to the dynamical crop model, in the particular case here considered, is limited by the skill of the seasonal forecasts. Before generalizing, further comparisons should be made, including a similar analysis for an area where quality meteorological and agricultural data are available and where the seasonal forecasts exhibit better skill.

Keywords: CFS v2, DSSAT, CSM-CERES-Rice, climate variability

II.1 Introduction

Crop yield prediction is an important component of the early warning system for the food security related planning (Thornton et al., 1997). It is also useful for trade, development policies and humanitarian assistance related to food security. Similarly, it helps farmers and/or decisions makers to prepare for the

crop growing season (Cabrera, 2009; Hansen, 2002). Moreover, it serves as an important indicator of the national income where agriculture contribution to gross domestic product (GDP) is high.

The crop yield for a given region and for a particular year or season can be predicted by estimating the area under a given crop and the yield per unit area. Carefully designed sampling techniques or aerial surveys can approximate the area under crop, as well as crop conditions. Yield can be predicted by establishing statistical relationships among yield per unit area, area under a given crop and crop conditions. All of these methods assume that weather conditions during the remainder of the growing season will be similar to those in previous years, which is not always the case. However, either statistical or dynamic models can estimate the following season's crop yield with a high degree of accuracy, if high-quality seasonal climate forecasts are available at the beginning of or during the cropping season.

These statistical models are based on the empirical relationship between the a region's final yield and mean weather variables, without taking physiological causalities into account (Thompson, 1969b; Thompson, 1969a). Statistical models have been used to determine the impact of increase in temperature on crop yield and to analyze the crop yield gap (Lobell et al., 2011; Lobell, 2013). In general, statistical models' results cannot be applied directly to other areas and time as the variations in factors affecting crop growth are not included in the population from which the models are derived.

Nonetheless, dynamic models are gradually replacing statistical models in agriculture due to the latter's many limitations (Abbaspour, 1992). Dynamic models are a mathematical representation of the plant growth and development process. Plant growth and development are determined by interactions among the soil, plant, atmosphere and management factors. Moreover, dynamic models are simulation models, as they involve a set of differential equations, calculate rate and produces output variables over time (Hoogenboom, 2000).

We are interested in predicting variability in crop yield associated with interanual variility in weather. Observation shows that the climate variability explains roughly a third of the crop yield variability globally (Ray, et al., 2015). Monsoon rainfall has been becoming more variable. Some studies have indicated that monsoon rainfall patterns have significantly changed in recent years, in terms of both magnitude and duration (Ramesh and Goswami, 2007; Goswami et al., 2006b). Extreme events, such as break periods or heavy rain events, have been increasing, while the total amount of rain has been declining. This trend has rendered rainfed cultivation areas more vulnerable to risks.

By inputting seasonal climate forecasts into a crop model at the beginning of the cropping season (or earlier), scientists can predict crop productivity for the coming season under different management options. Researchers are increasingly employing the dynamic cropping system model to study potential impact of interannual climatic variability and/or climate change on agriculture (Paz et al., 2007; Mikhail

and Francisco, 2007). The beauty of process-based crop models is that they can disentangle the effects of climate, soil and management on crop growth and productivity. Various types of seasonal forecasts have been used to predict yield.

One common approach to yield forecasting is on the basis of El Nino Southern Oscillation (ENSO) categories (Fraisse et al., 2006). Utilizing advance information on ENSO categories, scientists can predict the coming season's yield as the average of simulated yields for all years with similar ENSO phases. Using ENSO categories for yield prediction, however, have several limitations when applied to this study's area. First, ENSO's exact effect on weather is not clear for the study area. Shrestha et al. (2000) found a strong positive correlation between the All-Nepal monsoon precipitation and the Southern Oscillation Index (SOI) series but Ichiyanagi et al. (2007) found a weak positive correlation for the stations in western Nepal and negative correlation for the stations in eastern Terai. The SOI is measured by the Mean Sea Level Pressure difference between Tahiti and Darwin and is one of the most common indexes used to get an indication on the development and strength of ENSO events.

Secondly, the ENSO explains only a portion of variability (Goswami et al., 2006a; Blanford, 1884), and sometimes, other sources of variability compensate ENSO's effect. For example, effect of the strong El Nino in 1997 was, to a large extent, nullified by the Indian Ocean Dipole (IOD) (Saji et al., 1999; Gadgil et al., 2004; Ashok et al., 2001). Third, the relationship between ENSO and the Indian Summer Monsoon (ISM) is weakening in recent years (Kumar et al., 1999). Moreover, there is a mismatch in the life cycles of ENSO and the ISM. The rice-growing season extends from July to December, and monsoon season (JJAS) weather is crucial, as more than 80% of rainfall arrives during this time of year. However, ENSO's evolution does not exactly match the monsoon season. Rather, ENSO peaks in the cold season and dies during the spring or summer. Shrestha et al. (2000) found that the correlation coefficient between all-Nepal monsoon season precipitation and the SOI was higher with the SOI of the succeeding season (October-November) than the antecedent pre-monsoon (March-May) season. Therefore, it is difficult to predict whether the ENSO evolved during a particular year will be continued or dissipated away during the monsoon season.

Another common approach is to use seasonal climate forecasts from dynamic climate models. However, the mismatch in the dynamic climate models' and crop models' temporal and spatial scales present a challenge. Dynamic climate models' seasonal forecasts are issued in the form of a monthly or seasonal means or anomalies at a relatively low-resolution grid (approximately 100 km x 100 km in CFS v2), but crop models run on station-level daily data. To obtain daily data from these monthly or seasonal means or anomalies, Weather Generators (WG) have commonly been utilized. WGs generate daily data from the monthly or seasonal mean on the basis of the statistical methods using historical climatology (Dubrovský

et al., 2000). Ghosh et al. (2014) used statistical disaggregation to get daily data from seasonal means and to evaluate seasonal forecasts' performance by comparing simulated yields from the observed and forecasted weather.

For a WG, accurately generating precipitation (both occurrence and amount) is the most difficult task, especially for the tropical and sub-tropical regions (Schmidt et al., 1996; Jimoh and Webster, 1996). When using a dynamic crop model to simulate yield, the specific timing of dry spells is more essential rather than the total amount of rainfall (Baigorria et al., 2007). The crop yield is primarily affected by the stress caused by lack of soil-water.

In general, the process-based crop models can be categorized into three groups depending on the approach used for aboveground biomass (AGB) accumulation. The first category includes models which consider the net carbon accumulation as a balance between the carbon accumulation and consumption for growth and maintenance respiration. The SUCROS (Keulen and Wolf, 1986) is one example of this type of models. The requirement of large number of input variables and parameters makes this type of models difficult to use. The second category of crop models use the radiation-use-efficiency (RUE) approach to compute the AGB. The CERES group of models (Jones et al., 2003) and APSIM crop models (Keating et al., 2003) use this approach. The third category of crop models use the transpiration-use-efficiency approach (Tanner and Sinclair, 1983). One limitation of this approach is that the simulated yield becomes zero when the average saturated vapour pressure deficit is zero.

We utilized the CERES-Rice crop model from the DSSAT v4.6 (Hoogenboom et al., 2015), one of the most widely used models to forecast crop yields associated with climate variability and change (Bannayan et al., 2003; Soler et al., 2007; Pal et al., 2013; Shin et al., 2010). The DSSAT v4.6 includes 27 different process-based crop models, such as the CERES-Rice used in this study. The CERES-Rice model is used to simulate growth rate, duration and yield along with change in soil water, carbon and Nitrogen (Jones et al., 2003; Hoogenboom et al., 2012). The model's simulation processes are environment- and cultivar-specific, while the duration depends on the thermal environment and photoperiod. Various studies have used the CERES-Rice model in Nepal (Rai et al., 2011; Lamsal et al., 2013; Timsina and Humphreys, 2006), however none of these utilized seasonal forecasts for in-season yield prediction.

Using CERES-Maize and CROPGRO-Peanut crop models of DSSAT in the Southeast United States, Shin et al. (2010) compared how different types of seasonal forecasts affected simulated yields. They found that the downscaled global climate model data (statistical or dynamical) had greater predictive skill than the ENSO-based approach. However, they used an earlier model, the CFS v1 (Saha et al., 2006), which is relatively less skilful than the current version, the CFS v2, at predicting the ISM (Acharya et al.,

2014). Rainfall was the only variable taken from the CFS v1; temperature and solar radiation came from observed data. These dissimilar data sources might have led to physical inconsistency with other variables. Moreover, the impact of interannual weather variability on crop yield varies, not only across global regions, but also within individual countries. For example, rice yields in southern (non-southern) China are negatively (positively) affected during El Nino years (Iizumi et al., 2014).

We selected Nepal, because most (79%) of the rice production areas are still rainfed and 66% of the total rainfed areas are in the Terai (MOAC, 2008; IRRI, 2010; IRRI, 2009). Moreover, Nepal's Terai is the country's main rice cultivation area, covering 71% of the country's total rice area (MOAC, 2008). Furthermore, seasonal prediction systems (SPSs) have some skill to predict the monsoon over the South Asian region (Pokhrel Samir et al., 2013; Chaudhari et al., 2013).

We concentrated on the rice crop due to its economic significance in Nepal. Additionally, rice needs a considerable amount of water to grow. Rice is one of the most important staple foods for majority of Nepal's population. In Nepal, rice is cultivated on 1.53 million hectares (ha) of land, and annual production during 2011-2012 totalled 5.07 million tons (MOAD, 2012). Rice contributes to 23% of the country's agricultural GDP, and it comprises 52% of the total food grains produced in Nepal. Moreover, rice consumption meets half of the total calorie requirements of the Nepalese people (MOAD, 2012). Nearly two thirds (65.6%) of the country's total population is engaged in rice cultivation. Rice production needs high amounts of water as compared to other crops. On average, 2500 liters of water are required to produce one kilogram of rice (Bouman and Aureus, 2009).

Rainfed rice cultivation is entirely dependent on monsoon rain, and therefore is concentrated mostly during the monsoon season. Thus, rainfed rice production is subject to a high level of risk, due to the uncertainty posed by monsoon rain. These hazards include the late onset of the monsoon, droughts caused by breaks in the monsoon, and extremely heavy rainfall resulting in floods. This threats induce risk-averse farmers to adopt conservative strategies. As a result, the annual rice yield in Nepal is low (2.8 ton/ha) as compared to India (3.6 ton/ha), Bangladesh (4.4 ton/ha), Indonesia (5.2 ton/ha) and China (6.7 ton/ha) (FAOSTAT, 2015). Similarly, average fertilizer (N/P/K) application totals only 28.4 kg/ha in Nepal, as compared to 163.7 kg/ha in India, 278.6 kg/ha in Bangladesh, 194.8 kg/ha in Indonesia, and 647.6 kg/ha in China (WorldBank, 2015).

To our knowledge, this is the first study to predict rice yields using a dynamic climate model's daily forecasts as inputs for a dynamic crop model, particularly for Nepal. The findings of this study, therefore, could serve as a bench mark in a sense paving the way for using SPSs' seasonal forecasts daily input. The CFS v2's seasonal forecasts are able to accurately predict interannual variability of temperature maximums (T_{max}), temperature minimums (T_{min}), and solar radiations (S_{rad}), but they predict precipitation

relatively less precisely (Jha et al., 2016). We thus explored multiple approaches, all with the goal of improving yield predictions. First, we used all one-month-lead SF time series. Next, we employed a real-time simulation approach, in which we utilized observed weather data until the point of prediction, followed by the forecasts (one- or one-and-two month-lead time) supplemented with the historical climatology data for the remainder of the growing season.

Section II of this chapter describes the study area and weather data (including seasonal forecasts), the CERES-Rice model, the model data, and the calibration process. Section III describes and discusses the results, while the conclusion is in Section IV.

II.2 Methodology

II.2.1 Study area

The study area is centred on Hardinath station (26^0 48' N and 85^0 58' E) in Dhanusha district of Nepal's Terai. The Terai is comprised of flat lands in the south of Nepal, and it runs parallel to the foothills of the Himalayas. The Terai is a northern extension of the Indo-Gangetic plain, and its elevation ranges from 60 to 300 m. The Terai has tropical to subtropical climate and average daily temperature ranges from 7^0C to 24^0C in December/January and from 24^0C to 41^0C in June/July (Pariyar, 1998). The average annual rainfall ranges from 600 mm in the west to 1300 mm in the east (Pariyar, 1998). The average onset date of effective monsoon is the second week of June, and it ends in September. Alluvial soils are common, with old alluvial soils poor in nutrients more widespread than newer ones.

II.2.2 Daily meteorological data

The minimum weather variables required to run DSSAT are precipitation, T_{max}, T_{min} and S_{rad} on a daily basis (Jones et al., 2003). We focused on time series between 1983 to 2010, because of the availability of the CFS v2 hindcasts for that time period. We made use of different sources of weather data to explore their potential applicability. These sources included: weather station data, reanalysis data and CFS v2 forecasts.

II.2.2.1 Weather station data

The Department of Hydrology and Meteorology (DHM) Nepal's Janakpur Airport weather station is the closest (~7 km) weather station to the Hardinath agricultural research station. The weather variables incorporated from this weather station included daily T_{max}, T_{min}, and rainfall data for the period 1983 to

2010. For that periods, the weather station has less than 10% of missing data. However, the station did not have S_{rad} data for that period. Missing values were generated using the DSSAT Weatherman v4.6, while solar radiation was produced using the DSSAT Weatherman v4.6. conditioned on temperature. The Weatherman generated missing values from calculated mean and variances using the option fill short (<=7 days) with 10-day running mean. Although, it would be more accurate to use data from nearby stations, we did not find any weather stations nearby with complete data.

II.2.2.2 Reanalysis data

Along with the weather station data, ERA-Interim reanalysis (Dee et al., 2011) and APHRODITE data (Yatagai et al., 2012) were also used. For rainfall, the APHRODITE dataset was closer to observations in the South Asian region than was the ERA-Interim dataset. Therefore, we used APHRODITE rainfall values. The ERA Interim was available in 0.1^0 x 0.1^0 resolution, and APHRODITE was available in 0.25^0 x 0.25^0 resolution.

We used the reanalysis data for multiple reasons. First, it is difficult to obtain long-term weather station data for some regions in developing countries. Even when weather station data are available, the high number of missing values makes such data unusable. Finally, unlike weather station data, reanalysis data are easily available online, whilst some countries have strict policies on weather data sharing, and in some cases, the user must be physically present to submit an application for use and to pay. Chapter I contains a detailed assessment of the reanalysis weather data (T_{max}, T_{min}, S_{rad}, and precipitation) as compared to the weather station data. In brief, APHRODITE was drier and ERA-Interim was colder than the weather station data.

II.2.3 CFS v2 forecasts

Forecasts were taken from the CFS v2 SPS, which the NCEP made available (http://nomads.ncdc.noaa.gov/modeldata/cfs_reforecast_6-hourly_9mon_flxf). We selected the CFS v2 for its superior performance than the other General Circulation Models (GCMs) for the South Asia region, as reported by other studies (Pokhrel Samir et al., 2013). The CFS v2 consisted of a set of nine-month hindcasts initialized at five-day intervals, four times per day (00, 06, 12, and 18 UTC) from 1982 to 2010. Thus, there were 24 ensemble members per month, except in October and November, which each had only 20 members. We used all members of the daily hindcasts of four variables (precipitation, T_{max}, T_{min}, and S_{rad}) from 1983 to 2010 for the Terai's rice-growing season (June-December). The daily CFS v2 forecasts for each month had leads of one month and one-and-two months. For example, we took June forecasts from May initialization, July from June initialization and so on for one-month lead time.

Regarding the mixed forecasts one-and-two-month lead, the June and July forecasts were based on the May initialization, the August and September forecasts were based on the July initialization, and so on.

II.2.3.1 Skill of the forecasts and bias correction

In general, CFS v2 forecasts were colder and drier than the weather station data (Jha et al., 2016). Chapter I contains a comprehensive evaluation of the forecasts. The skill assessment indicated the presence of systematic biases in the CFS v2's T_{min} and T_{max} hindcasts. These biases were so significant that it was impossible to run the crop model using daily forecast data without correcting these biases.

Since the model simulates a cultivar's growth and development based on thermal degree-days, it takes fewer days for a cultivar to progress from one stage to the next in a warmer environment than in a colder environment. Given that the CFS v2 forecasts were colder than the weather station data, the crop model simulated an unrealistically lengthy crop growth and development period when forecasts were used. Therefore, bias correction was needed to achieve a realistic simulation. We thus corrected the bias of the CFS v2 forecasts against the climatology of weather station data. This is particularly relevant when not using a WG but raw daily data from the seasonal forecasts.

Therefore, before using seasonal forecasts, bias correction was completed for T_{min} and T_{max}. However, we did not correct the precipitation bias due to the complexity associated with correcting frequencies. Similarly, bias correction for S_{rad} was not undertaken, due to the absence of weather station data. Bias correction for crop models' weather variables also increases those models' predictability (Baigorria et al., 2008).

Bias correction was conducted by subtracting the average daily climatology of the observed weather variables for the Janakpur weather station from the average daily climatology of the CFS v2 hindcasts for the nearest grid point. The resulting bias in daily climatology was subtracted from each year's daily hindcasts from 1983 to 2010.

II.2.4 Real time simulation approach

When yield forecasting at long lead time is unable to produce the desired accuracy, a real-time simulation approach is one method to improve precision. Here, the model is updated with measured data over time (Bannayan et al., 2003). In our case, we combined daily CFS v2 forecasts with 28 years of historical daily weather data. We also included seasonal forecasts (one-month and one-and-two-month lead time) immediately after observed weather data to compare predictability with and without seasonal forecasts. The daily climatology, calculated by averaging all years, was not used, as it produced unrealistically high occurrences of rainfall because we are using the daily data.

Thus yield forecasts were conducted from every month, from July 1st to December 1st, for each year from 1983 to 2010, using a combination of weather data from observations, forecasts, and past year observations. For each year, weather data for yield forecasts consisted of observed daily weather data until the forecast date, combined with forecast data for the next one (two) month(s) and 28 years of daily historical weather data for the remainder of the growing season (Fig. II.1 a-b). For example, the weather data for yield forecasts from July 1st was comprised of June weather station data, CFS v2 seasonal forecasts for July, and 28 years of historical daily data from August to December. Similarly, weather data for yield forecasts from August 1st included June and July weather station data, CFS v2 forecasts for August, and 28 years of historical daily data from September to December. For the one-and-two-month lead seasonal forecasts, all details remained the same, except that two-month forecasts replaced the one-month forecasts.

(a)

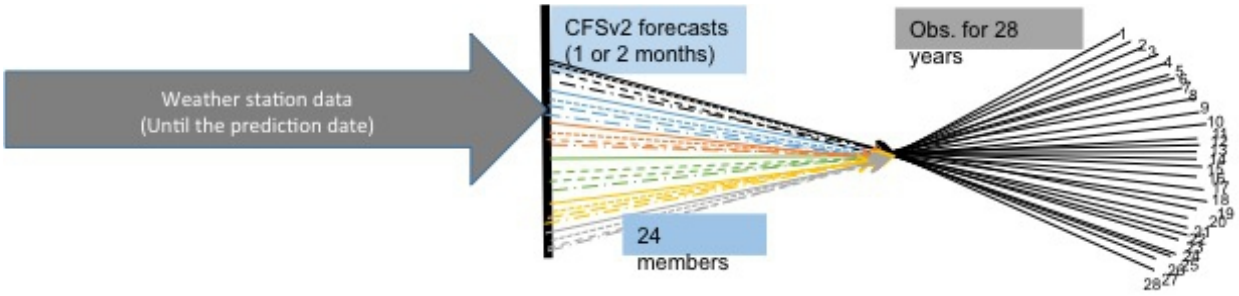

(b)

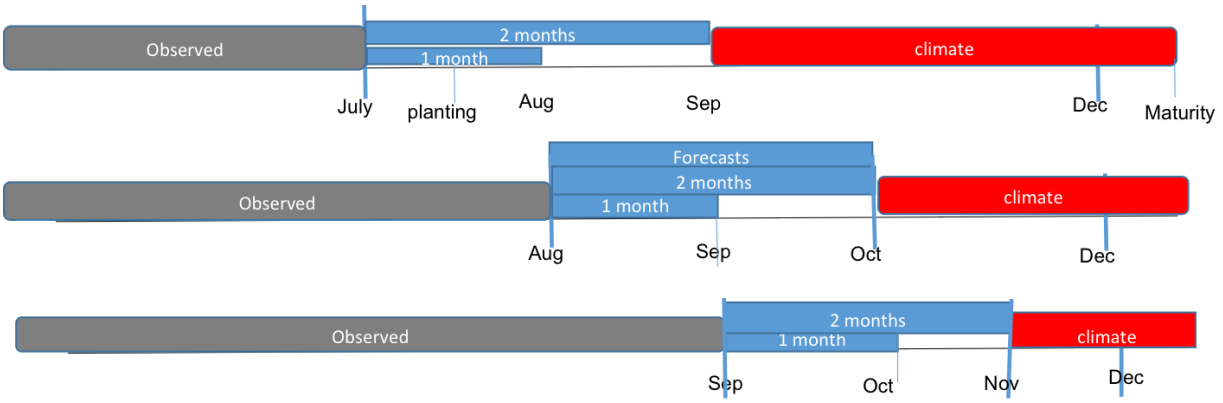

Fig. II.1 (a) Observed weather until the time of prediction (one time series), CFS v2 forecasts one (two)-month lead times (24 time series) and historical data (28 time series) and (b) change in composition of observed, forecasts and historical weather data with the progress in growing season.

Given that we had 24 CFS v2 ensemble members and 28 years of historical weather station data, we had 672 distinct virtual weather time series from June to November for each point of prediction, except for

December 1st. We only had 24 time series for December 1st, because we only used the observed weather until November for that date, followed by forecasts until the end of December. Thus, we did not need historical weather data for the December 1st prediction point, as the rice-growing season ends in that month. For the simulations not using seasonal forecasts, we had 28 virtual time series for every year from every points of prediction.

Considering the aforementioned weather time series, the model was run 672 times for each yield forecasting point (July 1st to November 1st), and 24 times for December 1st, for each year (1983 to 2010). In each case, we utilized the DSSAT v4.6's sensitivity analysis tool. The sensitivity analysis tool allows users to test model's sensitivity to a certain input by varying that input while keeping other inputs constant. In our case, we wanted to identify the impact of changes in weather; therefore, we selected a single treatment and different weather files under the model-levels. The average annual yield for each CFS v2 forecast ensemble member was calculated as the average of the 28 individual simulations from the 28 historical weather years. We thus had 24 mean simulated yields per year for each yield prediction point. For the simulations not using seasonal forecasts, every year's yield was calculated by averaging 28 individual runs using the historical weather.

II.2.4.1 Statistical tools for evaluating performance

The yields simulated using weather station data were the reference yields for comparison. The ensemble means and standard deviations were calculated from the annual mean yields for the 24 ensemble members for each year for each prediction point. Each prediction point's mean yield and standard deviation were plotted in an error bar diagram, along with the annual simulated yields based on weather station data. Also, the correlations between the reference yields and the yields simulated using CFS v2 forecasts were computed for 24 ensemble members for each yield prediction point from 1983 to 2010.

Similarly, the ensemble means of the simulated yields were compared with the reference yield for each year from 1983 to 2010. We evaluated model performance by calculating the mean percentage error (MPE), root mean square deviation (RMSD), correlation coefficients and model efficiency. The MPE and RMSD are defined by Bannayan et al. (2003) as follows:

$$\mathrm{MPE} = \left[\sum_{i=1}^{n}\left(\frac{|obs_{(i)} - model_{(i)}|}{obs_{(i)}}\right)100\right]/n \qquad [E.1]$$

$$\mathrm{RMSD} = \left[\left(\sum_{i=1}^{n}(model_{(i)} - obs_{(i)})^2\right)/n\right]^{0.5} \qquad [E.2]$$

Similarly, the efficiency (EF) index is defined by Loague and Green (1991) as follows:

$$EF = 1 - \frac{\sum_{i=1}^{n}(model_{(i)} - obs_{(i)})^2}{\sum_{i=1}^{n}(model_{(i)} - \overline{obs_{(i)}})^2} \quad [E.3]$$

Where $model_{(i)}$ is the i^{th} simulated yield, $obs_{(i)}$ is the i^{th} observed yield value, $\overline{obs_{(i)}}$ is the mean of the observed values and n is the number of observations.

The lower the MPEs and RMSDs values are, the better is the performance of models.

The EF index is one of the highly informative indices used for model evaluation. Its value range is [-∞, 1]. Models' performance is best when EF is 1. The negative values of EF indicate that the average observed values have better skill than the model.

Despite some caveats (Legates and McCabe, 1999), the Pearson's correlation coefficient is another commonly used diagnostic for evaluating models' performance. Its value can range from -1 (perfect negative correlation) to +1 (perfect positive correlation), with the values closer to +1 representing better model performance.

II.2.5 Crop yield simulation

II.2.5.1 How DSSAT simulates yield?

The DSSAT integrates species, weather, soil, and management-option effects to simulate growth and yield processes on a daily basis for a particular location. These factors collectively determine various dynamic variables, which DSSAT then uses to simulate a crop's growth and yield. Various DSSAT modules and sub-modules separately compute these variables for each day on the basis of various input files in DSSAT (e.g., species, cultivar, weather, and soil) through the experimental file (Jones et al., 2003). The calculated variables are then passed to an interface called the land-unit module (LUM), which makes them available to all modules.

The main program (MP) then calls the LUM and provides timing and simulation control variables. The MP starts the simulation by establishing the variables for initializing the run and calling the LUM (Jones et al., 2003). The MP then starts the season loop and calls the LUM for initializing variables at the start of every season loop. After that, it begins the daily loop and calls the LUM for rate calculations, integration, and output reporting. After the season loop is completed, the MP calls the LUM to produce season-end variables and summary output files.

The CERES-Rice model helps to include rice crop specific variations. Potential biomass production for a plant is calculated as a product of the RUE and fraction of the Photosynthetically Active Radiation (PAR) intercepted by the plant (Ritchie et al., 1998). The RUE value for rice is fixed from 2.6 to 4.0. The actual biomass is limited by the deficiency of water and nutrients. The biomass produced is then allocated among different parts of plant based on a sink-source concept. Crop yield is calculated by multiplying total number of grains per plant by unit grain weight at physiological maturity. Grain numbers per plant are estimated from the panicle weight at maturity, using the cultivar coefficient (G2), which is the single grain weight under ideal growing conditions. The grain weight is calculated by multiplying the cultivar specific potential growth rate by the grain filling duration.

We used the default simulation option in DSSAT v4.6 (Hoogenboom et al., 2015). This option took initial soil conditions and the reported weather from the soil input file. Evapotranspiration was calculated using the Priestley-Taylor/Ritchie method, and photosynthesis was estimated using the leaf photosynthesis response curve method. Similarly, the Ritchie water balance was used for hydrology, while infiltration was calculated using the Soil Conservation Services method. Likewise, the CERES (Godwin) computed the soil organic matter, the Suleiman-Ritchie method estimated soil evaporation, and the modified soil profile method gauged the soil layer distribution. Furthermore, the actual CO2 from Mauna Loa, Hawaii (Keeling curve), was used.

II.2.5.2 Management data

The experimental data on rice crop growth and yield came from the National Rice Research Program (NRRP) Hardinath of the Nepal Agricultural Research Council (NARC).

The management-related factors were fixed in all simulations, in order to assess the effects of changes in weather. All simulations were conducted for the Masuli cultivar. Although Masuli contributes only 3% of the total rice yield in Dhanusha district (CDD, 2015), we selected this cultivar because of the availability of data for calibration.

The planting date was fixed as July 14th, which is the common planting date for Masuli rice in the Terai's rainfed system (Personal communication with farmers). The 25-day-old transplants were planted at a depth of 3 cm, and at a rate of two plants per hill. The temperature of the transplants environment was assumed as 30^{0}C considering daily climatology. The row spacing was 20 cm x 20 cm, with a planting density of 25 plants per square meter (Akhtar et al., 2004; Chaoudhary et al., 2004). As our goal was to understand the effect of weather, all simulations assumed rainfed conditions. The average fertilizer application rate was fixed at 60:30:30 N:P:K kg/ha, and fertilizer was applied in two phases: at the time of

planting, and 25 days post-planting (Chaoudhary et al., 2004; Akhtar et al., 2004). In the model the harvest was set at physiological maturity.

II.2.5.3 Soils

The soil profiles were taken from the International Soil Reference and Information Center's (ISRIC) (World Inventory of Soil Emission Potentials) WISE soil database (Batjes, 1995; Batjes, 2002). The ISRIC is located in Wagenignen, The Netherlands (Batjes, 1995). Gijsman et al. (2007) converted 1,125 global soil profiles from WISE version 1.0 into a format that can be directly inputted into DSSAT using either WISE parameters or a theoretical approach (Jones et al., 2003; Hoogenboom et al., 2015). Romero et al. (2012) converted 4,382 soil profiles from WISE v1.1 into a DSSAT-compatible crop model format and applied various error-checking procedures.

Since the WISE database was compiled using different sources and methods, it cannot be considered error-free. And, these errors are further multiplied when converting WISE data into DSSAT inputs due to the uncertainty in several WISE parameters and theoretical estimations. Therefore, the WISE database only contains educated guesses regarding possible values for certain soil classes (Gijsman et al., 2007).

Hardinath soil falls into the CMIT043 category. This category has a silt loam texture, is 44% silt, 20% clay, and 36% sand, and reaches a depth of 1.2 m. Complete descriptions of each soil profile by soil horizon used in this study are shown in Table II.1.

Table II.1: CMIT043 Soil profile description (Source: (Romero et al., 2012)

Depth base of layer (m)	Master horizon	Wilting point (cm^3 cm^{-3})	Field capacity (cm^3 cm^{-3})	Max. water holding capacity (cm^3 cm^{-3})	Root growth factor	Saturated hydraulic conductivity (cm h^{-1})	Bulk density (G cm^{-3})	Organic carbon
15	A1	0.148	0.337	0.560	1.00	1.75	1.02	4.30
60	A2	0.068	0.232	0.451	0.47	3.40	1.37	1.10
120	B	0.183	0.274	0.374	0.17	0.70	1.58	0.05

Depth base of layer (m)	Master horizon	Clay (%)	Silt	Total Nitrogen (%)	pH in water	Magnesium (cmol kg^{-1})	Calcium, exchangeable, (Cmol kg^{-1})
15	A1	20	44.00	0.43	5.3	0.5	0.1
60	A2	22	31.00	0.11	5.4	0.5	0.1
120	B	12	18.00	0.01	5.6	0.6	0.1

II.2.6 Calibration of DSSAT model

CERES Rice model includes various cultivars of rice and each cultivar has a unique set of crop-specific parameters called genetic coefficients. Cultivars grown under the same environmental conditions have different yield and traits because of these coefficients (Bertin et al., 2010). Genetic coefficients can be broadly categorized into three types based on their relation to: life cycle, vegetative growth and reproductive growth. For CERES-Rice model we need the following eight genetic coefficients:

- P1 estimates the time period of vegetative phase of the plant in growing degree days (GDD);
- P2O estimates the longest day length at which the maximum development occurred;
- P2R estimates the delay in panicle initiation due to the per hour increase in P2O;
- P5 estimates the time period needed for grain filling to maturity;
- G1 is the spikelet number per gram of main culm;
- G2 is the single grain weight;
- G3 is the tillering coefficient; and
- G4 is the temperature tolerance coefficient.

Crop models should be calibrated for the study area if the results are to be credible (Timsina and Humphreys, 2006). Since not all cultivar traits can be confidently replicated using the genetic coefficients calibrated in different environment (Mavromatis et al., 2002), calibration is needed for better prediction.

Various methods have been used to estimate genetic coefficients and each method has its own strengths and limitations. Trial and error is the most common approach for the model parameter estimation (Wallach et al., 2001). In this method, various parameter values are tested until an acceptable fit to the observed data is found. Nonetheless, trial and error process has limitations such as lack of reliability and replicability (Lyneis and Pugh, 1996).

Considering our limitations (interpolated soil data, lack of time-series crop measurement data and some measured data from crops cultivated under environmental stresses), we did not rely on a single method alone.

We used the GLUE (Generalized Likelihood Uncertainty Estimation), a commonly used Bayesian method (Beven and Binley, 1992), which has been widely used in environmental modelling for model parameter

estimation (Blasone et al., 2008). The GLUE tool in DSSAT v4.6 uses the Gaussian likelihood function to assess the likelihood value of a given prior set of parameters (He et al., 2010; He et al., 2009). From the likelihood values, it is possible to get the estimated mean and variance of the posterior distribution of parameters.

Also, we considered the genetic coefficients calibrated by other studies in Nepal (Timsina and Humphreys, 2006; Rai et al., 2011; Lamsal et al., 2013) for the same cultivar but for different sites for comparison. We compared the RMSE, the index of agreement (d-stat) and coefficient of determination (R^2) of the simulated growth and yield values obtained using the genetic coefficients from GLUE and other studies with the measure data. Jones and Kiniry (1982) justified the use of mean and R^2 and Willmott et al. (1985); Willmott (1982) recommended using RMSE and d-stat for analysing model performance. Then we used trial and error process to adjust the coefficients until the RMSE was minimized, and until the d-stat and R^2 values neared to one.

$$RMSE = \left[N^{-1} \sum_{i=1}^{n} (s_i - o_i)^2\right]^{0.5} \quad \text{[E.4]}$$

$$RMSEn = 100 * RMSE/\bar{O} \quad \text{[E.5]}$$

$$d - stat = 1 - [\sum_{i=1}^{n} (s_i - o_i)^2 / \sum_{i=1}^{n} [|s_i'| + |o_i'|]^2] \quad \text{[E.6]}$$

$$s_i' = s_i - \bar{O}; \qquad o_i' = o_i - \bar{O}; \qquad \bar{O} = \sum o_i/n$$

A simulation was considered 'excellent' if the RMSEn was less than 10%, 'good' if between 10–20%, 'fair' if between 20–30%, and 'poor' if the RMSEn was higher than 30%.

Since most model users do not have controlled-environment facilities, measured data from the field are used. We used measured data on the Masuli rice cultivar from NRRP Hardinath varietal trial plots for the years 2002 to 2005 (Chaoudhary et al., 2004; Akhtar et al., 2004). The measured variables included: anthesis day, maturity day and yield at maturity. Before running the DSSAT, we entered the weather, soil, management, and measured data files in DSSAT format.

Model evaluation was done using the multiple statistics mentioned in the section II.2.4.1

II.3 Results and discussion

II.3.1 Genetic coefficients

Table II.2 provides the Masuli rice's genetic coefficients obtained from the calibration process. For set weather conditions, P1 and P5 were higher for the long duration cultivar and lower for the short duration cultivars. The genetic coefficients obtained from the calibration process were compared with the findings of other studies on the same cultivar in other parts of Nepal (Timsina and Humphreys, 2006; Rai et al., 2011; Lamsal et al., 2013). Although some coefficients were close to one another, other exhibited larger differences (Table II.2). The inconsistencies in the genetic coefficients calibrated using data from different regions were common, even for the same cultivar.

Table II.2: Calculated genetic coefficients for Masuli rice.

Cultivar	P1	P2R	P5	P2O	G1	G2	G3	G4	PHINT	References
Masuli	900.0	290.0	280.0	10.7	42.0	0.017	1.00	1.0	83.0	This study
Masuli	853.5	170.5	476.5	10.9	71.1	0.020	0.87	1.0	83.0	GLUE DSSAT
Masuli	830.0	200.0	600.0	11.4	35.0	0.030				(Timsina and Humphreys, 2006)
Masuli	840.7	186.1	251.0	10.8	42.0	0.020				(Lamsal et al., 2013)
Masuli	502.3	168.0	500.0	11.2	54.0	0.030				(Rai et al., 2011)

II.3.2 Main growth and development variables for Masuli rice

Table II.3 displays the main growth and development variables for Masuli rice from 2002 to 2005, both measured at the NRRP Hardinath station and simulated by the CERES-Rice model. The RMSEs for anthesis and maturity dates were excellent, and were good for the yield. In contrast, the d-stat for yield was better than the d-stat for the anthesis and maturity dates. Similarly, the correlation coefficient between the simulated and observed yields was also excellent, but fair for the other variables.

The high error in the maturity date's estimation could be due to the mismatch in dates between the model's simulation of physiological maturity and field measurements of the harvest maturity date. Similarly, the inconsistency in the anthesis dates could have stemmed from the subjective criteria used to measure them. Unlike these two variables, the yield could be measured very accurately, even under the local conditions. In personal communication with the scientists at the NRRP Hardinath during my field visit, they admitted that the measured maturity dates might not match the exact dates of physiological

maturity. They further told me that they use subjective criteria to estimate the anthesis dates, and that it was common for the measured anthesis date to be inaccurate by a few days.

Table II.3: Main growth and development variables for Masuli rice for the year 2002, 2003, 2004 and 2005 using the experimental data from NRRP Hardinath for calibration

Variable Name	Observed	Simulated	r-Square	RMSE	RMSEn (%)	d-Stat.
Anthesis day	120	121	0.4	2	2	0.7
Mat Yield kg/ha	2787	2355	0.8	534	19	0.8
Maturity day	150	159	0.4	12	8	0.6

II.3.3 Model evaluation

We evaluated the DSSAT's ability to predict rice yields by comparing simulated yields with district-average yield data. The mean simulated rice yields for the Hardinath point in Dhanusha district were compared against observed district-average rice yield data for Dhanusha district from the Ministry of Agricultural Development (MOAD) Nepal.

The model successfully simulated district-average yields for the shorter time period from 2002 to 2005, as demonstrated by the correlation coefficient of 0.7 and d-stat of 0.8. For the longer period from 1983 to 2010, however, its predictive skill dropped remarkably. The correlation coefficients were -0.1 and -0.2 for the weather station data, and for the ERA-Interim reanalysis combined with APHRODITE rainfall data respectively. The MPEs were as high as -23 (30) % and the RMSDs were as high as 804 (825) kg/ha for the simulations using weather station (ERA-Interim) data (Table II.4). Similarly, the model EF indexes were -3.6 (-4.0) for the simulations using weather station (ERA-Interim) data. The negative values of model efficiency indicate that the model did not have skill to simulate the district average yield data. We repeated the process for other representative stations (Parwanipur and Bhairahawa) in Terai, but without any success in improving the prediction skill (Table II.4 and Fig. II.2).

The model's drop in skill for district-average yields was related to the simulation's use of interpolated soil data and only a single management practice. The district is home to hundreds of thousands of small-scale farmers, who practice dissimilar management techniques in individual years and on different lands. In contrast, the simulation focused on a single point (Hardinath) with a fixed soil, and only one cultivar and management approach. It would have been impossible to acquire historical crop management data for all small-scale farms, because techniques differ from farm to farm, and farmers themselves would not be able to remember all data from past years.

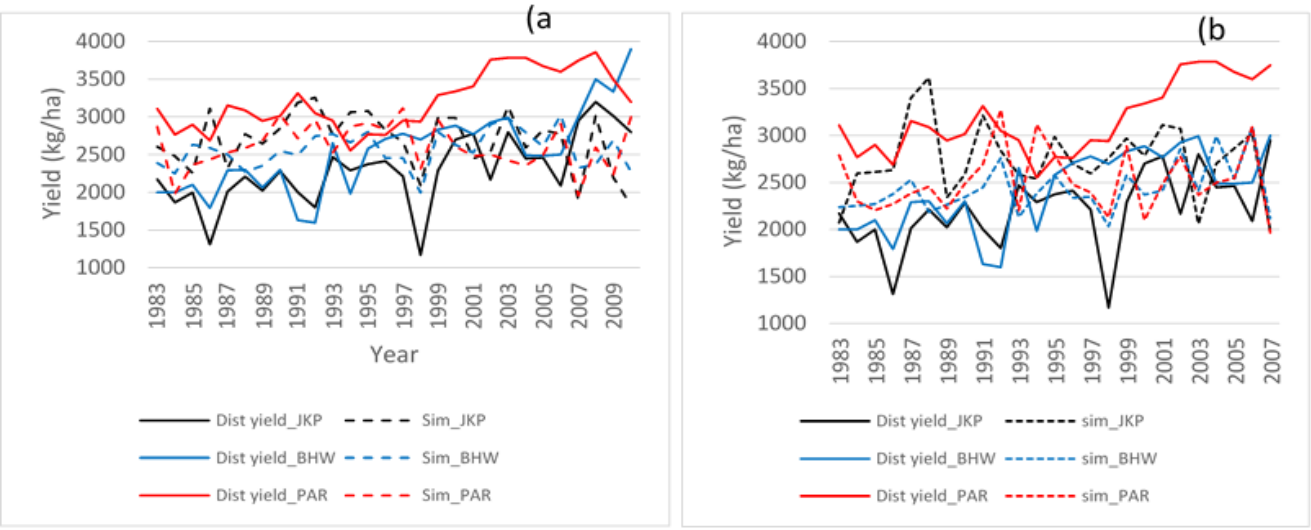

Figure II.2 Time series of simulated versus observed yield of rice for Dhanusha, Parwanipur and Bhairahawa for a) using weather station data b) using ERA-Interim data. The solid lines are for the district yield for the three stations and dashed line for the simulated yields. The simulated yields are obtained from the DSSAT-CERES-Rice model run while the measured yields are taken from the MOA.

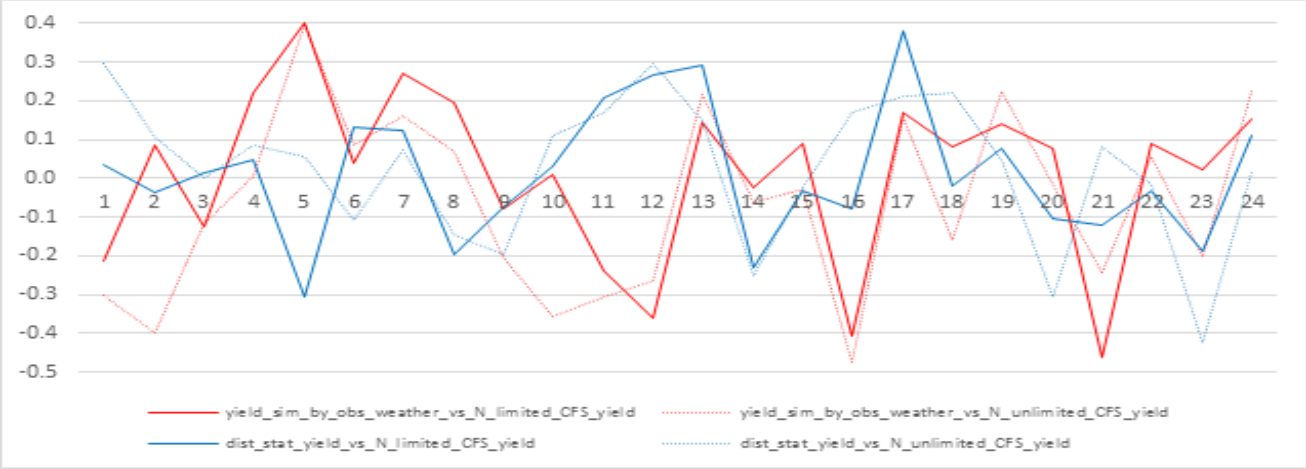

Fig. II.3 Correlation between district statistical yield, yield simulated using weather station data and yield simulated using CFS v2 forecasts July-Dec (all 1-month lead only) for 24 members for the periods 1983-2010. The simulations were done for both N-limited and N-unlimited yields.

Since the model did not have skill to simulate the district average yield data, we employed the yields simulated using observed weather as references for comparison. We used these reference yields, so as to capture the random errors related to the seasonal forecasts, while ignoring the crop model's inherent errors (Hansen et al., 2004). Then we calculated the correlation coefficients between yields simulated using one-month lead forecasts (24 ensemble members) and the reference yields. We found the correlation coefficients ranged from 0.4 to -0.5 for different ensemble members (Fig II.3). We tried to

improve skill by removing N limitation but it did not help (Fig II.3). Thus, we concluded that using seasonal forecasts alone could not accurately predict yields. Therefore, in the next step we used mixed weather data.

Table II.4: Model MPE, RMSD and EF for different sites compared to the district average yield data. The statistics are computed seperately for the simulations using weather station data and ERA-Inerim reanalysis data.

Sites	MPE (%)		RMSD (kg/ha)		EF	
	Station	ERA	Station	ERA	Station	ERA
Hardinath	-23	-30	737	812	-1.6	-3.0
Bhairahawa	-6	-4	593	490	-0.2	-0.4
Parwanipur	17	20	804	825	-3.6	-4.0

II.3.4 Model's skill in simulating yields using climatology and CFS v2 hindcasts

In this section, we are comparing performance of seasonal forecasts and climatology in simulating yields. Also, we are comparing the yield prediction skills of one-month lead and one-and-two-month lead forecasts. The assessment was done by quantifying yield prediction biases at different prediction time points, using the following tools: mean percentage error (MPE) and root mean square deviation (RMSD). Also, we compared correlation coefficients between the yields simulated using these hypothetical weathers and yields simulated using observed weather, hereafter named as reference yields.

II.3.4.1 Bias in prediction

In general, yield forecasts' improved in accuracy as successive monthly weather updates were incorporated, as demonstrated by the gradual decrease in MPE and RMSD (Fig. II.4). The reason that the yield predictions improved over time was that, as the season progressed, actual weather data replaced forecasts. This result is consistent with the finding of other studies (Hansen et al., 2004; Mishra et al., 2008; Pal et al., 2013).

Yield can be better predicted by using climatology alone than using forecasts combined with climatology. The MPE for the simulated grain yield using observations combined with one-month lead seasonal forecasts and climatology varied from 3% for the last date of prediction (December 1st) to 15% for the first date of prediction (July 1st), while the RMSD ranged from 83 kg/ha to 384 kg/ha (Table II.5). Normally, the MPE and RMSD for the simulated grain yield using observation and climatology was lower than the MPE for the simulated yield using observations combined with the one-month lead seasonal forecasts and climatology. The MPE for the simulated grain yield using observation and climatology varied from 3% for the last date of prediction (December 1st) to 12% for the first date of

prediction (July 1st), while the RMSD ranged from 85 kg/ha to 381 kg/ha. We repeated the process using observations combined with one-and-two-month lead forecasts and climatology. In general, prediction worsened when the one-month-lead forecasts were replaced by one-and-two-month forecasts. The MPEs for the simulated yields using weather data including one-and-two-month lead forecasts ranged from 6% for the last date of prediction (November 1st) to 19% for the first date of prediction (July 1st), while the RMSD ranged from 196 kg/ha to 484 kg/ha (Table II.5).

Careful analysis of individual year's prediction, however, suggested that during most of the years, the simulated yields predicted using weather data including seasonal forecasts have lower MPEs and RMSDs than the yields simulated without using seasonal forecasts. Consequently, the median MPEs and RMSDs values for the predictions with seasonal forecasts were lower than the prediction done without using seasonal forecasts.

By excluding four extreme years (out of 28 total years) from the analysis, the MPEs ranged from 6% to 25% (for the December 1st and July 1st predictions, respectively) (Table II.6). In order to understand the reasons for extreme biases in prediction in these years, we investigated the impact of weather on simulated yields for these years. Following paragraphs describes the results from these investigations.

The analysis illustrated that the years 1992, 2007, 2009, and 2010 were extreme in terms of biases (Fig II.4). Biases were excessive in these years, mainly due to the poor quality of rainfall forecasts. Although 1992 was, on average, a dry year, an above-average amount of rain fell in October during the panicle initiation, thus boosting crop yields. However, all forecast members predicted a dry October. The actual total monthly rainfall was 176 mm, while all CFS v2 ensemble forecasts ranged from 0 to 17 mm of rainfall. This caused the model to underestimate crop yields.

In contrast, the extreme biases in 2009 and 2010 were associated with all CFS v2 ensemble members' forecasts overestimation of rainfall in August. In 2009, from August 25 to October 7, a prolonged 43-day drought occurred during the crucial stages of rice growth. This led to decreased yields simulated with observed weather. However, in the CFS v2 forecasts, rain fell continuously for five days, bringing a total of 163 mm of rain during the last week of August in 2009. The forecasts' overestimation of rain amounts increased simulated yields. Similarly, extreme biases in 2010 were related to forecasts' overestimation of rainfall.

In 2007, rain fell continuously for 17 days during a 22-day period immediately after planting, with fields receiving 1,082 mm of rain. In a 3-day period from 26 July 2007 to 28 July 2007, total rainfall equalled 535 mm. However, all forecast members indicated normal rainfall, and therefore predicted higher yields as compared to the yields simulated using observed weather. Because of a decrease in rain from

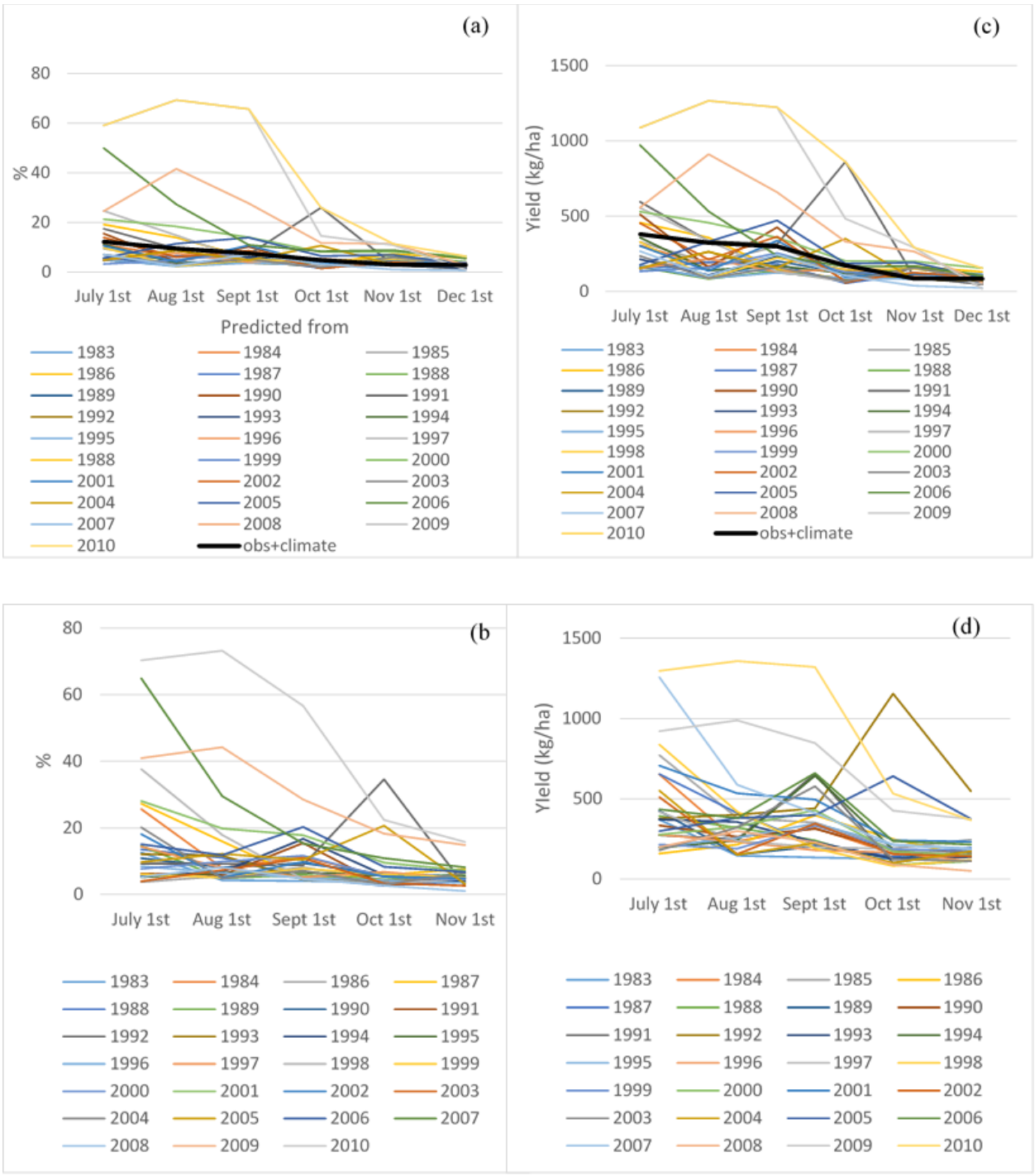

Fig. II.4 Mean Percentage Error (MPE) in simulated yield predicted at different months before harvest using: (a) one-month lead seasonal forecasts and (b) one-and-two-month lead forecasts. Root Mean Square Deviation (RMSD) of the predicted yield at different lead months before harvest using: (c) one-month lead seasonal forecasts and (d) one-and-two-month lead forecasts. The yield simulated using observed weather serve as the reference yields, and are compared against the yields simulated using weather station data/climatology from Janakpur Airport and CFS v2 forecasts.

September onwards after the end of the ISM, the mismatch declined between the observations and the forecasts. Consequently, the biases were reduced for predictions from September onwards.

We additionally analysed whether including the two-month lead forecasts reduced the extreme errors. For the yields predicted from 1 October 1992, the MPE was higher for the predictions using two-month lead forecasts than the predictions using one-month forecasts. This was because, for October 1st predictions, November weather came from forecasts and historical weathers for predictions using two-month and one-month lead respectively. The excessively dry forecasts substantially decreased the yields, and the error consequently increased. Similar results occurred when yields were predicted from 1 October 2005, 1 November 2009, and 1 November 2010. In general, yields predicted from September 1st using two-month lead forecasts had larger errors than yields predicted on that date with one-month lead forecasts. This is because of the poor quality of forecasts for those months, as compared to historical weather data.

Table II.5: Measures of maximum possible model deviation between the simulated yields using weather station data and forecast data considering all years

	Weather	July 1st	Aug 1st	Sep 1st	Oct 1st	Nov 1st	Dec 1st
MPE	Obs+climate	12	9	8	3	3	3
	Obs+1-mon-lead+Climate	15	13	12	6	5	3
	Obs+2-mon-lead+Climate	19	13	12	8	6	
RMSD	Obs+climate	381	324	300	173	87	85
	Obs+1-mon-lead+Climate	384	311	318	193	144	83
	Obs+2-mon-lead+Climate	484	363	404	235	196	

Table II.6: Measures of maximum possible model deviation between the simulated yields using weather station data and forecast data during average years (excluding extreme years 1992, 2007, 2009 and 2010)

	July 1st	Aug 1st	Sep 1st	Oct 1st	Nov 1st	Dec 1st
MPE (%)	25	18	14	11	8	6
RMSD (kg/ha)	555	456	472	351	200	156

II.3.4.2 Correlation coefficient

Correlation coefficients between the yields simulated using CFS v2 forecasts (24 members) mixed with historical weather data and the reference yields for the period from 1983 to 2010 were calculated from different months of prediction. CFS v2 forecasts included both one-month lead and one-and-two-month lead. These correlation coefficients were compared with the correlation coefficients between the simulated yields without using forecasts and reference yields at different months before harvest.

The correlation skill of predictions was consistent with our earlier findings related to MPEs and RMSDs that the correlation coefficients between the simulated and reference yields increased as successive monthly weather updates were incorporated regardless of the weather types. The correlation between the reference yields and the yields forecasted from July 1st was poor with the average correlation coefficient lower than 0.2 for all types of weather (Fig. II.5). This finding signifies a high degree of uncertainty in yield prediction at five months. The height of the boxes depicts the variations in correlation coefficient among 24 ensemble members. For early predictions (until September 1st), some of the ensemble members had better correlation coefficient than climatology, as shown by the height of the whiskers. The correlation skill of prediction increased as the growing season gradually advanced, as the duration of known weather increased and the duration of unknown weather thus decreased. The average correlation coefficient was satisfactory (0.7-0.9) when we predicted yields from end of September or from the beginning of October, two-and-a-half months before physiological maturity. As expected, the correlation coefficient was almost perfect (0.91-0.99) when we estimated yields from the end of October or from the beginning of November, one-and-a-half months before physiological maturity for all types of weather. However, by not using seasonal forecasts we can achieve almost perfect (0.91) correlation coefficient one month earlier (in October 1st) than when using seasonal forecasts.

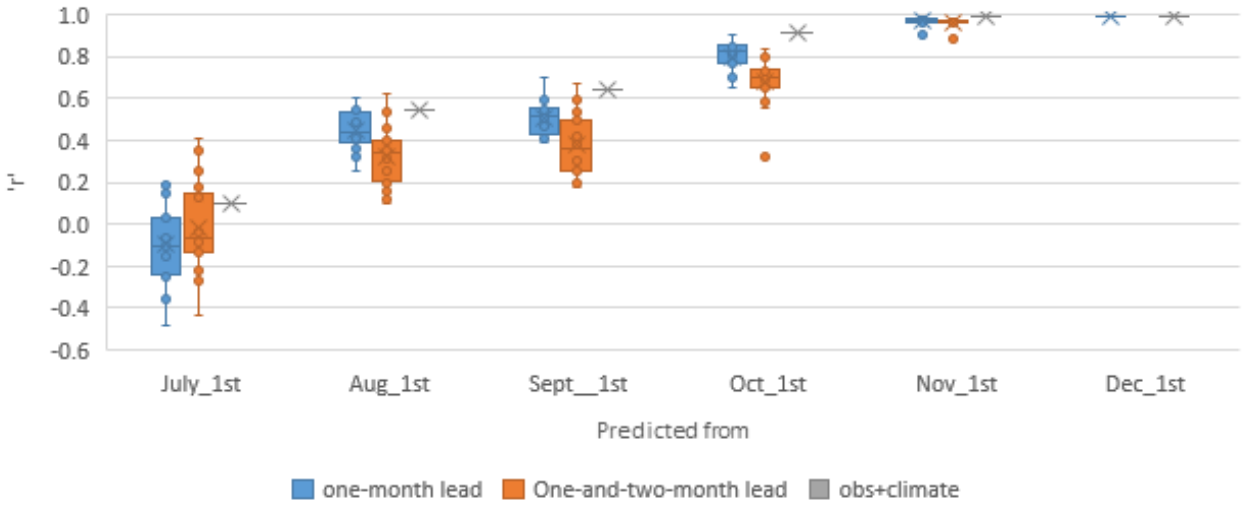

Fig II.5 Correlation coefficient between simulated yield using CFS v2 forecasts (24 members) and yield simulated using weather station data from Janakpur Airport for the period 1983-2010 at different months before harvest. CFS v2 forecasts included both one-month lead and one-and-two-month lead. These correlation coefficients are compared with the correlation coefficients between the simulated yields without using forecasts and simulated yields using weather station data at different months before harvest.

Our results related to increase in correlation coefficient between the simulated yields and reference yields with the successive monthly weather updates are supported from the findings of other studies (Pal et al., 2013; Mishra et al., 2008; Hansen et al., 2004).

The correlation coefficients between the yields simulated without using the seasonal forecasts and reference yields were always higher than the simulations using forecasts regardless of the time of prediction. Similarly, the yields simulated using two-month lead forecasts, from all ensemble members, had relatively lower correlation coefficient than the yields simulated with one-month lead forecasts except for the July 1st prediction. The poor correlation skill of the yields simulated using seasonal forecasts than using climatology and further worsening in correlation skill with the increase in seasonal forecasts' lead time are associated with poor quality of seasonal forecasts, particularly in predicting precipitation. This justified the use of observations and climatology alone rather than using forecasts.

Consistently and satisfactorily predicting yields two-and-a-half months before harvest for 28 years seems to be a promising result. Using a combination of actual daily weather data for 2002 and daily historical weather data for 25 years, Soler et al. (2007) were able to accurately predict the yields of four maize hybrids at least one-and-a-half months before the harvest in Brazil. Yield prediction is an important component of food security-related vulnerability analysis and planning (Thornton et al., 1997).

Duchon (1986) utilized a mix of observed weather before the forecast time, followed by historical weather sequences from the CERES-Maize model, and was able to perfectly predict yields between the beginning and the end of the grain filling stage for Peoria, Illinois. His findings were based on experiments from 1983 and 1976, and even during these years, there was a lack of consistency regarding maturity dates and accurate yield prediction dates.

II.3.4.3 Statistical significance of the difference between mean yields across members and years

To understand the statistical significance of the differences in mean yields across years and across members, we performed the analysis of variance (ANOVA) (Table II.7). The ANOVA analysis demonstrated that the interannual variations in mean yields were highly significant for the simulations using both one- and two-month lead times (Table II.7). Similarly, the differences among the ensemble members' predicted mean yields were significant for yields predicted from July 1st at both one- and two-month lead times.

Table II.7: ANOVA to find the statistical significance of the difference in mean yield across members and years.

Null hypotheses (one-month lead-time forecasts)	One-month-lead	p-value (One-month-lead)	Two-month-lead	p-value (Two-month-lead)
The inter-annual variation in yield related to weather is not significant	Reject	2.7e-14	Reject	1.52e-06
The mean yield predicted using different ensemble members does not differ significantly when predicted from July 1st	Reject	3.28e-05	Reject	0.02
The mean yield predicted using different ensemble members does not differ significantly when predicted from August 1st	Accept	0.65	Accept	0.83
The mean yield predicted using different ensemble members does not differ significantly when predicted from September 1st	Accept	0.30	Accept	0.28
The mean yield predicted using different ensemble members does not differ significantly when predicted from October 1st	Accept	0.72	Accept	0.62
The mean yield predicted using different ensemble members does not differ significantly when predicted from November 1st	Reject	0.03	Accept	0.19
The mean yield predicted using different ensemble members does not differ significantly when predicted from December 1st	Reject	0.004	-	-

For all other predictions points, the differences among the mean yields simulated by different ensemble members were not significant at a two-month lead. However, the differences were significant at a one-month lead for yield predictions from November 1st and December 1st (Table II.7).

II.3.4.4 Error bar

The crop was planted in mid-July and harvested in December. In most years, variability in yield forecasts, (shown by the bar) was higher when for yields predicted from July, August, and September (Fig. II.8). Theoretically, the standard deviation of the simulated yield should decrease as the duration of observed weather increases. This rule only seemed to apply one-and-half months after planting. The standard deviation indeed decreased as the duration of the observed weather grew in length as the growing season progressed. Standard deviation minimum values reached 30 kg/ha, 18 kg/ha, and 8 kg/ha, when predicted from October 1st, November 1st, and December 1st, respectively.

(a)

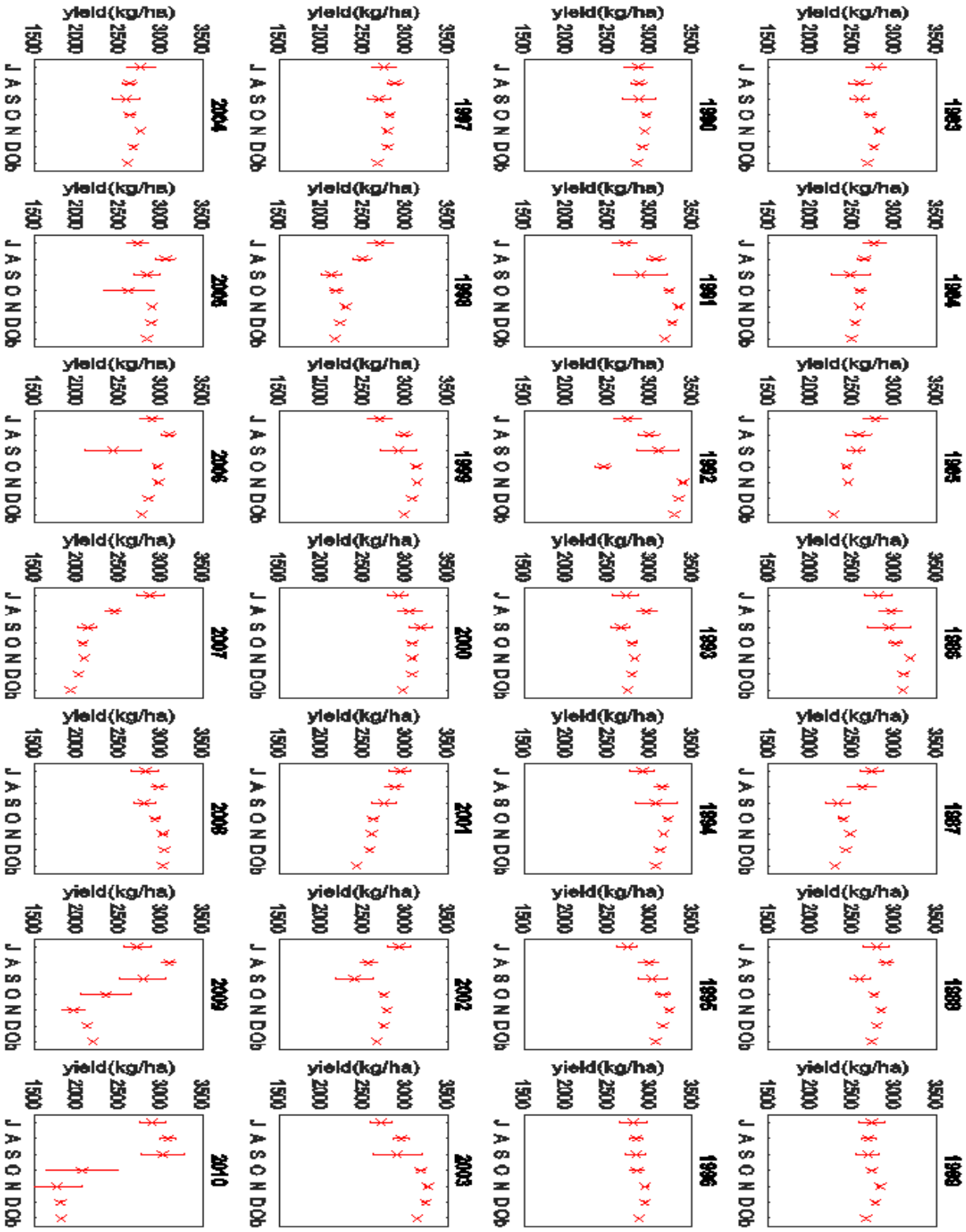
1983
1984
1985
1986
1987
1988
1989
1990
1991
1992
1993
1994
1995
1996
1997
1998
1999
2000
2001
2002
2003
2004
2005
2006
2007
2008
2009
2010
yield(kg/ha)
1500
2000
2500
3000
3500
J A S O N D Ob

(b)

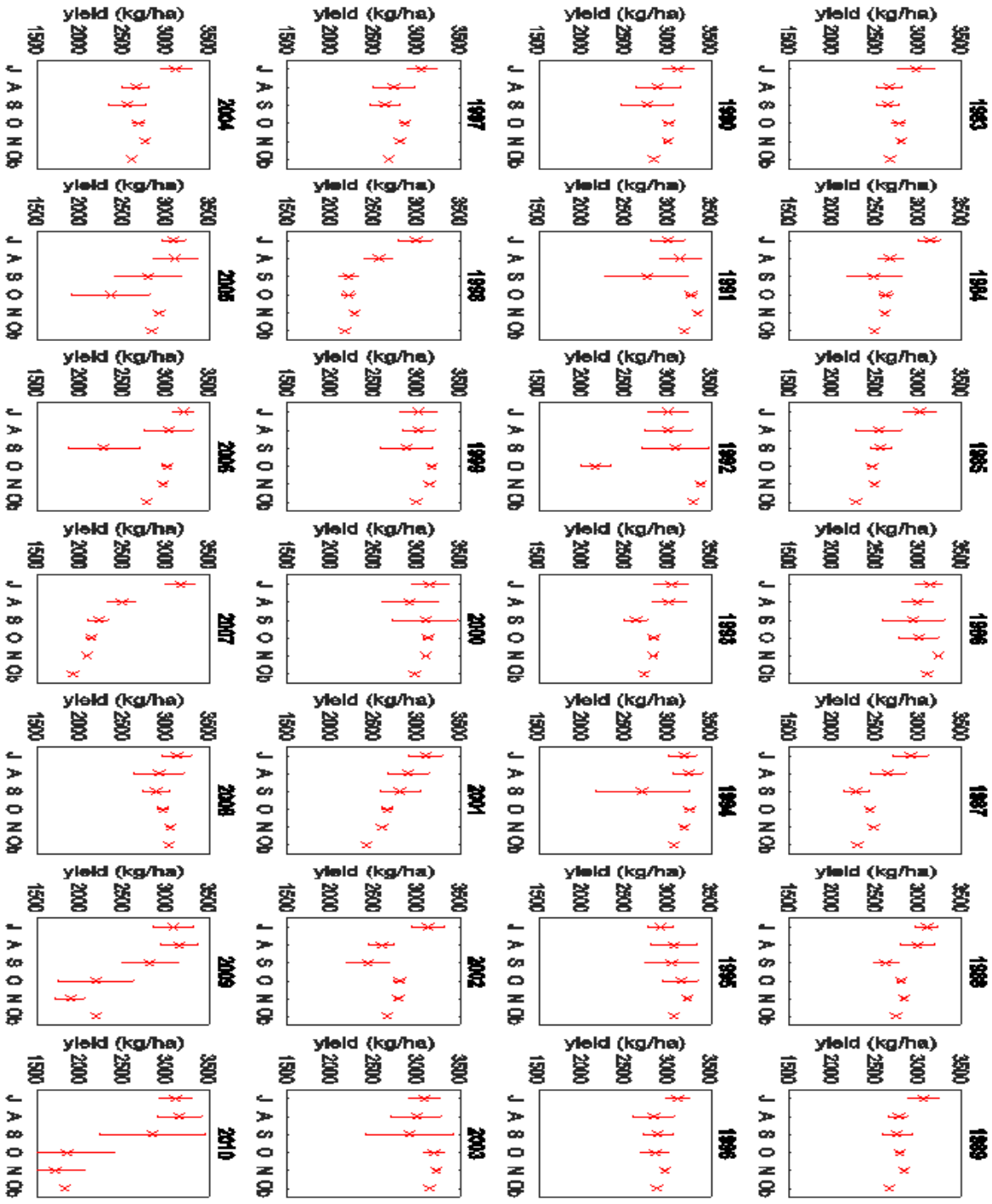

Fig. II.6: Average forecasted yield and standard deviation for year 1983-2008 (left to right) as a function of the forecast date and observed yield (kg/ha). Forecast date are 1st of July (J), August (A), September (S), October (O), November (N), December (D) and Observed (Ob). (a) one-month-lead time; (b) two-month-lead-time.

I.4 Conclusions

The study evaluated application of seasonal forecasts for rice yield prediction via a case study of Nepal's Terai. Rice is the country's main staple crop and contributes to half of the total calories required by the Nepalese people. In Nepal, rice is primarily cultivated in the lowland Terai region, and most rice production areas are still rainfed. Rainfed cultivation depends on the monsoon rain and entails a high degree of risk, due to the uncertainty posed by the monsoon (e.g., late onset, breaks, and extremely heavy rainfall).

Crop models provide an opportunity to quantify the effect of climate, soil, cultivar, and management on crop growth and productivity. We used the DSSAT v4.6's CERES-Rice model, which simulates cultivar-specific yields based on environmental conditions.

The DSSSAT v4.6 model was calibrated using experimental data from the NRRP Hardinath and weather station data from a nearby station for the Masuli cultivar. It was evaluated using district statistical yield data from the MOAD. Before using seasonal forecasts for yield prediction, we tested the crop model's ability to simulate the interannual district-average yield using observed weather and reanalysis data.

We found that the CERES-Rice model did not have satisfactory skill to simulate long-term district-average yield data, as demonstrated by the low correlation coefficient, high MPE, high RMSD and negative EF. Our results were consistent for other representative stations in Terai.

Our goal was to focus on how weather affects yields and to ignore crop-model errors. We thus took yields simulated using observed weather as reference yields for comparison. The reference yields were then compared against yields simulated using hypothetical weather data.

The study used the dynamic climate model CFS v2's seasonal forecasts to predict rice yields. In order to improve yield predictability, we tested a range of operational configurations. These included all one-month lead forecasts' time series for the entire growing season, so that July forecasts were based on June initializations, August forecasts were based on July initializations, and so on. We found the forecasts-only weather time series did not have a strong ability to predict yields, as evident from the low correlation coefficients (ranging from -0.4 to 0.4) between the yields simulated using forecasts and the yields simulated using weather station data.

Next, we followed the real-time simulation approach, using observed weather until the time of prediction, followed by the forecasts and historical weather data. Forecasts at one and one-and-two-month leads were employed combined with observed weather before prediction date and climatological time series after the end of the forecasts. Yields predicted using seasonal forecasts were then compared with yields predicted without using seasonal forecasts (using observed weather and climatology alone) to

understand the importance of seasonal forecasts. Yield predictions were conducted for the first date of every month, starting from July 1st and ending on December 1st. Statistical tools (e.g., MPE, RMSD, correlation, and error bar) were used to quantify biases and evaluate the predictive skill.

In general, yield forecasts improved by using climatology alone than using seasonal forecasts and climatology, as suggested by the gradual decrease in the MPE, and RMSD, and the increase in the correlation coefficients. Similarly, the prediction using one-and-two-month lead forecasts together with climatology had higher MPE, and RMSD and lower correlation coefficients than the prediction using one-month lead forecasts along with climatology. Likewise, the yield forecasts improved as successive monthly weather updates were incorporated. The MPEs of yields predictions from November 1st (July 1st) were 3% (12%) for the prediction using climatology alone, 5% (15%) for the prediction using one-month lead seasonal forecasts along with climatology and 6% (19%) for the prediction using one-and-two-month lead seasonal forecasts together with climatology. Similarly, the average correlation coefficients of yield predicted from November 1st (July 1st) were 0.99 (0.1) for the prediction using climatology alone, 0.97 (-0.1) for the prediction using one-month lead seasonal forecasts as well as climatology and 0.96 (0) for the prediction using one-and-two-month lead seasonal forecasts along with climatology.

Predicting yield within 5% error and with 99% correlation coefficient two-and-a-half months before harvest using climatology alone is an encouraging result. However, the predictions combining seasonal forecasts and climatology were less capable of predicting yields than were the one-month lead forecasts, as evident from the increase in MPE and the lower correlation coefficients as compared to the prediction using climatology alone. This justified using climatology alone rather than including seasonal forecasts. The worsening of skill by including seasonal forecasts were related to the poor quality of seasonal forecasts' daily data, particularly precipitation.

The study suggests to compare prediction skill using CFS v2's monthly mean and using WGs to generate daily data. We also recommend to explore the potential of using spatially downscaled precipitation data in improving prediction skill.

References

ABBASPOUR, K. C., HALL, J.W., MOON, D.E. 1992. A yield model for use in determining crop insurance premiums. *Agric. For. Meteorol.,* 60**,** 33-51.

ACHARYA, N., KULKARNI, M., MOHANTY, U. & SINGH, A. 2014. Comparative evaluation of performances of two versions of NCEP climate forecast system in predicting Indian summer monsoon rainfall. *Acta Geophysica,* 62.

AKHTAR, T., THAKUR, G., RAJAK, R. K., KHAN, S. U., GHIMIRE, S. P. & GHALE, G. Year. Rice varietal improvement works under irrigated sup tropical regions of Nepal. *In:* 24th Summer crop workshop 30-31 June 2004, 2004 National Rice Research Program Hardinath, Baniniya, Dhanusha. Nepal Agricultural Research Council Khumaltar.

ASHOK, K., GUAN, Z. Y. & YAMAGATA, T. 2001. Impact of the Indian Ocean Dipole on the relationship between the Indian monsoon rainfall and ENSO. *Geophysical Research Letters,* 28**,** 4499-4502.

BAIGORRIA, G. A., JONES, J. W. & O'BRIEN, J. J. 2008. Potential predictability of crop yield using an ensemble climate forecast by a regional circulation model. *Agricultural and Forest Meteorology,* 148**,** 1353-1361.

BAIGORRIA, G. A., JONES, J. W., SHIN, D., MISHRA, A. & BRIEN, J. J. 2007. Assessing uncertainties in crop model simulations using daily bias-corrected Regional Circulation Model outputs. *Climate Research,* 34**,** 211-222.

BANNAYAN, M., CROUT, N. M. J. & HOOGENBOOM, G. 2003. Application of the CERES-Wheat Model for Within-Season Prediction of Winter Wheat Yield in the United Kingdom. *Agronomy Journal,* 95**,** 114-125.

BATJES, N. H. 1995. A homogenized soil data file for global environmental research: a subset of FAO, ISRIC and NRCS profiles (version 1.0). *Working Paper and Preprint 95/10b.*

BATJES, N. H. 2002. A homogenized soil profile data set for global and regional environmental research. (WISE, version 1.1). Report 2002/01. Wageningen, The Netherlands: International Soil reference and Information Centre (ISRIC).

BERTIN, N., MARTRE, P., GÉNARD, M., QUILOT, B. & SALON, C. 2010. Under what circumstances can process-based simulation models link genotype to phenotype for complex traits? Case-study of fruit and grain quality traits. *Journal of Experimental Botany,* 61**,** 955-967.

BEVEN, K. & BINLEY, A. 1992. The future of distributed models: Model calibration and uncertainty prediction. *Hydrological Processes,* 6**,** 279-298.

BLANFORD, H. 1884. On the connection of Himalayan snowfall and seasons of drought in India *Proc R Soc Lond,* 37**,** 3-22.

BLASONE, R.-S., VRUGT, J. A., MADSEN, H., ROSBJERG, D., ROBINSON, B. A. & ZYVOLOSKI, G. A. 2008. Generalized likelihood uncertainty estimation (GLUE) using adaptive Markov Chain Monte Carlo sampling. *Advances in Water Resources,* 31**,** 630-648.

BOUMAN, B. & AUREUS, A. 2009. Every drop counts. *Rice Today.*: International Rice Research Institute. Los Banos, Laguna, Phillipines.

CABRERA, V. E., D. SOLIS, G. A. BAIGORRIA, AND D. LETSON (ed.) 2009. *Managing climate variability in agricultural analysis,* Inc. Hauppauge, NY: Nova Science Publishers.

CDD 2015. Rice Varietal Mapping in Nepal: Implication for development and adoption. Hariharvaban, Lalitpur, Nepal: Crop development directorate, Department of Agriculture, Ministry of Agricultural development.

CHAOUDHARY, D. K., MAHATO, B. P., SHRESTHA, L. L., THAKUR, G., GHALE, D. & GHIMIRE, K. H. Year. Rice varietal improvement for rainfed lowland areas in sub tropical region of Nepal. *In:* 24th Summer crop workshop, 2004 National Rice Research Program Hardinath, Baniniya, Dhanusha. Nepal Agricultural Research Council.

CHAUDHARI, H., POKHREL, S., MOHANTY, S. & SAHA, S. 2013. Seasonal prediction of Indian summer monsoon in NCEP coupled and uncoupled model. *Theoretical and Applied Climatology,* 114**,** 459-477.

DEE, D. P., UPPALA, S. M., SIMMONS, A. J., BERRISFORD, P., POLI, P., KOBAYASHI, S., ANDRAE, U., BALMASEDA, M. A., BALSAMO, G., BAUER, P., BECHTOLD, P., BELJAARS, A. C. M., VAN DE BERG, L., BIDLOT, J., BORMANN, N., DELSOL, C., DRAGANI, R., FUENTES, M., GEER, A. J., HAIMBERGER, L., HEALY, S. B., HERSBACH, H., HÓLM, E. V., ISAKSEN, L., KÅLLBERG, P., KÖHLER, M., MATRICARDI, M., MCNALLY, A. P., MONGE-SANZ, B. M., MORCRETTE, J. J., PARK, B. K., PEUBEY, C., DE ROSNAY, P., TAVOLATO, C., THÉPAUT, J. N. & VITART, F. 2011. The ERA-Interim reanalysis: configuration and performance of the data assimilation system. *Quarterly Journal of the Royal Meteorological Society,* 137**,** 553-597.

DUBROVSKÝ, M., ŽALUD, Z. & ŠŤASTNÁ, M. 2000. Sensitivity of Ceres-Maize Yields to Statistical Structure of Daily Weather Series. *Climatic Change,* 46**,** 447-472.

DUCHON, C. E. 1986. Corn Yield Prediction Using Climatology. *Journal of Climate and Applied Meteorology,* 25**,** 581-590.

FAOSTAT 2015. FAO statistics division, FAO Rome, Italy.

FRAISSE, C. W., BREUER, N. E., ZIERDEN, D., BELLOW, J. G., PAZ, J., CABRERA, V. E., GARCIA Y GARCIA, A., INGRAM, K. T., HATCH, U., HOOGENBOOM, G., JONES, J. W. &

O'BRIEN, J. J. 2006. AgClimate: A climate forecast information system for agricultural risk management in the southeastern USA. *Computers and Electronics in Agriculture,* 53**,** 13-27.

GADGIL, S., VINAYACHANDRAN, P. N., FRANCIS, P. A. & GADGIL, S. 2004. Extremes of the Indian summer monsoon rainfall, ENSO and equatorial Indian Ocean oscillation. *Geophysical Research Letters,* 31**,** L12213.

GHOSH, K., SINGH, A., MOHANTY, U. C., ACHARYA, N., PAL, R. K., SINGH, K. K. & PASUPALAK, S. 2014. Development of a rice yield prediction system over Bhubaneswar, India: combination of extended range forecast and CERES-rice model. *Meteorological Applications***,** n/a-n/a.

GIJSMAN, A. J., THORNTON, P. K. & HOOGENBOOM, G. 2007. Using the WISE database to parameterize soil inputs for crop simulation models. *Computers and Electronics in Agriculture,* 56**,** 85-100.

GOSWAMI, B. N., MADHUSOODANAN, M. S., NEEMA, C. P. & SINGUPTA, D. 2006a. A physical mechanism for North Atlantic SST influence on the Indian Summer Monsoon. *Geophysical Research Letters,* 33.

GOSWAMI, B. N., VENUGOPAL, V., SENGUPTA, D., MADHUSOODANAN, M. S. & XAVIER, P. K. 2006b. Increasing Trend of Extreme Rain Events Over India in a Warming Environment. *Science,* 314**,** 1442-1445.

HANSEN, J. W. 2002. Realizing the potential benefits of climate prediction to agriculture: Issues, approaches , challenges. *Agricultural System,* 74**,** 309-330.

HANSEN, J. W., POTGIETER, A. & TIPPETT, M. K. 2004. Using a general circulation model to forecast regional wheat yields in northeast Australia. *Agricultural and Forest Meteorology,* 127**,** 77-92.

HE, J., DUKES, M. D., JONES, J. W., GRAHAM, W. D. & JUDGE, J. 2009. Applying GLUE for Estimating CERES-Maize Genetic and Soil Parameters for Sweet Corn Production. *ASABE,* 52.

HE, J., JONES, J. W., GRAHAM, W. D. & DUKES, M. D. 2010. Influence of likelihood function choice for estimating crop model parameters using the generalized likelihood uncertainty estimation method. *Agricultural Systems,* 103**,** 256-264.

HOOGENBOOM, G. 2000. Contribution of agrometeorology to the simulation of crop production and its applications. *Agricultural and Forest Meteorology,* 103**,** 137-157.

HOOGENBOOM, G., J.W. JONES, P.W. WILKENS, C.H. PORTER, K.J. BOOTE, L.A. HUNT, U. SINGH, J.I. LIZASO, J.W. WHITE, O. URYASEV, R. OGOSHI, J. KOO, V. SHELIA & TSUJI., G. Y. 2015. Decision Support System for Agrotechnology Transfer (DSSAT) Version 4.6 (http://dssat.net). Prosser, Washington: DSSAT Foundation.

HOOGENBOOM, G., J.W. JONES, P.W. WILKENS, C.H. PORTER, K.J. BOOTE, L.A. HUNT, U. SINGH, J.L. LIZASO, J.W. WHITE, O. URYASEV, F.S. ROYCE, R. OGOSHI, A.J. GIJSMAN, G.Y. TSUJI & KOO, J. 2012. Decision Support System for Agrotechnology Transfer (DSSAT) Version 4.5 [CD-ROM]. Honolulu, Hawaii.: University of Hawaii.

ICHIYANAGI, K., YAMANAKA, M. D., MURAJI, Y. & VAIDYA, B. K. 2007. Precipitation in Nepal between 1987 and 1996. *International Journal of Climatology,* 27**,** 1753-1762.

IIZUMI, T., LUO, J.-J., CHALLINOR, A. J., SAKURAI, G., YOKOZAWA, M., SAKUMA, H., BROWN, M. E. & YAMAGATA, T. 2014. Impacts of El Niño Southern Oscillation on the global yields of major crops. *Nature Communications,* 5.

IRRI 2009. World Rice Statistics 2009 derived from FAO 2004-2006 Database - three years' average. International Rice Research Institute. Los Banos, Laguna, Phillipines.

IRRI 2010. Household survey data for Nepal collected under IFAD upland rice and STRASA (Stress tolerant rice for poor farmers in Africa and South Asia) projects. Social Sciences Division, International Rice Research Institute, Los Banos, Phillipines.

JHA, P. K., ATHANASIADIS, P. & GUALDI, S. 2016. *Chapter I: Evaluating the ability of the CMCC v1.5 and /CFS v2 Seasonal Prediction Systems (SPSs) for to predicting the South Asian Monsoon.* PhD thesis, University of Venice CA'Foscari.

JIMOH, O. D. & WEBSTER, P. 1996. The optimum order of a Markov chain model for daily rainfall in Nigeria. *Journal of Hydrology,* 185**,** 45-69.

JONES, C. A. & KINIRY, J. R. (eds.) 1982. *CERES-Maize: A Simulation Model of Maize Growth and Development,* College Station, Texas, TX: A&M University Press.

JONES, J. W., HOOGENBOOM, G., PORTER, C. H., BOOTE, K. J., BATCHELOR, W. D., HUNT, L. A., WILKENS, P. W., SINGH, U., GIJSMAN, A. J. & RITCHIE, J. T. 2003. The DSSAT cropping system model. *European Journal of Agronomy,* 18**,** 235-265.

KEATING, B. A., CARBERRY, P. S., HAMMER, G. L., PROBERT, M. E., ROBERTSON, M. J., HOLZWORTH, D., HUTH, N. I., HARGREAVES, J. N. G., MEINKE, H., HOCHMAN, Z., MCLEAN, G., VERBURG, K., SNOW, V., DIMES, J. P., SILBURN, M., WANG, E., BROWN, S., BRISTOW, K. L., ASSENG, S., CHAPMAN, S., MCCOWN, R. L., FREEBAIRN, D. M. & SMITH, C. J. 2003. An overview of APSIM, a model designed for farming systems simulation. *European Journal of Agronomy,* 18**,** 267-288.

KEULEN, H. V. & WOLF, J. 1986. *Modelling of agricultural production: weather, soils and crops,* Wageningen, Pudoc.

KUMAR, K. K., RAJAGOPALAN, B. & CANE, M. A. 1999. On the Weakening Relationship Between the Indian Monsoon and ENSO. *Science,* 284**,** 2156-2159.

LAMSAL, A., AMGAI, L. P. & GIRI, A. 2013. Modeling the sensitivity of CERES-Rice model: An experience of Nepal. *Agronomy Journal of Nepal,* 3**,** 11-21.

LEGATES, D. R. & MCCABE, G. J. 1999. Evaluating the use of "goodness-of-fit" Measures in hydrologic and hydroclimatic model validation. *Water Resources Research,* 35**,** 233-241.

LOAGUE, K. & GREEN, R. E. 1991. Statistical and graphical methods for evaluating solute transport models: Overview and application. *Journal of Contaminant Hydrology,* 7**,** 51-73.

LOBELL, D. B. 2013. The use of satellite data for crop yield gap analysis. *Field Crops Research,* 143**,** 56-64.

LOBELL, D. B., SCHLENKER, W. & COSTA-ROBERTS, J. 2011. Climate Trends and Global Crop Production Since 1980. *Science,* 333**,** 616-620.

LYNEIS, J. M. & PUGH, A. L. 1996. Automated vs. _hand_ calibration of system dynamics models: An experiment with a simple project model. *In:* RICHARDSON, G. P. & STERMAN, J. D. (eds.) *Proceedings of the 1996 International System Dynamics Conference.* Cambridge, MA: System Dynamics Society.

MAVROMATIS, T., BOOTE, K. J., JONES, J. W., WILKERSON, G. G. & HOOGENBOOM, G. 2002. Repeatability of Model Genetic Coefficients Derived from Soybean Performance Trials across Different States Florida Agricultural Experiment Station, Journal Series No. R-07981. *Crop Science,* 42**,** 76-89.

MIKHAIL, A. S. & FRANCISCO, J. D.-R. 2007. Utility of dynamical seasonal forecasts in predicting crop yield. *Climate Research,* 34**,** 71-81.

MISHRA, A., HANSEN, J. W., DINGKUHN, M., BARON, C., TRAORÉ, S. B., NDIAYE, O. & WARD, M. N. 2008. Sorghum yield prediction from seasonal rainfall forecasts in Burkina Faso. *Agricultural and Forest Meteorology,* 148**,** 1798-1814.

MOAC 2008. Statistical informaton on Nepalese Agriculture, 2008/09, Government of Nepal, Ministry of Agricultural Development, Agribusiness Promotion and Statistics Division, Singh Durbar, Kathmandu,Nepal.

MOAD 2012. Statistical informaton on Nepalese Agriculture, 2011/12, Government of Nepal, Ministry of Agricultural Development, Agribusiness Promotion and Statistics Division, Singh Durbar, Kathmandu,Nepal.

PAL, R. K., SEHGAL, A. K., MISRA, A. K., GHOSH, K., MOHANTY, U. C. & RANA, R. S. 2013. Application of Seasonal Temperature and Rainfall Forecast for Wheat Yield Prediction for Palampur, Himachal Pradesh *International Journal of Agriculture and Food Science Technology,* 4**,** 453-460.

PARIYAR, D. 1998. Country Pasture/Forage Resource Profiles Nepal. FAO Rome, Italy.

PAZ, J. O., FRAISSE, C. W., HATCH, L. U., GARCIA Y GARCIA, A., GUERRA, L. C., URYASEV, O., BELLOW, J. G., JONES, J. W. & HOOGENBOOM, G. 2007. Development of an ENSO-based irrigation decision support tool for peanut production in the southeastern US. *Computers and Electronics in Agriculture,* 55**,** 28-35.

POKHREL SAMIR, DHAKATE, A., CHAUDHARI, H. S. & SAHA, S. K. 2013. Status of NCEP CFS vis-a-vis IPCC AR4 models for the simulation of Indian summer monsoon. *Theor. Appl Climatol,* 11**,** 65-78.

RAI, Y. K., ALE, B. B. & ALAM, J. 2011. Impact Assessment of Climate Change on Paddy Yield: A Case Study of Nepal Agriculture Research Council (NARC),Tarahara, Nepal. *Journal of the Institute of Engineering,* 8**,** 147-167.

RAMESH, K. V. & GOSWAMI, P. 2007. Reduction in temporal and spatial extent of the Indian summer monsoon. *Geophysical Research Letters,* 34**,** n/a-n/a.

RAY, D. K., GERBER, J. S., MACDONALD, G. K. & WEST, P. C. 2015. Climate variation explains a third of global crop yield variability. *Nature Communications,* 6, 5989.

RITCHIE, J. T., SINGH, U., GODWIN, D. C. & BOWEN, W. T. 1998. Cereal growth, development and yield. *In:* TSUJI, G. Y., HOOGENBOOM, G. & THORNTON, P. K. (eds.) *Understanding Options for Agricultural Production.* Dordrecht: Springer Netherlands.

ROMERO, C. C., HOOGENBOOM, G., BAIGORRIA, G. A., KOO, J., GIJSMAN, A. J. & WOOD, S. 2012. Reanalysis of a global soil database for crop and environmental modeling. *Environmental Modelling & Software,* 35**,** 163-170.

SAHA, S., NADIGA, S., THIAW, C., WANG, J., WANG, W., ZHANG, Q., DOOL, H. M. V. D., PAN, H.-L., MOORTHI, S., BEHRINGER, D., STOKES, D., PEÑA, M., LORD, S., WHITE, G., EBISUZAKI, W., PENG, P. & XIE, P. 2006. The NCEP Climate Forecast System. *Journal of Climate,* 19**,** 3483-3517.

SAJI, N. H., GOSWAMI, B. N., VINAYACHANDRAN, P. N. & YAMAGATA, T. 1999. A dipole mode in the tropical Indian Ocean. *Nature,* 401**,** 360-363.

SCHMIDT, G. M., SMAJSTRLA, A. G. & ZAZUETA, F. S. 1996. Parametric uncertainty in stochastic precipitation models: wet day amounts. *Transactions of the ASAE,* 39**,** 2093-2103.

SHIN, D. W., BAIGORRIA, G. A., LIM, Y.-K., COCKE, S., LAROW, T. E., O'BRIEN, J. J. & JONES, J. W. 2010. Assessing Maize and Peanut Yield Simulations with Various Seasonal Climate Data in the Southeastern United States. *Journal of Applied Meteorology and Climatology,* 49**,** 592-603.

SHRESTHA, A. B., WAKE, C. P., DIBB, J. E. & MAYEWSKI, P. A. 2000. Precipitation fluctuations in the Nepal Himalaya and its vicinity and relationship with some large scale climatological parameters. *International Journal of Climatology,* 20**,** 317-327.

SOLER, C. M. T., SENTELHAS, P. C. & HOOGENBOOM, G. 2007. Application of the CSM-CERES-Maize model for planting date evaluation and yield forecasting for maize grown off-season in a subtropical environment. *European Journal of Agronomy,* 27**,** 165-177.

TANNER, C. B. & SINCLAIR, T. R. 1983. Efficient Water Use in Crop Production: Research or Re-Search?1. *In:* TAYLOR, H. M., WAYNE, J. R. & THOMAS, S. R. (eds.) *Limitations to Efficient Water Use in Crop Production.* Madison, WI: American Society of Agronomy, Crop Science Society of America, Soil Science Society of America.

THOMPSON, L. M. 1969a. Weather and technology in the production of corn in the US corn belt. *Agron. J.,* 61**,** 453-456.

THOMPSON, L. M. 1969b. Weather and technology in the production of wheat in the United States. *J. Soil Water Conserv.,* 24.

THORNTON, P. K., BOWEN, W. T., RAVELO, A. C., WILKENS, P. W., FARMER, G., BROCK, J. & BRINK, J. E. 1997. Estimating millet production for famine early warning: an application of crop simulation modelling using satellite and ground-based data in Burkina Faso. *Agricultural and Forest Meteorology,* 83**,** 95-112.

TIMSINA, J. & HUMPHREYS, E. 2006. Performance of CERES-Rice and CERES-Wheat models in rice–wheat systems: A review. *Agricultural Systems,* 90**,** 5-31.

WALLACH, D., GOFFINET, B., BERGEZ, J.-E., DEBAEKE, P., LEENHARDT, D. & AUBERTOT, J.-N. 2001. Parameter Estimation for Crop Models. *Agronomy Journal,* 93**,** 757.

WILLMOTT, C. J. 1982. Some Comments on the Evaluation of Model Performance. *Bulletin of the American Meteorological Society,* 63**,** 1309-1313.

WILLMOTT, C. J., ACKLESON, S. G., DAVIS, R. E., FEDDEMA, J. J., KLINK, K. M., LEGATES, D. R., O'DONNELL, J. & ROWE, C. M. 1985. Statistics for the evaluation and comparison of models. *Journal of Geophysical Research: Oceans,* 90**,** 8995-9005.

WORLDBANK 2015. Fertilizer consumption rate (kg/ha) of arable land. Data catalogue of the World Bank datasets. The World Bank Group

YATAGAI, A., KAMIGUCHI, K., ARAKAWA, O., HAMADA, A., YASUTOMI, N. & KITOH, A. 2012. APHRODITE: Constructing a Long-Term Daily Gridded Precipitation Dataset for Asia Based on a Dense Network of Rain Gauges. *Bulletin of the American Meteorological Society,* 93**,** 1401-1415.

CHAPTER III: Using ENSO conditions to optimize rice crop management for Nepal's Terai

Abstract

Seasonal prediction systems (SPSs) are gradual improving in terms of their ability to predict the El Nino Southern Oscillation (ENSO). This advance provides an opportunity to link the coming season's weather with dynamic crop models to evaluate various crop management options. Assessment of these crop management approaches can help farmers to make better decisions before the beginning of the planting season. Although the potential benefits of this approach have been tested in many areas of the world, to our knowledge, limited scientific evidence exists regarding its application in South Asian (SA) regions. Most rice cultivation in SA regions remains rainfed and is heavily reliant on monsoon rainfall. By incorporating ENSO- and rainfall-based weather categories into the Decision Support System for Agrotechnology Transfer's (DSSAT) v4.6 Cropping System Model (CSM) Crop Estimation through Resource and Environment Synthesis (CERES)-Rice crop model, this study evaluates planting dates and fertilizer levels for Nepal's Terai region. The Terai is Nepal's principal rice-growing region, and the majority of its lands are still under rainfed cultivation. The model simulations indicated that rice yields were higher in below-average rainfall (dry) years and in El Nino years. Moreover, rice yields were lower in above-average (wet) rainfall years and La Nina years. Rice yields increased as additional Nitrogen (N) fertilizer was added, but they decreased with late planting from 14 June onwards. The lower yields during La Nina and wet years were associated with high (low) N leaching (uptake) resulting from high drainage and runoff levels. Furthermore, the reduced yields in La Nina years were also related to a high minimum temperature anomaly during the second half of growing season. However, the addition of fertilizer increased yields in all years, although the efficiency of fertilizer use was greater in dry years and El Nino years than at other times. Considering the existing practices of mid-July planting and low-level N fertilizer application, rice yields could be increased in an efficient manner by adding N fertilizer in dry years and El Nino years, and by adopting earlier planting dates. In El Nino years, a 14 June planting date, coupled with an increase in fertilizer to 90 kg/ha and 60 kg/ha, resulted in net gross margins of US$ 34/ha and US$ 15/ha, respectively, as compared with similar changes in other years. These results should be taken as indicative only as the ENSO signal was not strong in the study area, and soil profiles were based on reanalysis data.

Keywords: ENSO, DSSAT, Terai, rice, planting date, fertilizer

III.1 Introduction

Climate variability is a major sources of interannual crop yield variability, explaining roughly a third of the observed yield variability globally (Ray et al., 2015). The high interannual variability in weather variables, including rainfall, constitutes the primary obstacle that limits risk-averse farmers from fully realising their farms' potentials. This is particularly true for rainfed farming systems and for crops requiring high amounts of water. The uncertainty associated with climate variability and unpredictability compel risk-averse farmers to adopt low risk strategies than those which are more profitable on average.

As dynamic climate models gradually become more skilled at ENSO prediction, crop models can be run using historical weather data representing ENSO categories for a particular year. By utilizing a crop model to evaluate alternative crop-management options for given weather categories, farmers' optimum management options for the coming growing season can be identified (Hoogenboom, 2000). This knowledge will help famers to optimize their farming management techniques. Intensifying inputs (fertilizers) and technologies during favourable weather, while simultaneously preventing resource losses during unfavourable weather, will allow farmers to achieve maximum potential production.

The ENSO is irregular variations in sea surface temperature (SST) and wind in the equatorial Pacific, and its effect can be felt around much of the globe. Various studies have demonstrated that positive ENSO phases – a condition called El Nino – are associated with low levels of summer monsoon rainfall in SA regions. Similarly, negative ENSO phases – a condition called La Nina – are associated with increased rainfall during the summer monsoon season (Sikka, 1980; Shukla, 1987; Rasmusson and Carpenter, 1983). Thus, ENSO prediction, along with dynamic crop models' use of predicted ENSO categories to evaluate management options, has substantial potential to increase production and to minimize input losses for regions like Nepal's Terai. We selected the Terai, because rice is the main staple food in Nepal (MOAD, 2012), and the Terai is the country's primary rice-growing region (MOAC, 2008). Moreover, rice production requires significant amounts of water (Bouman and Aureus, 2009) and the Terai is home to the majority of Nepal's rainfed rice cultivation areas (MOAC, 2008).

The ENSO's exact effect on the monsoon in Nepal's Terai region is unclear. Shrestha et al. (2000) found a strong positive (0.64) correlation between the average annual Southern Oscillation Index (SOI) and all-Nepal summer monsoon precipitation for the period from 1970 to 1994. In contrast, Ichiyanagi et al. (2007) established a weak positive relationship between the SOI and the summer monsoon precipitation for the weather stations in western Terai and negative correlation for the weather stations in eastern Terai from 1987 to 1996. They also demonstrated that monsoon precipitation significantly varied across regions of Nepal. While Shrestha et al. (2000) found the relationship became stronger after 1970, Kumar et al. (1999) wrote that the relationship has weakened in recent years. Therefore, it is necessary to revisit the

relationship between the ENSO and monsoon precipitation in Terai. Additionally, dynamic climate models' ability to predict the ENSO for Nepal's Terai region must be assessed before ENSO is employed as a planning tool.

Various studies have determined that advance information on the coming season's ENSO phase can be utilized as a planning tool to optimize farm management practices, so as to increase yields and profits (Jones et al., 2000; Asseng et al., 2012). The ENSO's influence on rice yields varies, not only across global regions, but also within individual countries. For example, rice yields in southern (other) China are negatively (positively) affected during El Nino years (Iizumi et al., 2014). The economic value of forecasting information varies across regions and crops, and quantitative assessments of forecast values for smallholder rainfed farmers in developing countries are virtually absent (Meza et al., 2008).

Crop growth does not depend solely on rainfall. Therefore, even if the ENSO and precipitation are not strongly related, crop yield could be different due to other weather variables such as temperature as crops are the integrator.

The chapter's objectives are to reassess the link between the ENSO and the summer monsoon and ENSO's predictability for Nepal's Terai region. After evaluating the ENSO-monsoon link and predictability, the study's second objective is to evaluate how various crop management options affect rice yields for different ENSO phases, using the CERES-RICE model of the DSSAT v4.6 (Hoogenboom et al., 2015), with the aim of maximizing crop yield while minimizing the loss of inputs.

III.2 Methods

III.2.1 Climate data

To examine the relationship between the ENSO and the monsoon in the Terai, the observed Nino 3.4 seasonal (JJAS) anomaly for the period from 1982 to 2005 was calculated from the NOAA Reynold v2 SST (Reynolds and Smith, 1994). The ensemble means of the monthly SST forecasts, which were based on May initializations, were taken from the Centro Euro-Mediterraneo sui Cambiamenti Climatici Version 1.5 (CMCC v1.5) (Borrelli et al., 2012) and the coupled forecast system model version 2 (CFS v2) (Saha et al., 2010). Seasonal (JJAS) Nino 3.4 index anomalies for both CMCC v1.5 and CFS v2 were calculated from their corresponding SSTs.

Similarly, the observed precipitation data were taken from different sources including the Global Precipitation Climatology Project (GPCP) (Adler et al., 2003) and the Asian Precipitation - Highly-Resolved Ob-

servational Data Integration Towards Evaluation (APHRODITE) (Yatagai et al., 2012). Finally, daily precipitation data came from four Department of Hydrology and Meteorology (DHM) weather stations: Janakpur, Parwanipur, Bhairahawa, and Nepalgunj. The standardized monsoon-season (JJAS) precipitation anomaly was calculated separately from these data for every year. These standardized values were then correlated with the Nino 3.4 index.

III.2.2 Categorizing years

III.2.2.1 On the basis of ENSO phase

There is no consensus regarding the most appropriate index for ENSO phase classification (Hanley et al., 2003). Some common indexes used for ENSO classification include: the SOI (Stone et al., 1996), the Nino 3.4 index (Trenberth and Stepaniak, 2001) and the Japan Meteorological Agency (JMA) Index (Hanley et al., 2003). In the context of the weakening relationship between the ENSO and the Indian monsoon, (Kumar et al. (1999) demonstrated that the central equatorial Pacific's SST anomaly is becoming more effective at predicting the Indian monsoon (Kumar et al., 2006). The Nino 3.4 (5^{o}N-5^{o}S, 120^{o}-170^{o}W) index more accurately represents the central equatorial Pacific region than does the Nino 3.0 (5^{o}N-5^{o}S, 150^{0}W-90^{0}W) (Trenberth and Stepaniak, 2001).

In this study, the seasonal (JJAS) average of the Nino 3.4 index anomalies assigned rice growing seasons to the El Nino (La Nina) phase for anomalies at or above (at or below) 0.5^{0}C. The historical years were categorized as El Nino, La Nina or Neutral years based on the above threshold (Table III.1).

Table III.1: ENSO classification following the mean seasonal (JJAS) anomalies for Nino 3.4 index from 1983 to 2010

El Nino	1987, 1991, 1997, 2002, 2009
La Nina	1984, 1985, 1988, 1989, 1998, 1999, 2000, 2010
Neutral	1983, 1986, 1990, 1992, 1993, 1994, 1995, 1996, 2001, 2003, 2004, 2005, 2006, 2007, 2008

III.2.2.2 On the basis of rainfall amount

Because the ENSO signal had a weak link with rainfall at many stations, we repeated the simulations by categorizing historical years according to their average annual rainfall. Years with above-average rainfall (based on the standardized normal anomaly >0.5), were defined as wet years. Similarly, years with below-average rainfall (based on the standardized normal anomaly <-0.5) were deemed dry years, while years with rainfall within the standardized normal anomaly (between -0.5 to 0.5) were described as normal years (Table III.2).

Table III.2: Year categories based on the standardized normal anomaly of seasonal (JJAS) rainfall from 1983 to 2010.

Dry	1983, 1985, 1987, 1991, 1992, 1993, 1994, 2002, 2004, 2006
Wet	1984, 1988, 1989, 1996, 1998, 1999, 2001, 2003, 2010
Normal	1986, 1990, 1995, 1997, 2000, 2005, 2007, 2008, 2009

II.2.2.3 Relation between ENSO and precipitation

In order to understand the interaction between ENSO signal and precipitation in our study area, we categorized years based on both ENSO phases and precipitation categories. From the categorization, we found that neither all El Nino years were dry years nor all La Nina years were wet years. For example, 1997 and 2009 were El Nino years but were normal in terms of precipitation (Table III.3). Similarly, 1985 was a La Nina year but was dry and 2000 was a La Nina year but was normal in terms of precipitation. On the other hand, the ENSO-Neutral years were on all categories in terms of precipitation but majority of them were either dry or normal.

Table III.3: Year categories based on ENSO phases and precipitation combined.

	El Nino	**La Nina**	**Neutral**
Dry	1987, 1991, 2002	1985	1983, 1992, 1993, 1994, 2004, 2006
Wet		1984, 1988, 1989, 1999, 2010	1996, 2001, 2003
Normal	1997, 2009	2000	1986, 1990, 1995, 2005, 2007, 2008

III.2.3 Crop model

The DSSAT v4.6's CERES-RICE model (Hoogenboom et al., 2015) was run using the Seasonal Analysis tool for the historical weather years that are representatives of ENSO events, to determine rice yield's sensitivity to N fertilizer levels and to different planting dates. The DSSAT v4.6 is a dynamic model that simulates plant growth, development, yield, soil water and N balance, based on the daily crop development process for a particular location (Jones et al., 2003). The model employs user-specified inputs to calculate dynamic variables using various modules, sub modules and a main program.

All simulations assumed rainfed conditions and focused on the Masuli cultivar. We selected the Masuli cultivar, because it is grown in the Terai, and previous studies have used the CERES-RICE model to calibrate its genetic coefficients for Terai (Timsina and Humphreys, 2006; Lamsal et al., 2013). We designed 20 individual treatments to examine how the planting date and N fertilizer level affected yields, soil N

levels, and the water balance in different weather-year categories. These 20 treatments included five planting dates (at two-week intervals, starting from 14 June) and four N fertilizer levels (0 kg/ha, 30 kg/ha, 60 kg/ha, and 90 kg/ha). The N fertilizer was applied in two phases: once during planting, and again at 25 days post-planting. We selected the initial planting date of 14 June, because in rainfed systems, rice transplanting starts after the monsoon's onset. Considering onset of monsoon in Kerala in 1 June and time needed for monsoon to arrive in Nepal, June 14 is taken as the start date. Further, rice is not commonly planted after mid-August in Terai.

In all simulations, 25-days-old transplants were planted at a depth of three centimetres (cm) and at a rate of two plants per hill. All simulations assumed a soil temperature of 30^0C, a row spacing of 20 cm x 20 cm, and a planting density of 25 plants per square metre (Akhtar et al., 2004). The representative soil type for the Terai, CMNP002, was taken from the World Inventory of Soil Emission Potentials (WISE) database (Gijsman et al., 2007; Batjes, 2002), which was also available in DSSAT v 4.6 format. The soils'(all layers) stable organic carbon percentage was fixed to 90%, the initial soil water was set at half of the field's capacity and no initial soil N was assumed at the start of simulations. Daily weather data from Bhairahawa airport weather station were utilized for the simulations, as strong ENSO signal was found for that station. The model was run using the DSSAT v 4.6's default simulation option, except that the organic matter simulation made use of the Century option. For each planting date, the simulation began exactly one month before the day of planting. DSSAT v4.6 has adapted the Ritchie's soil water balance model for use by all crop models (Ritchie and Otter, 1985) (Ritchie, 1998). Daily rainfall was portioned into runoff and infiltration using the Soil Conservation Service (SCS) method (S.C.S, 1972). For each weather-year category, simulated yields, soil water, and N were then compared to identify the effects of the different management options.

III.2.4 Informal discussion

In order to understand the existing rice-cultivation practices, informal discussions were held with farmers from the Terai's Dhanusha district. The goal of the conversations was to learn more about rice planting dates, N fertilizer application, fertilizer costs, and rice prices in the Terai's local market. Biases related to rapport building were minimal, because the respondents had been acquainted with the researcher for the last 30 years. Moreover, as the researcher was born in Dhanusha district and completed school there, he had insight into the existing rice cultivation practices. The information from these discussions was then verified using the available literature.

III.3 Results and Discussion

III.3.1 How strong is the ENSO signal in the study area?

We found the strong negative correlation between seasonal (JJAS) anomalies of the Nino 3.4 index and precipitation from the GPCP for Nepal from 1982 to 2005. The correlation coefficients varied from -0.5 to -0.8 except some regions (7 of the 30 grid boxes) in the Eastern Terai and Eastern Mid mountains, where relationship was weaker (Fig. I.12 Chapter I). Results for the APHRODITE daily precipitation data were consistent with those for the GPCP data. Again the correlation coefficients were stronger for western Nepal than for eastern Nepal. The correlation coefficients were -0.6 for the weather stations (Bhairahawa airport and Tikapur) in the western Terai and -0.2 for the eastern weather stations (Janakpur airport and Parwanipur). In contrast, when weather station data from the DHM was used, the relationship was only strong for the Bhairahawa airport station (correlation coefficient -0.6) and weak-to-very-weak (correlation coefficients -0.1 to -0.2) for the other three stations for the period 1983 to 2010. Therefore, Bhairahawa airport weather station data was used for crop model simulation.

III.3.2 Can we predict ENSO?

The models, the CFS v2 and the CMCC v1.5, successfully captured the negative correlation between the ENSO and the summer monsoon in the SA region. The correlation coefficients between the models' simulated seasonal (JJAS) Nino 3.4 index anomalies and all-India region average precipitation were -0.6 and -0.5 for the CFS v2 and the CMCC v1.5, respectively.

For Nepal, the CFS v2 model came closer to the observed data in capturing the relationship between the ENSO and the summer monsoon. It established a weak to non-existent relationship in the Eastern Terai and a negative relationship for other areas, including a strong, negative relationship in Western Nepal (correlation coefficients varying from -0.4 to -0.8). The CMCC v1.5 model exhibited an unrealistically strong and positive relationship between the two variables in some parts of the Eastern Terai and near the Indo-Nepal border in the east. Both models simulated the Nino 3.4 index very closely. The correlation coefficients between the observed and model-simulated seasonal (JJAS) Nino 3.4 index anomalies from May initializations were 0.8 and 0.7 for the CFS v2 and the CMCC v1.5, respectively. Thus, it is expected that these models can predict the ENSO from May initializations fairly well. Failures occurred in years when SSTs in the Nino 3.4 region drastically changed after May, resulting in an ENSO phase change (Torrence and Webster, 1998).

However, not all El Nino years were drier, as the ENSO explains only a part of the interannual variability. Other sources of variability include: snow cover variations over Eurasia (Blanford, 1884), the North Atlantic Ocean circulation (Goswami et al., 2006), Indian Ocean dipole (Saji et al., 1999; Ashok et al.,

2001) and internal dynamics (Krishnamurthy and Shukla, 2000; Cherchi and Navarra, 2003).

III.3.2 Weather conditions

On average, the monsoon onset was earlier in La Nina years than in other years, as demonstrated by the higher rainfall amounts in June in La Nina years (Fig III.1). Additionally, the seasonal total rainfall amount was higher in La Nina years. In contrast, El Nino years were drier than others.

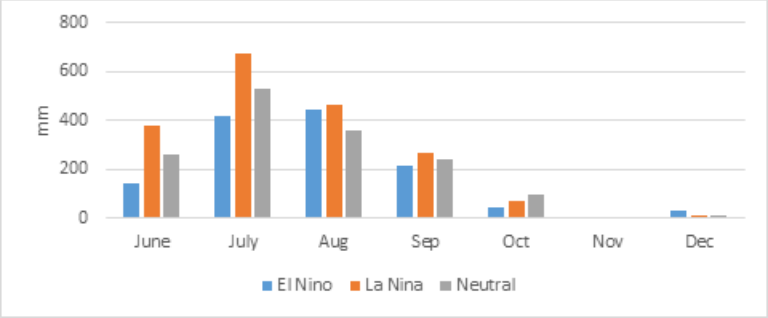

Fig III.1 Monthly mean precipitation (mm) for Bhairahawa from 1983 to 2010 for each ENSO phase.

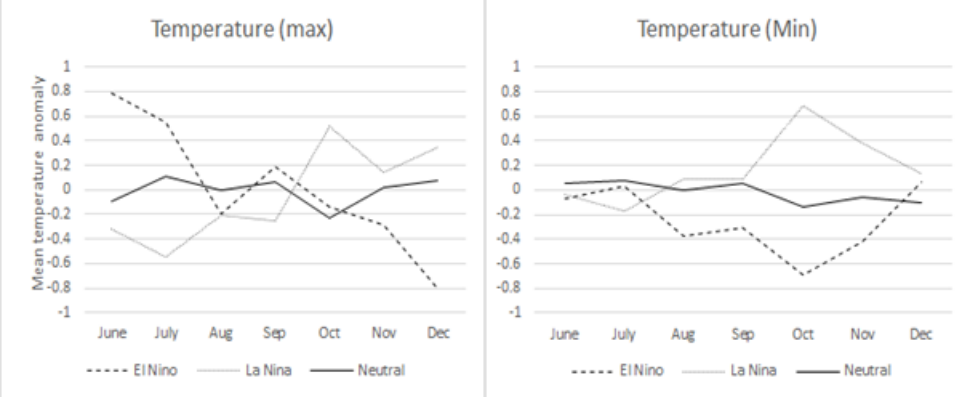

Fig III.2 Monthly mean temperature anomaly (^{0}C) for Bhairahawa, from 1983 to 2010, for: (a) average maximum temperature and (b) average minimum temperature for each ENSO phases - El Nino phase (dashed line), La Nina phase (dotted line) and Neutral phase (solid line).

The El Nino (La Nina) years had a positive (negative) maximum temperature anomaly (Fig. III.2). The highest maximum temperature anomaly of 0.8 ^{0}C (-0.6 ^{0}C) occurred during June (July) in El Nino (La Nina) years. The trend, however, reversed after the second half of the growing season.

The El Nino years displayed a negative minimum temperature anomaly during the entire growing season, with a maximum value of -0.7 ^{0}C in October (Fig.III.2). In contrast, La Nina years had a positive minim-

um temperature anomaly from August onwards, which reached a maximum (0.7 ^{0}C) in October.

These temperature and rainfall variations contributed to differences in yields across the ENSO phases.

III.3.3 Effect of weather, fertilizer and planting date on yields

III.3.3.1 Wet/dry categories

In general, rice yield was higher in dry years, average in normal years and lower in wet years for all fertilizer application levels and planting dates (Fig. III.3). These results are in alignment with the findings from Mavromatis et al. (2002), who achieved higher peanut yields in La Nina years with below-average rainfall. Regardless of the year, rice yields depended on the amount of N fertilizer applied and on the planting date. Normally, yields increased in proportion to amount of the N fertilizer utilized. Furthermore, yields slightly decreased for planting dates after 14 June, and sharply declined for planting dates after 28 June.

Thus, the average highest yield 2,578 kg/ha, was obtained in dry years under 90 kg N/ha for the crops planted on 14 June. And, the lowest yield, 64 kg/ha was produced in wet years with without N fertilizer for crops planted on 14 June. Fig. III.3 illustrates interannual variations in rice yields for different categories of years, corresponding to various fertilizer application levels and planting dates.

Interannual variability in rice yields, demonstrated by the box heights, was high, particularly during dry years with late planting dates and high N fertilizer levels. Therefore, we have more confidence that yields increased in dry years with higher levels of fertilizer and early planting dates than that late planting dates led to declining yields.

In Nepal rice planting usually starts from July's so called "plantation day" *(Ropain Diwas in Nepali*), peaks in mid-July and ends in July. Moreover, under existing practices, farmers apply less than 90 kg/ha of N fertilizer. Thus, rice yields in the Terai could be increased with an earlier planting date (approximately 14 June) and by amplified N fertilizer application, regardless of weather categories. However, any conclusions of this type should be first tested and verified by research stations locally.

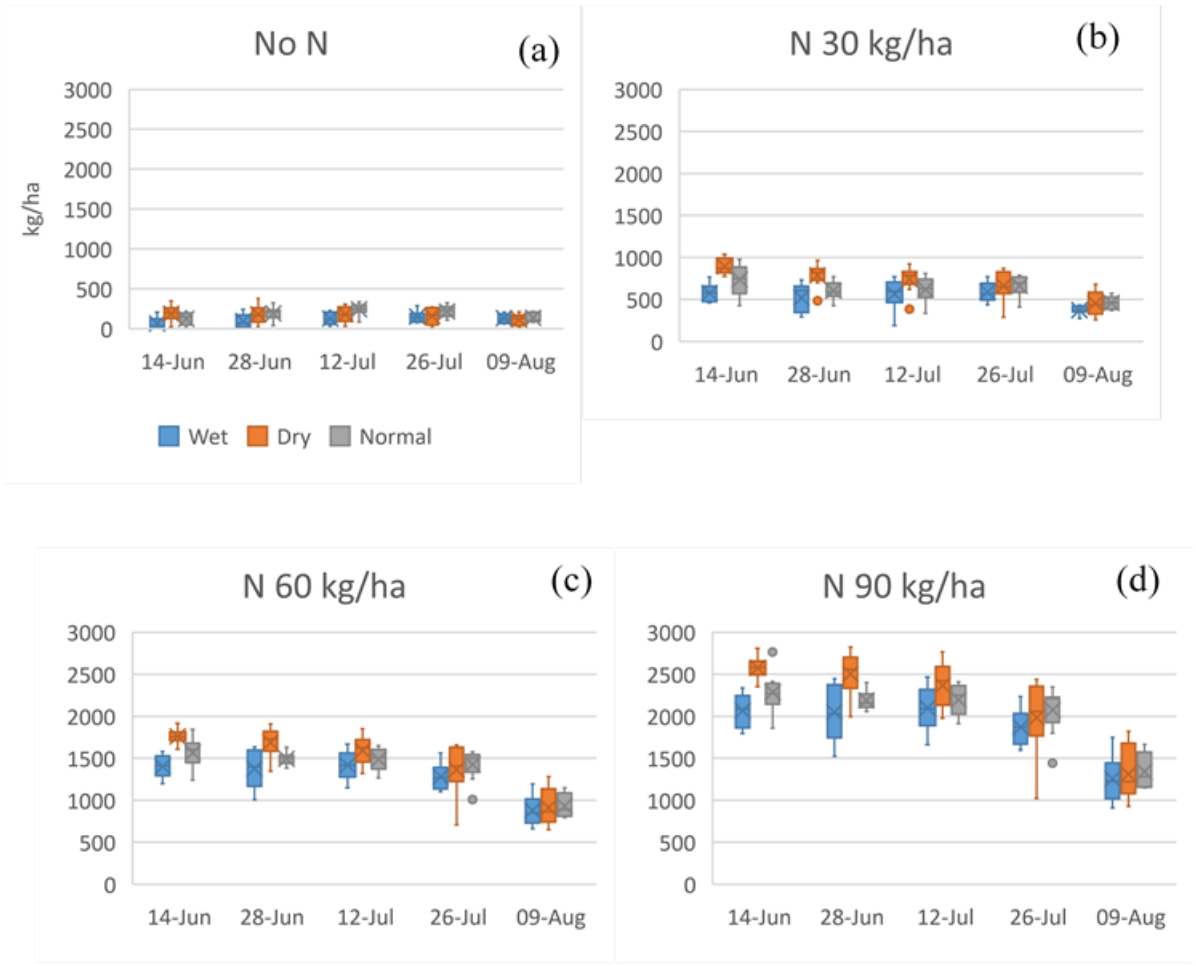

Fig. III.3 Simulated yield as a function of planting date and rainfall for: (a) without N fertilizer, (b) 30 kg/ha N fertilizer, (c) 60 kg/ha N fertilizer, and (d) 90 kg/ha N fertilizer for Bhairahawa station from 1983 to 2010.

III.3.3.2 ENSO categories

In general, rice yields were higher in El Nino years and lower in the La Nina years, with the Neutral years in the middle (Fig. III.4). These results agreed with findings by Mavromatis et al. (2002), who found higher peanut yields in La Nina years with below-average rainfall. Moreover, rice yields also depended on the planting date and on the amount of N fertilizer was applied. Normally, yields increased in proportion to the amount of N fertilizer applied but decreased slightly if planted after 14 June, and fell sharply for planting dates after 28 June.

Thus, the average highest yield, 2,512 kg/ha, was obtained in El Nino years under 90 kg N/ha for crops planted on 14 June. And, the lowest yield, 83 kg/ha, was produced in La Nina years without N fertilizer for crops planted as late as 14 June. Fig. III.4 depicts rice yields in different years, corresponding to various fertilizer application levels and planting dates.

The lower yields in La Nina years were associated with above-average minimum temperature during the latter parts of the growing season, high (low) N leaching (uptake) and above-average rainfall. Peng et al. (2004) also found that rice yields declined as minimum night-time temperatures (T_{min}) increased.

The interannual variability in rice yield was lower in El Nino years than other years, particularly for the early planting dates. As a result, it is more certain that the selection an earlier planting date and the application of additional N fertilizer can increase rice yields in El Nino years than that other year categories and later planting dates.

In light of these findings and existing planting practices, rice yields could be increased in the Terai if earlier planting dates (approximately 14 June) were adopted and if N fertilizer levels were increased, regardless of weather categories. However, these practices would have a higher likelihood of leading to greater yields and profits in El Nino years. The use of additional N fertilizer would be more profitable in El Nino years than in other years, because the marginal increase in yields due to the extra fertilizer would be higher during those years. Yet, these conclusions should be first verified by research stations before farmers are advised accordingly.

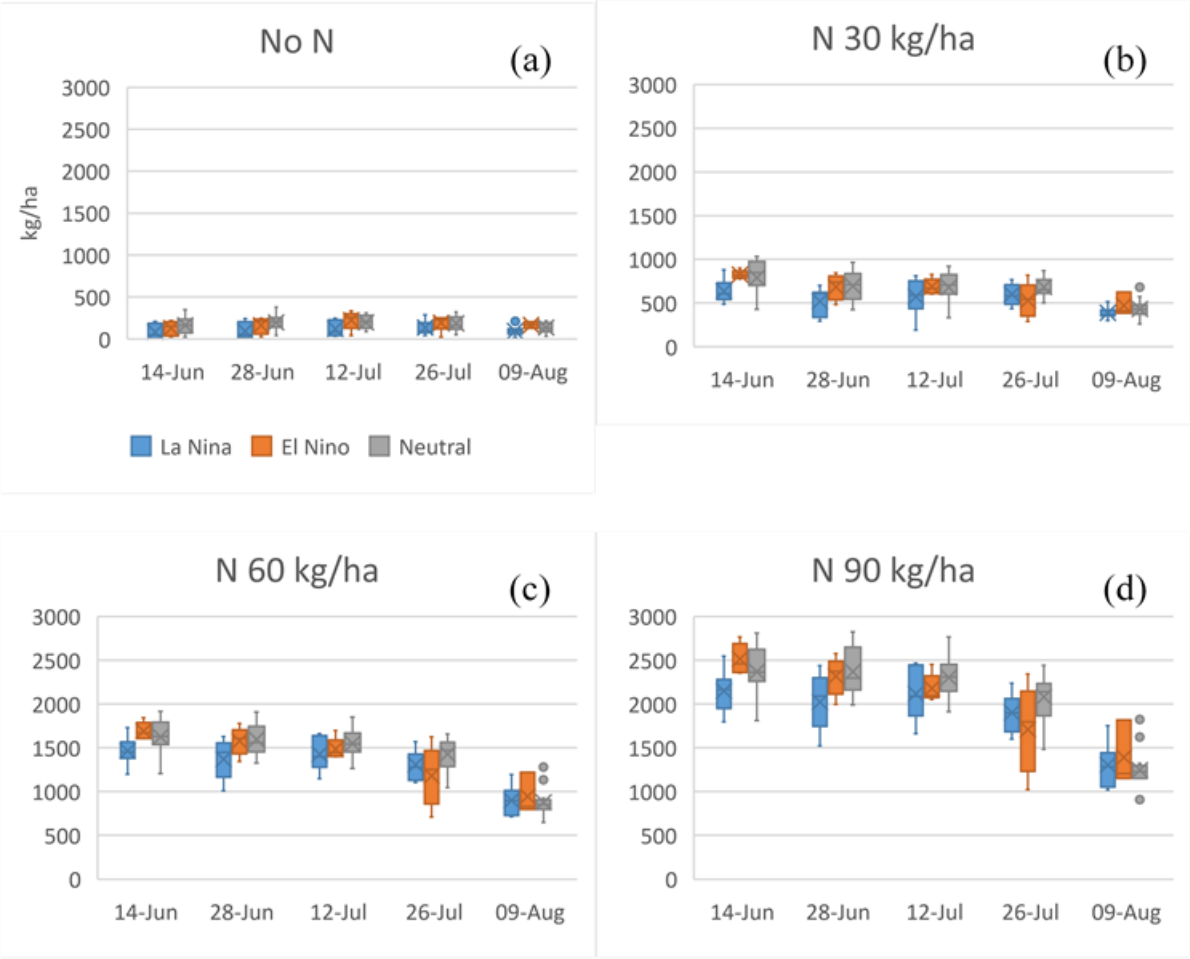

Fig. III.4 Simulated yield as a function of planting date and ENSO phases for: (a) without N fertilizer, (b) 30 kg/ha N fertilizer, (c) 60 kg/ha N fertilizer, and (d) 90 kg/ha N fertilizer for Bhairahawa station from 1983 to 2010.

To investigate the causes behind the low yields realised in wet years and Lan Nina years, we analysed the model-simulated N leaching from the soil and plants' N uptake for the various weather-year categories. Similarly, we conducted a separate evaluation of simulated drainage and runoff for the different categories of years.

III.3.4 Effect of precipitation on Nitrogen leaching

III.3.4.1 Wet/dry categories

N leaching increased in proportion to the amount of rainfall, as evident from the fact that N leaching was higher in above-average rainfall years, medium during normal years and low during below-average years (Fig. III.5). Mavromatis et al. (2002) also found 15-40 % more N leaching in the cropping season

followed by an El Nino phase with above-average rainfall. The rate of N leaching gradually declines if planting is delayed past 14 June, but it increases disproportionally as additional N fertilizer is added.

The highest N leaching rate, 38 kg/ha, occurred in the above-average rainfall years for the crops planted on 14 June with 90 kg N/ha. The lowest N leaching rate, 7 kg/ha, occurred during dry years for crops planted on 09 August without N fertilizer application. The yearly variations in N leaching, according to different fertilizer application levels and planting dates, are illustrated in Fig. III.5. The interannual variabilities in N leaching, depicted by the height of the boxes, increased as fertilizer was added.

These findings imply that it is less efficient to use high levels of N fertilizers in wet years and normal years. In order words, increasing N fertilizer levels more efficiently boosts rice yields in dry years than in other years.

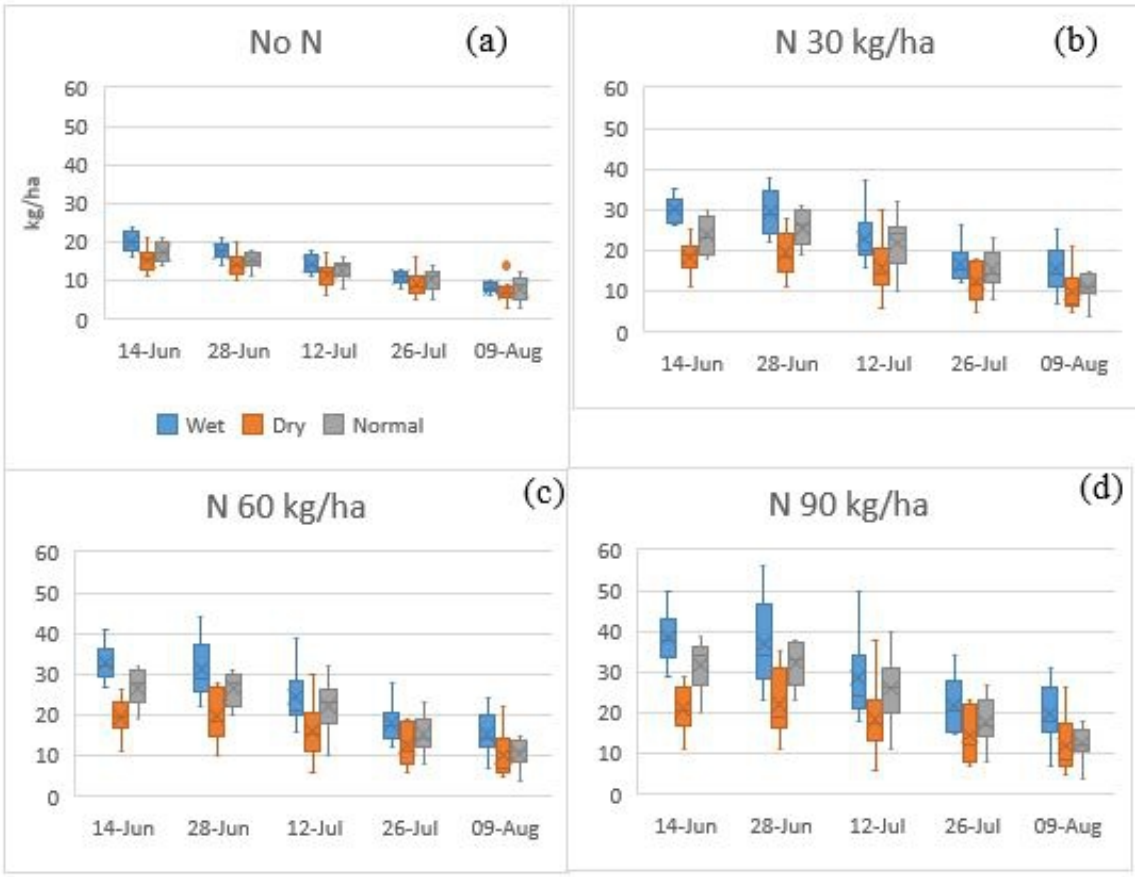

Fig III.5 Simulated N leaching as a function of planting date and rainfall for: (a) without N fertilizer, (b) 30 kg/ha N fertilizer, (c) 60 kg/ha N fertilizer, and (d) 90 kg/ha N fertilizer for Bhairahawa station from 1983 to 2010.

III.3.4.2 ENSO categories

Regarding the ENSO categories, the N leaching rate was high in La Nina years, medium in El Nino years and low in Neutral years (Fig. III.6). In terms the leaching rate, La Nina years were closer to wet years, El Nino years were closer to dry years and neutral years were closer to normal years. The N leaching rate increased in proportion to the amount of N fertilizer applied, and it decreased over time as planting dates were delayed. However, the increase in N leaching was disproportionally higher in La Nina years, when higher levels of N fertilizer were applied. Similarly, the N leaching rate slightly increased for crops planted on 28 June than on 14 June, followed by moderate but steady decrease. For the planting without N fertilizer, however, leaching rate steadily decreased after 14 June.

The highest N leaching rate, 38 kg/ha, occurred in La Nina years with an early planting date (28 June) and 90 kg N/ha, while the lowest N leaching rate, 7 kg/ha, was found for El Nino years with a late planting date (09 August) without N fertilizer. Fig. III.6 provides the variations in annual N leaching rates, according to fertilizer levels and planting dates.

Interannual variabilities in N leaching, illustrated by box height, increased as additional fertilizer was applied. This growth, however, was disproportionally high for La Nina years, as demonstrated by the long whiskers of the wet years' boxes.

These findings imply that it is less efficient to use high level of N fertilizers in La Nina years, and they also suggest that early planting can reduce N leaching. This proves that when large amounts of N are applied during wet years, plants are unable to make use of the fertilizer, as it is instead leached away from the soil. Thus, applying high levels of N fertilizers during La Nina years is a waste of resources.

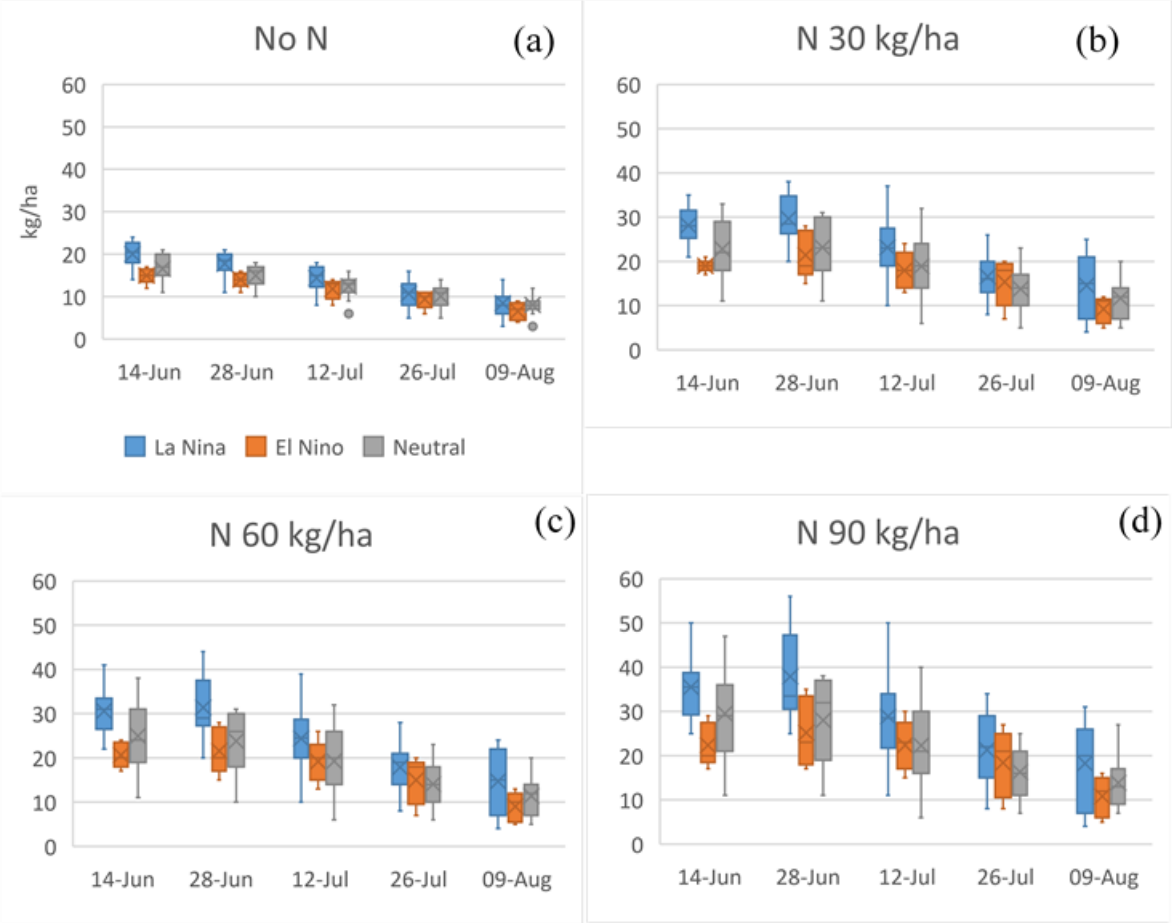

Fig III.6 Simulated Nitrogen leaching as a function of planting date and ENSO phases for: (a) without N fertilizer, (b) 30 kg/ha N fertilizer, (c) 60 kg/ha N fertilizer, and (d) 90 kg/ha N fertilizer for Bhairahawa station from 1983 to 2010.

III.3.5 Effect of precipitation on Nitrogen uptake

III.3.5.1 Wet/dry categories

N uptake was high during below-average rainfall years, medium during normal years, and low during above-average years (Fig. III.7). Normally, at high levels of N fertilizer, the rate of N uptake slowly fell when planting was delayed from past 14 June. However, it increased disproportionally as more N fertilizer was added.

The highest N uptake rate, 120 kg/ha, occurred during below-average rainfall years for the 14 June planting date and 90 kg N/ha. Similarly, the lowest N leaching rate, 15 kg/ha, occurred during above-average rainfall years for crops planted on 14 June without N fertilizer. These yearly variations in the N uptake rate differed according to fertilizer level and the planting date are demonstrated in Fig. III.7.

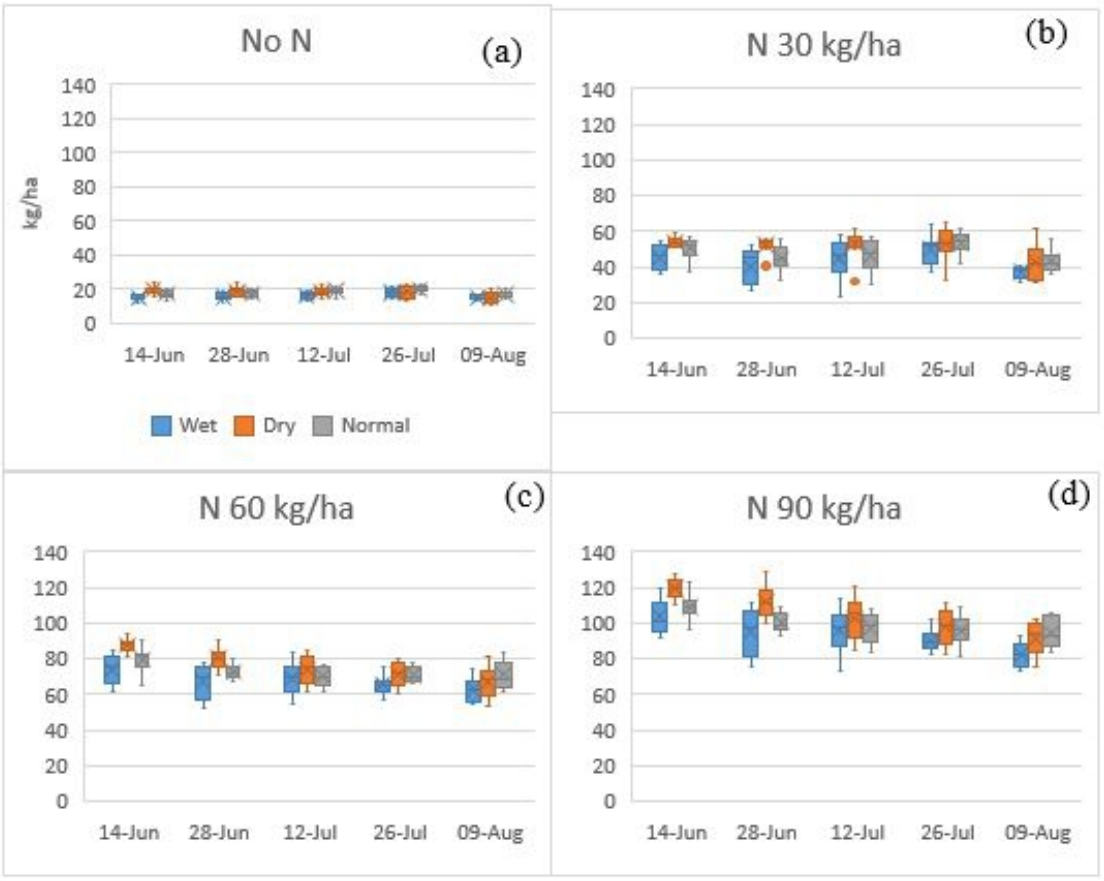

Fig III.7 Simulated Nitrogen uptake as a function of planting date and rainfall for: (a) without N fertilizer, (b) 30 kg/ha N fertilizer, (c) 60 kg/ha N fertilizer, and (d) 90 kg/ha N fertilizer for Bhairahawa station from 1983 to 2010.

These findings indicate that high levels of N fertilizers are less efficient in wet years and normal years. In general, applying large volumes of fertilizer in wet years is less efficient, especially for late planting dates, as the plants can only access a small portion of the fertilizer, while the majority of it is lost.

III.3.5.2 ENSO categories

N uptake was higher (lower) during the El Nino (La Nina) years. On average, the N uptake in Neutral years was very close to El Nino years (Fig. III.8). The N uptake rate slowly declined when planting was delayed past 14 June, but it increased out of proportion to additional N fertilizer levels.

The average highest N uptake rate, 116 kg/ha, occurred during El Nino years when planting took place on June 14 June and when 90 kg N/ha was applied. In contrast, the average lowest N leaching rate, 16 kg/ha,

was for La Nina years when planting took place on 14 June without N fertilizer. The annual variations in N uptake fluctuated according to fertilizer application level and planting date, and are depicted in Fig. III.7. The interannual variabilities in the N uptake rate, expressed by the box heights, increased for higher N fertilizer levels.

These results infer that it is less efficient to use high levels of N fertilizers in La Nina years. In general, high volumes of fertilizer are less efficient in La Nina years, especially for late planting dates, as only a small portion of the fertilizer is taken up by the plants, and while the greater part is lost.

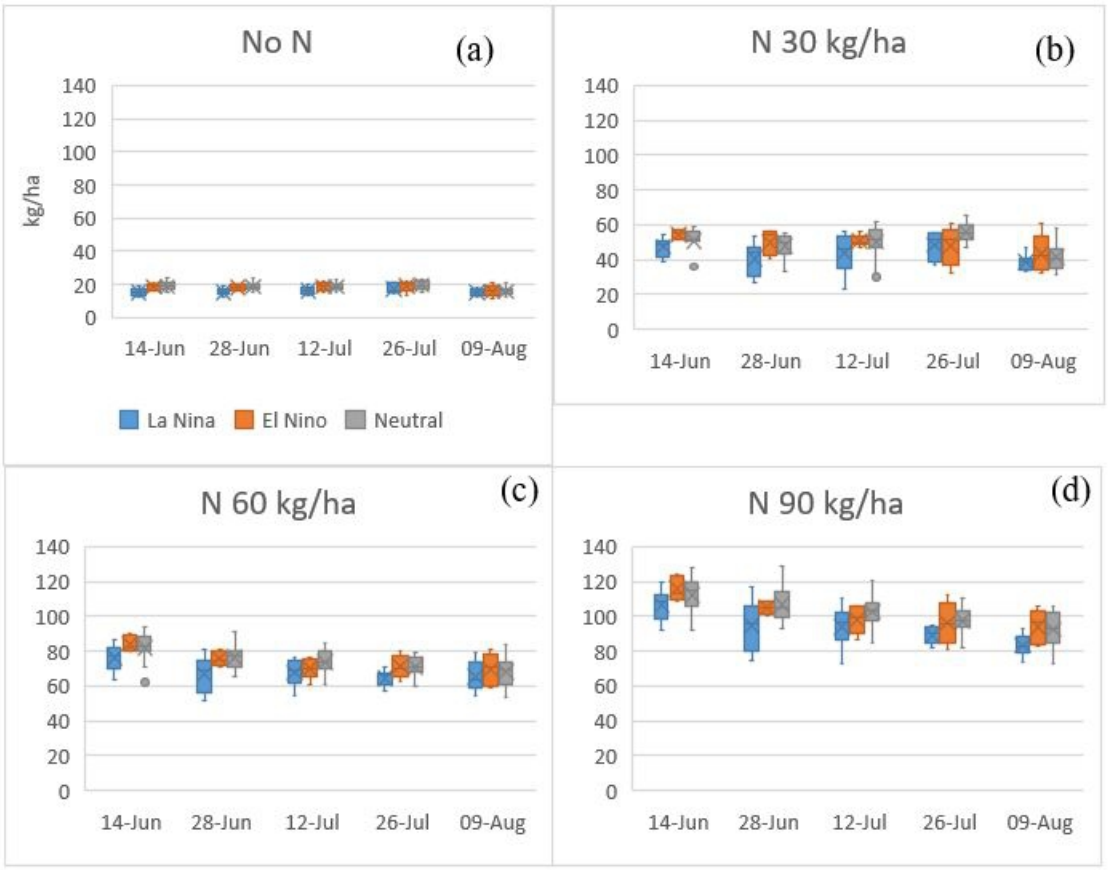

Fig III.8 Simulated N uptake as a function of planting date and ENSO phases for: (a) without N fertilizer, (b) 30 kg/ha N fertilizer, (c) 60 kg/ha N fertilizer, and (d) 90 kg/ha N fertilizer for Bhairahawa station from 1983 to 2010.

III.3.6 Drainage and runoff

La Nina and above-average rainfall years experienced more drainage, not only due to the high precipitation levels, but also the higher percentage of precipitation contribution to drainage than the runoff (Fig. III.9). The drainage-to-precipitation ratio was higher (40-42 %) in wet and La Nina years and lower in dry and El Nino years (34-35 %).

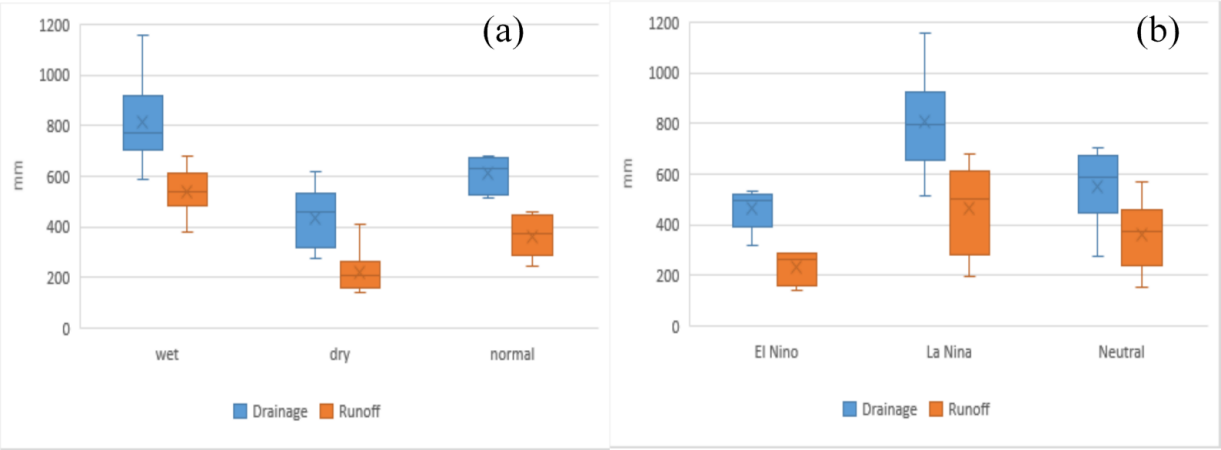

Fig. III.9 Drainage and runoff for: (a) rainfall categories of years and (b) ENSO categories of years.

The average drainage (runoff) varied from 436 (220) mm during dry years to 816 (541) mm during wet years (Fig III.11). Similarly, the average drainage (runoff) varied from 465 (230) mm in El Nino years to 811 (465) mm in La Nina years. The upper whiskers for drainage reached approximately 1,200 mm for wet years and La Nina years (Fig. III.11).

III.3.7 Value of forecasts

III.3.7.1 Existing practice

Based on informal discussion with farmers, we found that rice planting dates in the Terai's rainfed system varied according to the monsoon onset date and the amount of soil water available in the soil. Usually, seeds are sown a few days after the monsoon' onset, and transplanting takes place when the seedlings are 25 days old. However, in extreme weather years, rainfall amounts and the available soil water can lead to altered transplanting dates. For example, when there is a monsoon break or heavy flooding, farmers must delay transplanting. In general, however, the transplanting date is around mid-July, although it can occur a few weeks before or after, depending on labour availability.

Like the planting date, the N fertilizer level is not fixed. Rather, it varies from farmer to farmer, and individual farmers apply dissimilar amounts in different years. However, the most common application is 75 kg/ha Diammonium Phosphate (DAP) during planting and 45 kg/ha Urea in top dressing, about 25 days post-planting. Since DAP is comprised of 18% N, and Urea is comprised of 46% N, this is equivalent to 34 kg N/ha. Moreover, this figure is close to the World Bank's data on Nepal's average fertilizer application rate of 28.4 kg/ha, which includes, Nitrogen, Phosphorus and Potassium (WorldBank, 2015). Therefore, an average 15 July planting date and 30 kg N/ha are considered to constitute the existing rice cultivation practices in the Terai, which we employed as a baseline for comparison.

III.3.7.2 Value of forecasts

A forecast's value is calculated as the additional benefits from switching from existing rice cultivation practices to optimal management techniques. In our case, the model simulations identified the following optimal management methods: 14 June planting date, high levels of N fertilizer (60 kg/ha and 90 kg/ha), and El Nino years. The analysis indicated that increasing N fertilizer levels could boost rice yields in all years. However, net gross margins increased more substantially for crops planted on 14 June in El Nino years.

To that end, informal discussions at the local level estimated the cost of additional N fertilizer, as well as paddy prices. At the local level, Urea costs US$ 0.19/kg (1 US$=106 Nepali Rupees [Nrs.]) and a paddy with husk costs US$ 0.23/kg. The necessary quantity of Urea fertilizer was estimated on the basis of its 46% N content. It was assumed that all Nitrogen came from Urea.

The net gross margins associated with 60 kg N/ha and 90 kg N/ha were US$ 15/ha and US$ 34/ha, respectively, for a June 14 planting date in El Nino years, as compared with similar change in other years. The values of the ENSO-based forecasts differed considerably from those found by other studies. For example, Ramirez-Rodrigues et al. (2014) determined the ENSO-persistence-based forecasts were valued up to US$ 178/ha, while Asseng et al. (2012) found lower figure, only A$ 50/ha.

III.4 Conclusions

This study's objective was to evaluate different management options' effect on the coming season's rice yields to better understand optimal management methods for maximizing yields and minimizing resource wastage. The analysis employed the DSSAT v4.6's CERES-RICE model and employed advance information on the coming season's ENSO category.

The historical years were categorized into El Nino, La Nina, or Neutral years, according to the Oceanic Nino Index (ONI). Similarly, the standardized annual precipitation anomaly, obtained from weather station data, classified years as wet, dry, or normal. The DSSAT version 4.6's Seasonal Analysis tool simulated yields for different weather categories under various fertilizer levels and planting dates.

In general, rice yields were higher during dry and El Nino years and were lower in wet and La Nina years. The lower yield in La Nina years and wet years were associated with higher N leaching rates, as well as with reduced N uptake by plants (in wet years). Moreover, the reduced yields in La Nina years were related to an increase in minimum temperatures during the second half of the growing season. Similarly, the high leaching rate during wet years was associated with high drainage and runoff during wet years. In contrast, the N leaching (uptake) were lower (higher) during dry and El Nino years.

Rice yield also depended on the amount of N fertilizer applied and on the planting date. Overall, additional N fertilizer caused yields to increase, but this effect weekend for crops planted from 14 June onwards. Considering that under existing practices in the Terai, rice planting takes place in mid-July and with low levels of N fertilizer, all years' rice yields could be enlarged with additional N fertilizer and earlier planting dates. However, the marginal increase in yield associated with additional N fertilizer was higher during dry years and El Nino years. These conclusions must be verified by research stations.

Therefore, extra N fertilizer is more efficient in dry years and El Nino years. This is also because a high portion of N leached away in wet years and La Nina years. Consequently, plants could only access a limited amount of fertilizer in those years. We calculated a forecast's value as the additional benefit to be achieved from switching from existing practices to optimal management techniques in El Nino years, as compared with similar changes in other years. Increasing fertilizer levels to 90 kg/ha and 60 kg/ha resulted in net gross margins of US$ 34/ha and US$ 15/ha, respectively, for rice planted on 14 June in El Nino years.

The interannual variability of N leaching and uptake was lower for crops planted on 14 June in dry and El Nino years than for other planting dates and other categories of years. This reduced interannual variability increases our confidence that N leaching (uptake) was lower (higher) in dry years for earlier planting dates than those currently employed. However, every La Nino years is not necessarily a wet year and every wet years has different intraseasonal variability. Therefore, the study's conclusions have a statistical value but may lead to failures and losses. From an operational viewpoint, one should assess the probabilities and the cost of these "failures".

References

ADLER, R. F., HUFFMAN, G. J., CHANG, A., FERRARO, R., XIE, P.-P., JANOWIAK, J., RUDOLF, B., SCHNEIDER, U., CURTIS, S., BOLVIN, D., GRUBER, A., SUSSKIND, J., ARKIN, P. & NELKIN, E. 2003. The Version-2 Global Precipitation Climatology Project (GPCP) Monthly Precipitation Analysis (1979–Present). *Journal of Hydrometeorology,* 4, 1147-1167.

AKHTAR, T., THAKUR, G., RAJAK, R. K., KHAN, S. U., GHIMIRE, S. P. & GHALE, G. Year. Rice varietal improvement works under irrigated sup tropical regions of Nepal. *In:* 24th Summer crop workshop 30-31 June 2004, 2004 National Rice Research Program Hardinath, Baniniya, Dhanusha. Nepal Agricultural Research Council Khumaltar.

ASHOK, K., GUAN, Z. Y. & YAMAGATA, T. 2001. Impact of the Indian Ocean Dipole on the relationship between the Indian monsoon rainfall and ENSO. *Geophysical Research Letters,* 28, 4499-4502.

ASSENG, S., MCINTOSH, P. C., WANG, G. & KHIMASHIA, N. 2012. Optimal N fertiliser management based on a seasonal forecast. *European Journal of Agronomy,* 38, 66-73.

BATJES, N. H. 2002. A homogenized soil profile data set for global and regional environmental research. (WISE, version 1.1). Report 2002/01. Wageningen, The Netherlands: International Soil reference and Information Centre (ISRIC).

BLANFORD, H. 1884. On the connection of Himalayan snowfall and seasons of drought in India *Proc R Soc Lond,* 37, 3-22.

BORRELLI, A., MATERIA, S., BELLUCCI, A., ALESSANDRI, A. & GUALDI, S. 2012. Seasonal Prediction System at CMCC. *Research Papers Issue RP0147*.

BOUMAN, B. & AUREUS, A. 2009. Every drop counts. *Rice Today.*: International Rice Research Institute. Los Banos, Laguna, Phillipines.

CHERCHI, A. & NAVARRA, A. 2003. Reproducibility and predictability of the Asian summer monsoon in the ECHAM4-GCM. *Climate Dynamics,* 20, 365-379.

GIJSMAN, A. J., THORNTON, P. K. & HOOGENBOOM, G. 2007. Using the WISE database to parameterize soil inputs for crop simulation models. *Computers and Electronics in Agriculture,* 56, 85-100.

GOSWAMI, B. N., MADHUSOODANAN, M. S., NEEMA, C. P. & SINGUPTA, D. 2006. A physical mechanism for North Atlantic SST influence on the Indian Summer Monsoon. *Geophysical Research Letters,* 33.

HANLEY, D. E., BOURASSA, M. A., O'BRIEN, J. J., SMITH, S. R. & SPADE, E. R. 2003. A Quantitative Evaluation of ENSO Indices. *Journal of Climate,* 16, 1249-1258.

HOOGENBOOM, G. 2000. Contribution of agrometeorology to the simulation of crop production and its applications. *Agricultural and Forest Meteorology,* 103, 137-157.

HOOGENBOOM, G., J.W. JONES, P.W. WILKENS, C.H. PORTER, K.J. BOOTE, L.A. HUNT, U. SINGH, J.I. LIZASO, J.W. WHITE, O. URYASEV, R. OGOSHI, J. KOO, V. SHELIA & TSUJI., G. Y. 2015. Decision Support System for Agrotechnology Transfer (DSSAT) Version 4.6 (http://dssat.net). Prosser, Washington: DSSAT Foundation.

ICHIYANAGI, K., YAMANAKA, M. D., MURAJI, Y. & VAIDYA, B. K. 2007. Precipitation in Nepal between 1987 and 1996. *International Journal of Climatology,* 27, 1753-1762.

IIZUMI, T., LUO, J.-J., CHALLINOR, A. J., SAKURAI, G., YOKOZAWA, M., SAKUMA, H., BROWN, M. E. & YAMAGATA, T. 2014. Impacts of El Niño Southern Oscillation on the global yields of major crops. *Nature Communications,* 5.

JONES, J. W., HANSEN, J. W., ROYCE, F. S. & MESSINA, C. D. 2000. Potential benefits of climate forecasting to agriculture. *Agriculture, Ecosystems & Environment,* 82, 169-184.

JONES, J. W., HOOGENBOOM, G., PORTER, C. H., BOOTE, K. J., BATCHELOR, W. D., HUNT, L. A., WILKENS, P. W., SINGH, U., GIJSMAN, A. J. & RITCHIE, J. T. 2003. The DSSAT cropping system model. *European Journal of Agronomy,* 18, 235-265.

KRISHNAMURTHY, V. & SHUKLA, J. 2000. Intraseasonal and interannual variability of rainfall over India. *Journal of Climate,* 13, 4366-4377.

KUMAR, K. K., RAJAGOPALAN, B. & CANE, M. A. 1999. On the Weakening Relationship Between the Indian Monsoon and ENSO. *Science,* 284, 2156-2159.

KUMAR, K. K., RAJAGOPALAN, B., HOERLING, M., BATES, G. & CANE, M. 2006. Unraveling the Mystery of Indian Monsoon Failure During El Nino. *Science,* 314, 115-119.

LAMSAL, A., AMGAI, L. P. & GIRI, A. 2013. Modeling the sensitivity of CERES-Rice model: An experience of Nepal. *Agronomy Journal of Nepal,* 3, 11-21.

MAVROMATIS, T., JAGTAP, S. S. & JONES, J. W. 2002. El NiÃƒÂ±o-Southern Oscillation effects on peanut yield and nitrogen leaching. *Climate Research,* 22, 129-140.

MEZA, F. J., HANSEN, J. W. & OSGOOD, D. 2008. Economic Value of Seasonal Climate Forecasts for Agriculture: Review of Ex-Ante Assessments and Recommendations for Future Research. *Journal of Applied Meteorology and Climatology,* 47, 1269-1286.

MOAC 2008. Statistical informaton on Nepalese Agriculture, 2008/09, Government of Nepal, Ministry of Agricultural Development, Agribusiness Promotion and Statistics Division, Singh Durbar, Kathmandu,Nepal.

MOAD 2012. Statistical informaton on Nepalese Agriculture, 2011/12, Government of Nepal, Ministry of Agricultural Development, Agribusiness Promotion and Statistics Division, Singh Durbar, Kathmandu,Nepal.

PENG, S., HUANG, J., SHEEHY, J. E., LAZA, R. C., VISPERAS, R. M., ZHONG, X., CENTENO, G. S., KHUSH, G. S. & CASSMAN, K. G. 2004. Rice yields decline with higher night temperature from global warming. *Proceedings of the National Academy of Sciences of the United States of America,* 101, 9971-9975.

RAMIREZ-RODRIGUES, M. A., ASSENG, S., FRAISSE, C., STEFANOVA, L. & EISENKOLBI, A. 2014. Tailoring wheat management to ENSO phases for increased wheat production in Paraguay. *Climate Risk Management,* 3, 24-38.

RASMUSSON, E. M. & CARPENTER, T. H. 1983. The relationship between eastern equatorial Pacific sea surface temperatures and rainfall over India and Sri lanka. *Mon. Wea. Rev,* 111, 517-528.

RAY, D. K., GERBER, J. S., MACDONALD, G. K. & WEST, P. C. 2015. Climate variation explains a third of global crop yield variability. *Nature Communications,* 6, 5989.

REYNOLDS, R. W. & SMITH, T. M. 1994. Improved Global Sea Surface Temperature Analyses Using Optimum Interpolation. *Journal of Climate,* 7, 929-948.

RITCHIE, J. T. 1998. Soil water balance and plant stress. *In:* TSUJI, G. Y., HOOGENBOOM, G. & THORNTON, P. K. (eds.) *Understanding Options for Agricultural Production.* Dordrecht, The Netherlands: Kluwer Academic Publishers.

RITCHIE, J. T. & OTTER, S. 1985. Description and performance of CERES-Wheat: a user-oriented wheat yield model. *ARS Wheat Yield Project. ARS-38.* Springfield, Missouri: Natl Tech Info Serv.

S.C.S 1972. *National Engineering Handbook, Hydrology* Soil Conservation Service (SCS).

SAHA, S., MOORTHI, S., PAN, H.-L., WU, X., WANG, J., NADIGA, S., TRIPP, P., KISTLER, R., WOOLLEN, J., BEHRINGER, D., LIU, H., STOKES, D., GRUMBINE, R., GAYNO, G., WANG, J., HOU, Y.-T., CHUANG, H.-Y., JUANG, H.-M. H., SELA, J., IREDELL, M., TREADON, R., KLEIST, D., VAN DELST, P., KEYSER, D., DERBER, J., EK, M., MENG, J., WEI, H., YANG, R., LORD, S., VAN DEN DOOL, H., KUMAR, A., WANG, W., LONG, C., CHELLIAH, M., XUE, Y., HUANG, B., SCHEMM, J.-K., EBISUZAKI, W., LIN, R., XIE, P., CHEN, M., ZHOU, S., HIGGINS, W., ZOU, C.-Z., LIU, Q., CHEN, Y., HAN, Y., CUCURULL, L., REYNOLDS, R. W., RUTLEDGE, G. & GOLDBERG, M. 2010. The NCEP Climate Forecast System Reanalysis. *Bulletin of the American Meteorological Society,* 91, 1015-1057.

SAJI, N. H., GOSWAMI, B. N., VINAYACHANDRAN, P. N. & YAMAGATA, T. 1999. A dipole mode in the tropical Indian Ocean. *Nature,* 401, 360-363.

SHRESTHA, A. B., WAKE, C. P., DIBB, J. E. & MAYEWSKI, P. A. 2000. Precipitation fluctuations in the Nepal Himalaya and its vicinity and relationship with some large scale climatological parameters. *International Journal of Climatology,* 20, 317-327.

SHUKLA, J. 1987. Interannual variability of monsoons. *In:* FEIN, J. S. & STEPHENS, P. L. (eds.) *Monsoons.* Wiley and Sons.

SIKKA, D. R. 1980. Some aspects of the large scale fluctuations of summer monsoon rainfall over India in relation to fluctuations in the planetary and regional scale circulation parameters. *Earth and Planetary Sciences,* 89, 179-195.

STONE, R. C., HAMMER, G. L. & MARCUSSEN, T. 1996. Prediction of global rainfall probabilities using phases of the Southern Oscillation Index. *Nature,* 384, 252-255.

TIMSINA, J. & HUMPHREYS, E. 2006. Performance of CERES-Rice and CERES-Wheat models in rice–wheat systems: A review. *Agricultural Systems,* 90, 5-31.

TORRENCE, C. & WEBSTER, P. J. 1998. The annual cycle of persistence in the El Nño/Southern Oscillation. *Quarterly Journal of the Royal Meteorological Society,* 124, 1985-2004.

TRENBERTH, K. E. & STEPANIAK, D. P. 2001. Indices of El Niño Evolution. *Journal of Climate,* 14, 1697-1701.

WORLDBANK 2015. Fertilizer consumption rate (kg/ha) of arable land. Data catalogue of the World Bank datasets. The World Bank Group

YATAGAI, A., KAMIGUCHI, K., ARAKAWA, O., HAMADA, A., YASUTOMI, N. & KITOH, A. 2012. APHRODITE: Constructing a Long-Term Daily Gridded Precipitation Dataset for Asia Based on a Dense Network of Rain Gauges. *Bulletin of the American Meteorological Society,* 93, 1401-1415.